SYNTHESIS AND CHARACTERIZATION OF Ln(BTFA)$_3$DMPHEN COMPLEXES (Ln= Eu^{3+}, Er^{3+}, Ho^{3+}, Tb^{3+}, Tm^{3+}, AND Yb^{3+}, BTFA=4,4,4-TRIFLUORO-1-PHENYL-1,3-BUTANEDIONE, DMPHEN=4,7-DIMETHYL-1,10-PHENANTHROLINE) AND SOL-GEL MATERIALS FOR POTENTIAL OPTICAL APPLICATIONS

A thesis presented to the faculty of the Graduate School of Western Carolina University in partial

fulfillment of the requirements for the degree of Master of Science in Chemistry

By

Louis Christopher Martin

Director: Dr. Channa R. De Silva

Associate Professor,

Department of Chemistry and Physics

Committee Members: Dr. Brian D. Dinkelmeyer, Chemistry

Dr. David D. Evanoff Jr., Chemistry

November 2016

ACKNOWLEDGEMENTS

TABLE OF CONTENTS

LIST OF TABLES

LIST OF FIGURES

LIST OF SCHEMES

LIST OF ABBREVIATIONS

Ce- element 58, Cerium

dmphen- 4,7-dimethyl,1,10-phenanthroline

Dy- element 66, Dysprosium

Er- element 68, Erbium

Eu- element 63, Europium

Gd- element 64, Gadolinium

g- [gram] The SI unit of mass

Hacac- 2,4-pentanedione

Hbtfa- 4,4,4-trifluoro-1-phenyl-1,3-butanedione

Ho- element 67, Holmium

ICP-OES - Inductively Couple Plasma Optical Emission Spectroscopy

IR- Infra red

L- [litre] The SI unit of Volume

La- element 57, Lanthanum

LED- Light Emitting Diode

Ln- General chemical abbreviation used to denote a compound containing a lanthanide series element

Lu- element 71, Lutetium

mg- [milligram] 1/1000 of a gram

mL- [milliliter] 1/1000 of a liter

mmol-[millimole] 1/1000 of a mole

mol- [mole] number of atoms in a unit of a substance. Represented by Avogadro's number 6.022×10^{23}

Nd- element 60, Neodymium

phen- 1,10-phenanthroline

Pm- element 61, Promethium

Pr- element 59, Praseodymium

Sm- element 62, Samarium

STEM- Scaning Transmission Electron Microscopy

Tb- element 65, Terbium

Tm- element 69, Thulium

Yb- element 70, Ytterbium

ABSTRACT

SYNTHESIS AND CHARACTERIZATION OF Ln(BTFA)$_3$DMPHEN COMPLEXES (Ln= Eu^{3+}, Er^{3+}, Ho^{3+}, Tb^{3+}, Tm^{3+},AND Yb^{3+}, BTFA=4,4,4-TRIFLUORO-1-PHENYL-1,3-BUTANEDIONE, DMPHEN=4,7-DIMETHYL-1,10-PHENANTHROLINE) AND SOL-GEL MATERIALS FOR POTENTIAL OPTICAL APPLICATIONS

Louis Christopher Martin, M.S

Western Carolina University (November 2016)

Director: Dr. Channa R. De Silva

Lanthanide-based materials are attractive candidates for the use in light emitting devices, immunoassays, and *in-vitro* cellular imaging technologies. Their superior luminescent properties include sharp emission bands arising from *f-f* electronic transitions and longer luminescence lifetimes compared to traditional organic dyes. Major problems in biological applications are the toxicity, stability, and the delivery of insoluble lanthanide chelators to targeted cells. Silica encapsulation of the lanthanide chelators provides a promising approach to minimize the toxicity and improve the dispersion of the lanthanide chelators in an aqueous environment with higher stability. This research is focused on the synthesis of novel lanthanide(III) complexes and their silica-based solgel materials. Lanthanide complexes have the general formula of Ln(btfa)$_3$(dmphen) where btfa = 4, 4, 4-trifluoro-1-phenyl-1,3-butanedione and dmphen = 4,7-dimethyl,1,10-phenanthroline. All complexes demonstrate the common formula, Ln(btfa)$_3$(dmphen) where Ln= Eu^{3+},Er^{3+}, Tb^{3+}, Ho^{3+}, Tm^{3+}, and Yb^{3+}. Eu^{3+} and Tb^{3+} complexes emit red and green light, respectively, whereas Er^{3+}, Ho^{3+}, and Yb^{3+} complexes have near-infrared emission characteristics. The molecular structures of the complexes were characterized using single crystals X-ray diffraction studies. The complexes and sol-gel materials were characterized using absorption and fluorescence spectroscopy,

time-resolved luminescence spectroscopy, and ICP-OES studies. Structural and the luminescent properties

of the complexes are discussed.

CHAPTER 1: BACKGROUND AND INTRODUCTION TO RESEARCH

1.1 LANTHANIDES PAST AND PRESENT

The lanthanides, or lanthanoids[1], are a series of chemically similar metals comprising the 4f block of the periodic table, and include the elements 58 (cerium, Ce) through 71 (lutetium, Lu).[1] Though not technically a lanthanide due to having no 4f electrons, element 57 lanthanum (La) is typically included in discussions of the lanthanides.[1] Along with elements 21 (scandium, Sc) and 39 (yttrium, Y), the lanthanides make up a group of metals referred to as the rare earth elements, though they are by no means exceptionally rare.[2] The most abundant lanthanide, Ce, has the same relative abundance as copper (Cu), and is in much higher abundance than boron (B), cobalt (Co), germanium (Ge), lead (Pb), tin (Sn), and uranium (U) on the planet.[3] The least abundant naturally occurring lanthanide, element 69 (thulium, Tm), is more abundant than cadmium (Cd), iodine (I), mercury (Hg), silver (Ag), gold (Au), and platinum (Pt).[3]

The history of the lanthanides begins in 1787. During this time, Swedish artillery officer and geology enthusiast, Lt. Carl Axel Arrhenius (1757-1824), was exploring a quarry in the small Swedish town of Ytterby.[1,3] Arrhenius found a sample of a black mineral that he termed ytterbite. Speculation at the time said that this ytterbite contained the recently discovered element tungsten (W). With the work of Finnish chemist and mineralogist, Johan Gadolin (1760-1852), it was shown that the mineral contained a previously unidentified "earth" (a term loosely applied to insoluble metal oxides) which he termed "Yttria."[1] Yttria would later be shown to contain six different rare earth/lanthanide oxides. The rest of the lanthanides would be discovered through the 19th and 20th century, with the last naturally occurring lanthanide, lutetium (Lu), being discovered in 1907.[1] It would be 1947 before the final element, promethium (Pm), was synthesized and characterized.[1,3] Table 1 shows the discovery dates and origins of the lanthanide names.

Table 1. Brief History of Lanthanide Series.

Name	Year	Name Origin
lanthanum	1839	From the Greek lanthanein meaning "to lie hidden"
cerium	1803	Ceres, an asteroid discovered in 1801
praesodymium	1885	Named from Greek prasios meaning "green," and didymos meaning "twin"
neodymium	1885	Named from Greek neo meaning "new," and didymos meaning "twin"
promethium	1947	Named from Greek god Prometheus, who stole fire from the gods.
samarium	1879	Named from samarskite, a mineral that was named after Russian mining official Col. Samarski
europium	1901	Europe
gadolinium	1886	Named from the mineral gadolinite that gets its name from Johan Gadolin
terbium	1843	Ytterby, Sweden
dysprosium	1886	Named from Greek disprositos meaning "hard to get at."
holmium	1878	Holmia, Latin name for Stockholm Sweden
erbium	1842	Ytterby, Sweden
thulium	1879	Named from Thule, ancient name of Scandinavia
ytterbium	1878	Ytterby, Sweden
lutetium	1907	Lutetia, ancient name for Paris

It should be noted that although the lanthanides have been known since the 19th and early 20th centuries, it has only been since the 1950's that sufficiently pure samples have been prepared.[3] In modern times,

lanthanides have seen an explosion in commercial use with the common uses summarized in Table 2.

Table 2. Commercial uses for lanthanides.[1]

Application	Percentage
catalytic converters	45
petroleum refining catalysts	25
permanent magnets	12
glass polishing and ceramics	7
metallurgical	7
phosphors	3
other	1

The current surge in lanthanide interest is bolstered by the growing need of luminescent materials that meet stringent requirements for telecommunications, lighting, sensors electroluminescent materials, and bio-imaging devices.[4] With the rise in the commercial use of lanthanide materials due to their unique electronic and magnetic properties, three major areas of lanthanide research have been developed. These three major developments of lanthanide research are in the areas of light-emitting devices (LED's), bio immunoassays, and *in vitro* cellular imaging technologies.[4-28] Though much progress has been made in all areas of lanthanide utilization, this work will focus on the use of lanthanides as materials for possible bio-imaging, biomedical applications, light emitting materials as well as an exploration of the molecular structures and coordination chemistry of new lanthanide complexes. Lanthanide based materials are attractive for these applications due to their many advantages as a base for luminescent materials. Bio-imaging and biomedical uses of lanthanides will be discussed in section 1.2. The advantages of lanthanide chelators, with particular attention to lanthanide β-diketonates, that make them such appealing candidates for bio-imaging technologies as well as the current problems with utilization will be discussed

in section 1.3.

1.2 BIO-IMAGING AND BIOMEDICAL USE OF LANTHANIDES

Lanthanide emission has been used heavily in biological systems.[4-28] One method is the labeling of biological molecules with lanthanide probes which are used to detect cell functions. In order to help with diagnosis of medical conditions and early stage detection of diseases like cancer, a way to view (image) inside a patient's body is needed. This has led to the use of luminescent materials that can be used to tag various conditions, and to visualize the areas being examined. Much progress has been made in the field of biological imaging, and lanthanide use as luminescent materials in these applications has been increased. Joseph Leonard and colleagues presents the luminescent lanthanides that quench upon anion recognition of a specific substrate in a displacement assay.[8] Most of these applications are done *in vitro* as immunoassays of biological samples such as blood. Given these major problems, the advantages of lanthanides and the doping of them into biologically favorable carrier constituents continue to be a growing area of study. The broad luminescent capabilities of trivalent lanthanide ions are intriguing due to possible applications in biological and chemical sensors, medical diagnostics, cellular imaging, and high sensitivity detection of biomolecules, and biomedical imaging. Lanthanide materials have become an area of interest in varying fields of medical and biological research due to the unique luminescent properties they possess.[5] This has led to the development of new lanthanide organometallic complexes that have novel applications in immunoassay, DNA hybridization, high-throughput screening assays, and imaging.[5,6] Fluorescent labels based on lanthanides have been used in highly sensitive time resolved immunoassay technologies.[6] The remarkable improvement in the assay is due to the time-resolved detection technique which eliminates cellular background fluorescence.[6,7]

1.3 ADVANTAGES AND DISADVANTAGES OF LANTHANIDE CHELATORS

Ever since Weissman described a highly photoluminescent europium complex in 1942, interest in lanthanides has increased due to their high potential for imaging applications.[29] Lanthanides exhibit

many characteristics that make them attractive candidates for biological imaging applications, due to their superior luminescent and unique electronic and magnetic properties caused by shielded f electrons, sharp emission bands originating from f-f electronic transitions, a unique energy transfer mechanism for lanthanide centered luminescence, large Stokes shifts, limited photo bleaching, wavelength tunability dictated by the lanthanide ion chosen, high luminescent quantum yields, high signal to noise ratios during measurements, ease of synthesis, wide availability of well characterized and studied chelator ligands, and luminescence lifetimes that are much longer than traditional organic dyes. Many lanthanides also exhibit emission in the infrared (IR) region, and some lanthanides can be used in the process of photon up-conversion. In addition to these properties, the fluorescence of many lanthanides is outside the range of the cell background fluorescence, which reduces possible interference from normal cell fluorescent activity. With these advantages over more traditional phosphors, much progress has been made, but there are still several problems with lanthanide materials used for the purpose of biological imaging.

The problems arising from the use of lanthanide based materials for biological imaging applications vary from common concerns of metal toxicity and stability of the synthesized complexes in an aqueous environment. Many of the highly luminescent lanthanide complexes are water insoluble, and of the ones that can be dispersed in water, the potential quenching effects of the aqueous environment matching the vibrational states of the lanthanide material become problematic and produce diminishing returns on the highly luminescent properties of the material. One way to get around this issue is the use of silica based sol gel materials. These materials will be discussed further in section 1.5.5.

1.3.1 Lanthanide β-diketonates

To utilize lanthanide ions and make luminescent complexes, chelating groups are necessary. This is due to trivalent lanthanide cations (Ln^{3+}) being hard Lewis acids with a coordination number of 8 or 9.[7] This also means that "hard" donors with oxygen or nitrogen in the chelating ligands is necessary. There are many types and combinations of chelators that can be used in conjunction with lanthanides to make lanthanide chelator complexes. The chelators can range from monodentate and up to bidentate and

tridentate varieties. Bidentate ligands are a good choice for making chelator complexes because they can be added to the central lanthanide metal ion through simple synthetic methods and still provide an enhanced energy transfer between the ligand and the lanthanide metal ion. Among the various classes of lanthanide chelators, β-diketonates are the most widely studied lanthanide complexes[3]. Many lanthanide β-diketonate complexes use a derivative of the 2, 4-pentanedione (acac) ligand (Figure 1).
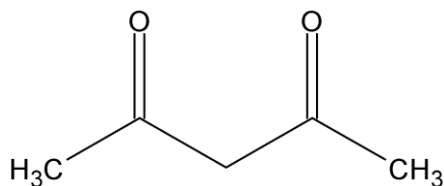
Figure 1. Molecular structure of acac

Lanthanide β-diketonate complexes are attractive candidates for luminescent applications of lanthanides because the ligands are commercially available, well characterized, and inexpensive. This class of ligands provide materials with high luminescent quantum yields with an easy route to the synthesis of chelator complexes. Lanthanide β-diketonates have been used in *in vitro* luminescent assays including Dissociation Enhanced Lanthanide Fluoroimmunoassay [DELFIA] Technology that was suggested conceptually more than 30 years ago.[7]

The use of Lanthanide β-diketonates could allow for improved bio-imaging and this type of assay can be used in early detection of cancer. Despite the recent progress of utilizing this class of materials in biomedical imaging applications, they suffer from several drawbacks. The disadvantages of lanthanide β-diketonates for the use in biomedical imaging applications include stability, toxicity, and poor water solubility of the complexes. Another major challenge is the targeted delivery of the chelator agents to a desired cell type.

1.3.2 N-Donor Ligands

The β-diketonate ligand serves as a charge balance to the central lanthanide cation. The three bidentate β-diketonate ligands replace six of the eight coordination sites on a typical lanthanide ion. This still leaves

two water ligands attached from the reaction of the β-diketonate and the lanthanide chloride or nitrate hydrate. The last two coordination sites containing water ligands can be replaced by a neutral bidentate ligand such as 1,10-phenanthroline (phen) (Figure 2.)
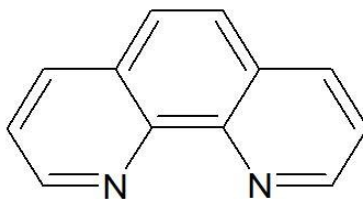
Figure 2. Molecular structure of phen

The 1 and 10 positions on phen contain nitrogen atoms. These two nitrogen atoms will coordinate to the central lanthanide ion and replace the water ligands. The new complex now has the bidentate neutral ligand with the nitrogen atoms attached. It can also act as a secondary source for absorbing light energy during excitation and is referred to as an N-Donor Ligand.

1.3.3 Lanthanide-Centered Luminescence

Luminescence is a process where a substance absorbs light at one wavelength and then emits it at another wavelength that is generally higher.[5] The absorbed energy excites the molecule from the ground singlet state (S_0) to an excited higher level such as S_1. From this state, many options can occur. The energy can relax from a singlet state back down to the S_0 state (fluorescence). Other pathways include radiative and non-radiative transitions that can return the molecule to any of its rotational or vibrational ground states. Transitions from the S_1 state to the triplet state (T_1) can be followed by phosphorescence or non radiatively. T_1 can also transition the excitation energy to another species such as chelated lanthanide ions. It is from this state that luminescence can occur. The ligand to metal energy transfer is called the antenna effect and can lead to intense luminescence of lanthanide ions that would absorb energy poorly without the ligand. The *f-f* electronic transitions are parity and spin forbidden and are highly inefficient. In order to efficiently utilize the *f-f* electronic transitions of the trivalent lanthanides, it must be sensitized by a coordinating ligand capable of light absorption. This ligand is an organic chromophore and acts as

an "antenna" to efficiently sensitize the lanthanide ions (Figure 3). Figure 4 shows this process for the excited states of Eu^{3+} complexes. The lanthanide ion luminesces upon relaxation. This process is known as lanthanide-centered luminescence. Each lanthanide ion has characteristic emission bands. Eu^{3+} has four electronic transitions arising from a $^5D_0$ to ^7F_n energy levels. The electronic transitions for Eu^{3+} are $^5D_0$ to $^7F_1$ (595 nm), $^5D_0$ to $^7F_2$ (615 nm), $^5D_0$ to $^7F_3$ (655 nm), and $^5D_0$ to $^7F_4$ (688 nm)[8]. The $^5D_0$ to $^7F_2$ (615 nm) is the strongest transition for Eu^{3+} and is ideal for biological imaging due to being far away from the cell background fluorescence usually observed in the blue and green region of the electromagnetic spectrum.[1] The electronic transitions for Tb^{3+} are $^5D_4$ to $^7F_6$ (480 nm), $^5D_4$ to $^7F_5$ (535 nm), $^5D_4$ to $^7F_4$ (580 nm), $^5D_4$ to $^7F_3$ (615 nm), and $^5D_4$ to $^7F_2$ (640 nm)[8]. Er^{3+} has an emission at 1550 nm ($^4I_{13/2}$ to $^4I_{15/2}$)[12]. Tm^{3+} has an emission at 975 nm ($^3F_4$ to $^3H_6$) and 1465 nm ($^3F_4$ to $^3H_4$)[13]. Ho^{3+} has an emission at 975 nm ($^5F_5$ to $^5I_7$), ~1187 nm ($^5I_6$ to $^5I_8$), and 1479 nm (5F5 to 5I6)[13]. Yb^{3+} has one luminescent transition at 980 nm ($^2F_{5/2}$ to $^2F_{7/2}$)[12]. These lanthanides were chosen due to their near-infrared emission characteristics, which are even farther away from the cell background fluorescence. Since the *f* electrons have minimum participation in metal-ligand bonding, the emission is characteristic of the lanthanide ion. For example, Eu^{3+} complexes produce a sharp emission peak at 615 nm upon ligand excitation (Figure 5).
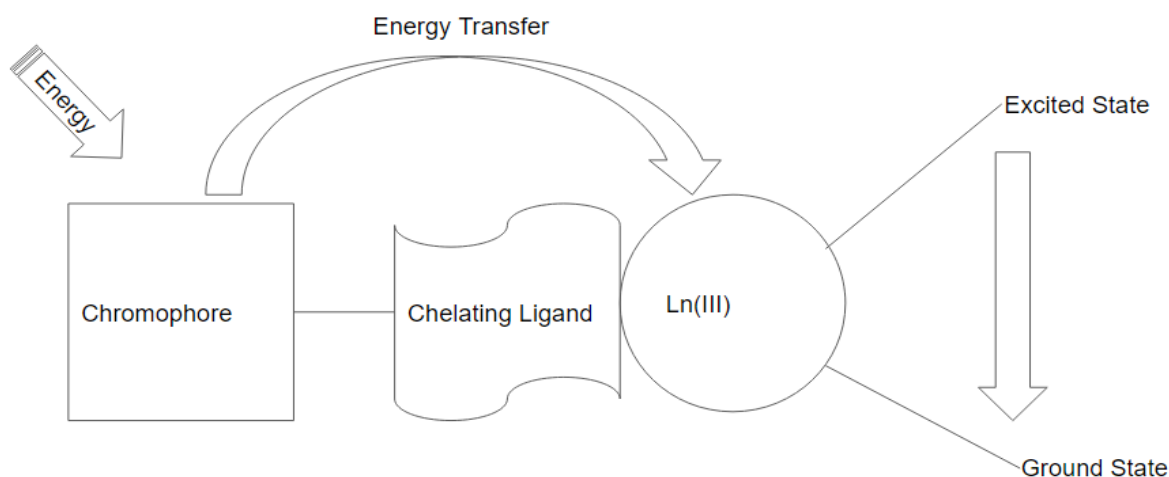
Figure 3. Lanthanide-Centered Luminescence.
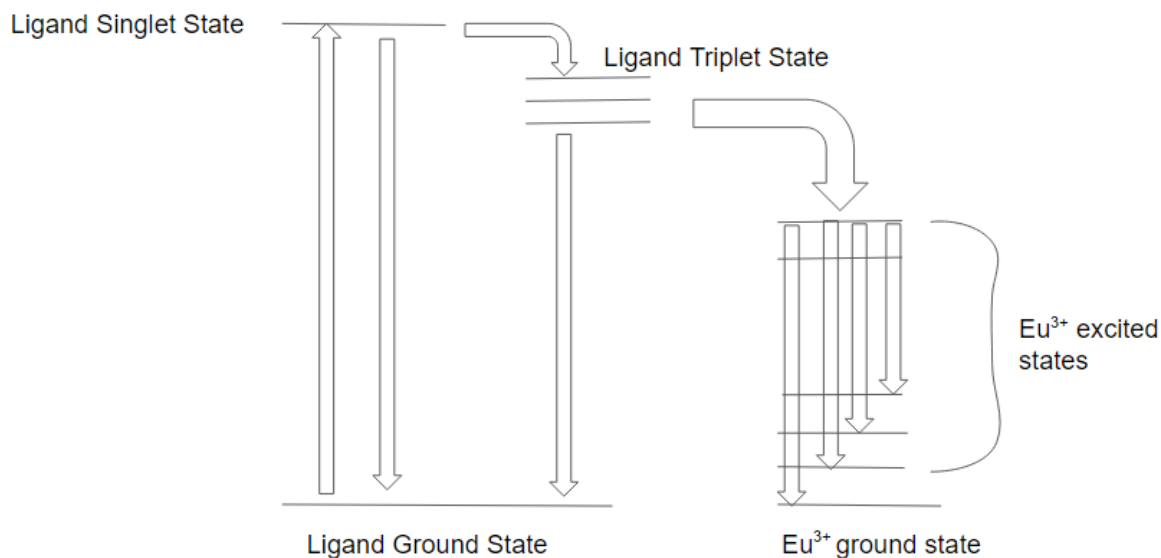
Figure 4. Energy transfer diagram for a typical Eu^{3+}-complex.
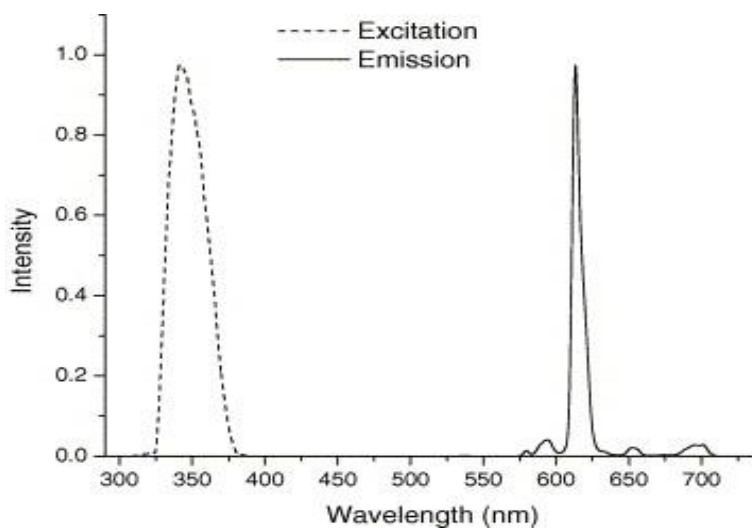
Figure 5. Photo-physical properties of a typical Eu^{3+} complex

1.3.4 Comparison with Traditional Organic Dyes

Detecting particular analytes in an assay is critical to biomedical and imaging applications. Due to biological samples having high background fluorescence, it is difficult to get good sensitivity for traditional and simple fluorophores.[7] Luminescent lifetimes from conventional fluorescent dyes and sample interference lifetimes occur at a nanosecond scale. Scattering of the excitation light by the instrument optics, sample vessel, and matrix are additional problems with conventional fluorophores,

because of their generally small Stokes shifts. A final problem with conventional fluorophores is self-quenching because of substantial overlap between their excitation and emission spectra, meaning that multiply-labeled biomolecules fluoresce much less compared to the luminescence expected from the degree of labeling. With their large Stokes shifts, narrow emission bands, and no overlap between excitation and emission spectra, lanthanide chelates are not susceptible to this problem and so are ideal candidates for highly sensitive protein-detection assays.[7]

Lanthanide chelator complexes are of interest due to their differences from organic dyes such as the large stokes shift, sharp emission, and long luminescent lifetime in the microsecond to millisecond range.[6] In order to determine if lanthanide based materials are better for biological imaging type applications, it is important to compare the lanthanide materials to traditional organic dyes that are used. Traditional organic dyes have broad excitation and emission spectra as shown in Figure 5. This is due to the π-π^* transitions of the organic dyes[30]. This allows for a broader range of excitations to be used during studies, but these organic dyes have relatively short luminescence lifetimes in the nanosecond range. This may also interfere with the cell background fluorescence during measurements, as part of the emission and excitation spectra could fall in the blue to green range of normal cell background fluorescence. Lanthanide complexes, on the other hand, have lifetimes that are relatively much longer than the cell background fluorescence with reported lifetimes in the millisecond (msec) range. Thus, time-gated measurements can be used to study cells of interest with lanthanide based luminescent tracers (Figure 6). Time-resolved luminescence produces sensitive detection with a higher signal-to-noise ratio allowing for shorter and more accurate read times.
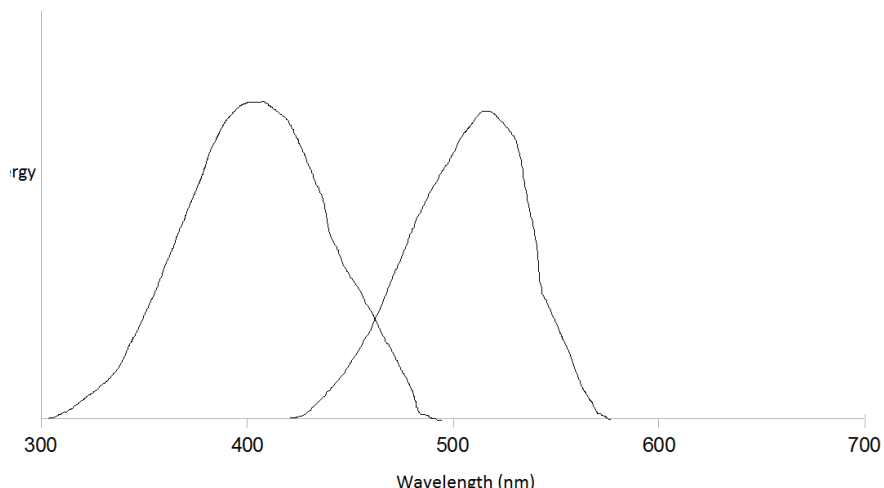
Figure 6. Absorption (left) and emission (right) spectra of a "typical" organic dye.

In this time-resolved luminescence, there is an initial burst of light that may cause not only the lanthanide complex, but also the cell components to emit radiation. Once the short-lived cell background completely decays, a delayed window is opened. This window then only has the luminescence of the lanthanide complex used. This allows for the measurement and observation of cells of interest with high accuracy. These advantages make lanthanide complexes ideal candidates for luminescent tracer studies as they have a much higher signal to noise ratio compared to those observed for traditional organic dyes.

1.4 INTRODUCTION TO RESEARCH

Given the advantages of lanthanide based luminescent materials, the De Silva group is interested in the synthesis and characterization of novel lanthanide (III) complexes that can be used for biological applications such as imaging and new immunoassay technologies with the ultimate goal of creating materials that can be used for *in vivo* real-time diagnostics. Many octacoordinated and nonacoordinated chelator complexes of Eu (III) and Tb (III) have been developed and characterized in the form $Ln(\beta$-diketonate)$_3$L where Ln= Eu (typically),Tb ;β-diketonate= thenoyltrifluoroacetone (tta),4,4,4-trifluoro-1-phenyl-1,3-butanedione(btfac),1,1,1,5,5,5-hexafluoro-2,4-pentanedionate(hfac),2, 4-pentanedione (acac), and dibenzoylmethane (DBM), 1-benzoylacetone (BA); and L= an N-donor ligand such as 2,4,6-tri(2-pyridyl)-1,3,5-triazine (tptz),1,10-phenanthroline(phen),and 4,7-dimethyl,1,10-phenanthroline

11

(dmphen).[31,32] These complexes have had coordination numbers of 8 or 9, and have had molecular geometries in the shape of capped antiprisms and square antiprisms. The complexes of europium have shown bright luminescent characteristics with impressive lifetimes in the microsecond time scale.

Fluorinated β-diketonates are commonly used due to the electronegativity of the F^- ion. All previously made complexes have been characterized by methods such as single crystal X-ray diffraction, UV-Vis, FT-IR, ^{1}H NMR, steady state and time-resolved fluorescence spectroscopy, elemental analysis, and luminescent quantum yield measurements. Previous high quantum yields have been suggestive of high ligand to metal transfer efficiencies, and "antenna" effects have also been suggested. Due to the intense characteristic 615 nm emission peak of Eu^{3+} luminescence, it has been a main focus of much work with β-diketonate systems to take advantage of the luminescence being outside the cell background fluorescence, while calculations involving Tb^{3+} systems with β-diketonates have been less promising. This is due to a higher energy gap triplet state needed by the "antenna" ligand to flow to the triplet state of the Tb^{3+} ion. One area less explored by the De Silva group has been the use of IR emitting or magnetic lanthanides with the β-diketonate systems to make chelators with other potential applications.

This research is focused on the development of novel lanthanide β-diketonate complexes and solgel materials based on the 4, 4, 4-trifluoro-1-phenyl-1,3-butanedione (btfa) and 4,7-dimethyl,1,10-phenanthroline (dmphen) ligand system for potential biological imaging applications. The chelator complexes will have the common formula, $Ln(\beta\text{-diketonate})_3$dmphen where $Ln= Eu^{3+}$, Er^{3+}, Tb^{3+}, Ho^{3+}, Tm^{3+}, and Yb^{3+}. Eu^{3+} and Tb^{3+} complexes emit visible light. Er^{3+}, Ho^{3+}, Tm^{3+}, and Yb^{3+} complexes have near-infrared emission characteristics, and Gd^{3+}, is magnetic. The new complexes and europium sol gel materials are characterized by UV-Vis spectroscopy, steady state, and time-resolved fluorescence spectroscopy, elemental analysis, and single crystal X-ray-diffraction technique. The luminescent lifetimes and quantum yields were calculated for the Eu^{3+} complex. Luminescence lifetime for the Ho^{3+} was also evaluated. The luminescence of the dmphen complexes, quantum yield, and lifetime decays were compared the aqua complexes, while new non-visible light emitting lanthanide β-diketonate

complexes were characterized to find new potential applications in biological imaging and beyond.

1.5 PROJECT DESIGN

1.5.1 Lanthanide Metal Targets

The lanthanide metals used in this work are Eu^{3+}, Er^{3+}, Gd^{3+}, Ho^{3+}, Tb^{3+}, Tm^{3+}, and Yb^{3+}. The lanthanides chosen range from visible to near infrared emitters. Gd^{3+} was chosen for its magnetic properties.
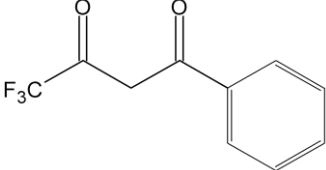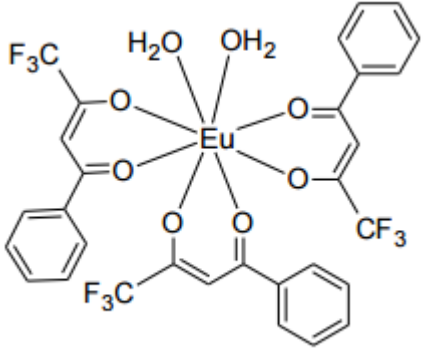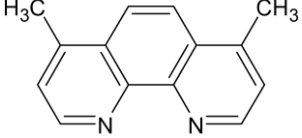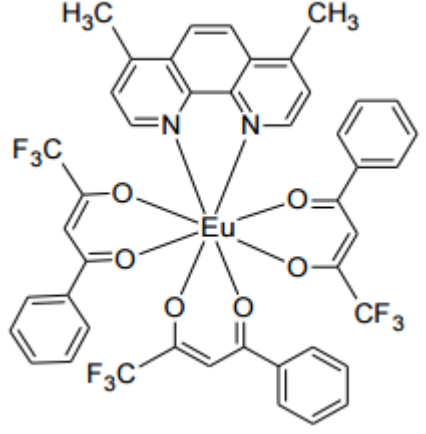
1.5.2 Chelator Ligands

The chelator ligands chosen to synthesize the new lanthanide β-diketonates are 4,4,4-trifluoro-1-phenyl-1,3-butanedione and 4,7-dimethyl,1,10-phenanthroline. Table 3 shows the structures of the ligands chosen for this project along with examples of the ligands bound to Eu^{3+}.

Table 3. Molecular structures and example lanthanide compounds of the β -diketonate and N-donor ligands used in this study.

Hbtfa

Dmphen

1.5.3 Synthesis of Lanthanide β-diketonates

The β-diketonate complexes in this research are easily made using the general reaction using lanthanide(III) chloride or nitrate salts (Scheme 1). The coordination of three β-diketonate ligands to the lanthanide center is controlled by the stoichiometry between the β-diketonate ligand and the lanthanide(III) chloride or nitrate.
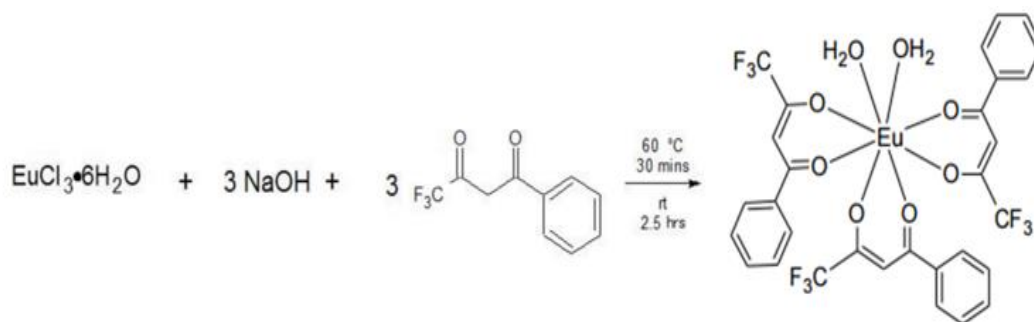
Scheme 1. General Reaction Scheme for the Synthesis of Eu(btfa)$_3$(H$_2$O)$_2$

1.5.4 Attachment of N-donor ligands

Once the Ln(β-diketonate)$_3$(H$_2$O)$_2$ complex has been synthesized, it could be used for luminescent studies and for the preparation of sol gel materials. However, there are some potential pitfalls in that the water could cause some quenching effects due to some of the vibrational states matching the states of the luminescent lanthanide. This interference would reduce the effectiveness of the lanthanide chosen and provide a luminescence that is much lower than expected. To avoid these potential quenching effects, another neutral ligand is coordinated to the Ln(β-diketonate)$_3$(H$_2$O)$_2$ to replace the water ligand. To maintain charge balance, this ligand would have to be neutral. This ligand would have nitrogen atoms with lone pairs of electrons to chelate the lanthanide complex. Like the H$_2$O ligand, this new ligand would be neutral, and is referred to as an N-donor ligand. A bidentate version of this type of ligand is used to replace the coordinated water in the lanthanide complex, and may also contribute to the overall luminescent quantum yield. Coordinated H$_2$O ligands are substituted by this N-donor ligand to form the Ln(β-diketonate)$_3$N-donor complex (Scheme 2)
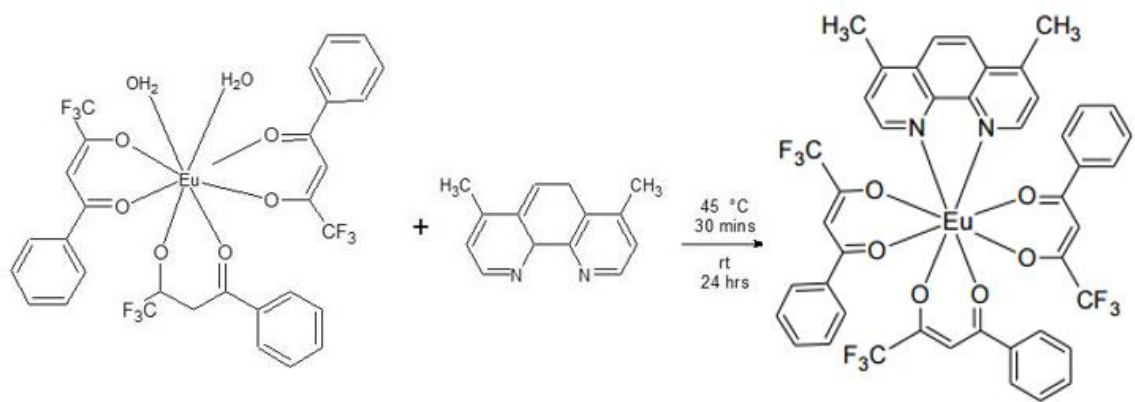
Scheme 2. General reaction scheme for the synthesis of a Ln(β-diketonate)₃(N-donor Ligand) complex

1.5.5 Silica Sol Gel Materials

Because many of the lanthanide based materials that were synthesized are not water dispersible, a way to make this happen is to encapsulate them with a material that is able to go into the aqueous environment.[33-39] This is a major problem of using β-diketonates for biological imaging. To address this issue, silica sol gels can be synthesized by doping the above synthesized chelators in a silica matrix that has been prepared using materials like tetraethylorthosilicate (TEOS) and a surfactant to start the process. A silica sol gel is made up of the luminescent chelator encapsulated in a silica matrix, with possible surface attachment for the targeting of specific cells (Figure 7).
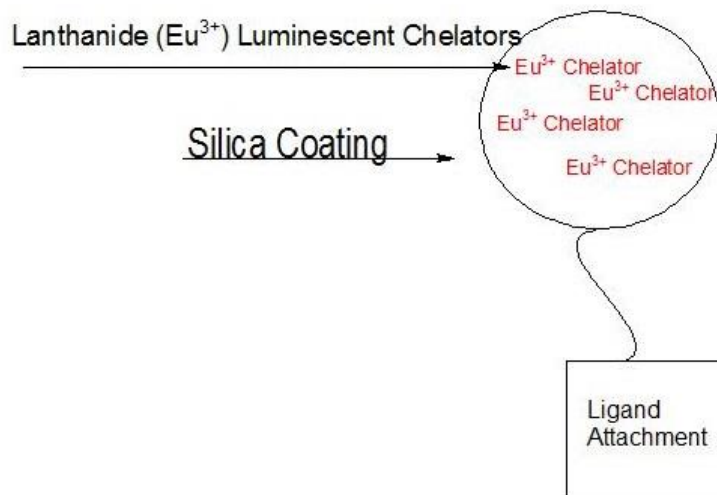
Figure 7. A representative chelator-doped silica solgel

Silica sol gels have a number of advantages over the pure lanthanide β-diketonate chelator complexes. The silica matrix is bio-compatible. This means that there is no inherent harm in using it as a means of encasing the chelator complex for use in *in vitro* or *in vivo* studies. Silica is also water dispersible, which means that the sol gels can be used for biological assays in an aqueous environment. They are less prone to leakage, and so the toxic materials inside do not escape into the biological environment. As mentioned previously, the surface of these nanoparticles can then be functionalized so that they are able to target cells of interest while still providing the benefits of the doped material. This part of the research focuses on the development of these sol gel materials, while characterizing them in comparison to their pure chelator counterparts.

SUMMARY

Three major areas of lanthanide based material research include applications in optical devices, bio immunoassays, and cellular imaging. Lanthanides are attractive candidates for biological imaging technologies due to their superior luminescent properties arising from electronic structure, tunability, lanthanide-centered luminescence, and longer luminescent lifetimes compared to traditional dyes. β-diketonate adducts of lanthanide materials are simple to synthesize, have lower costs, and provide a high enough triplet state to act as an effective antenna in lanthanide-centered luminescence. While these properties make them attractive, concerns about the stability and toxicity of the materials remain a challenge in their utilization. The use of doping and biocompatible sol gel materials has been proposed for delivery of chelators to targeted cells in immunoassays. Despite the challenges and due to the properties that make them excellent luminescent materials, the De Silva group has characterized many different lanthanide β-diketonates of the form Ln(β-diketonate)$_3$L where Ln= Eu (typically), Tb ;β-diketonate=(tta)(btfac),(hfac),(acac), and (DBM),(BA); and L=(tptz),1,10-phenanthroline(phen),and (dmphen). Due to the intense characteristic emission peak of Eu^{3+} luminescence, it has been a main focus of much work with β-diketonate systems, while calculations involving Tb^{3+} systems has been less promising.[32]

This research is focused on the development of novel lanthanide β-diketonate complexes and sol gel materials based primarily on btfa and dmphen ligands. Most complexes will have the common formula, Ln(β-diketonate)$_3$dmphen where Ln= Eu^{3+}, Er^{3+}, Tb^{3+}, Ho^{3+}, Tm^{3+}, and Yb^{3+}. Eu^{3+} and Tb^{3+} with some lanthanides chosen for non-visible light luminescence properties. The new complexes and sol gels are characterized by UV-Vis, steady state, and time-resolved luminescent spectroscopy, FTIR, elemental analysis, and single crystal X-ray-diffraction studies. The luminescent lifetimes and quantum yields were calculated. The luminescence measurements of dmphen complexes, quantum yield measurements, and lifetime decays of the Eu^{3+} were compared the aqua complexes, while new, non-visible light emitting lanthanide β-diketonate complexes were characterized to find new potential applications.

18

CHAPTER 2: METHODS, MATERIALS, AND CALCULATIONS

2.1 MATERIALS

2.1.1 Lanthanide Materials

The lanthanide metals used for the project were Eu^{3+}, Er^{3+}, Gd^{3+}, Ho^{3+}, Tb^{3+}, Tm^{3+}, and Yb^{3+}. The metal salts were purchased through Fisher Scientific and were the hydrated form of the lanthanide chloride or lanthanide nitrate. All lanthanide materials were dried and kept in a desiccator until used without further purification.

2.1.2 β-diketonate and N-donor Ligands

β-diketonate ligands chosen for this project was 4,4,4-trifluoro-1-phenyl-1,3-butanedione (Hbtfa). These ligands act as the primary antenna. The N-donor ligand used in this project was 4,7-dimethyl,1,10-phenanthroline (dmphen). Dmphen is the neutral ligand that will replace the H_2O in the Ln(β-diketonate)$_3$(H_2O)$_2$ complexes. All ligands were purchased from Sigma-Aldrich and kept in a desiccator until used without further purification.

2.1.3 Solvents and Other Materials

The solvents used in this project were used for various stages of synthesis, analysis and crystallization of the complexes. The solvents chosen were acetone, ethanol, chloroform, cyclohexane, methylene chloride, and nanopure H_2O with a resistivity of 18.2 MΩ from a Barnstead NANOpure Diamond system with 0.2 μm hollow fiber filter and argon purged for 1 hr prior to use. The solvents excluding the nanopure water were purchased from Fisher and used without further purification. Other reagents and materials used for this project were tetraethyl orthosilicate (TEOS), triton-x 100, NaOH which were purchased from Fisher and used without further purification.

2.2 METHODS

2.2.1 Synthesis

2.2.1.1 General Reactions and Synthesis

All of the lanthanide chelator complexes made follow a general two step reaction procedure. In this method, a 1:3 stoichiometric ratio of lanthanide (Ln= Eu^{3+}, Er^{3+}, Gd^{3+}, Ho^{3+}, Tb^{3+}, Tm^{3+}, and Yb^{3+}) to β-diketonate was maintained and then the resulting aqua complex was reacted with the N-donor ligand (dmphen) to form the final complex in a 1:1 stoichiometric ratio. Scheme 3 and Scheme 4 show the general reaction schemes of the Ln(β-diketonate)$_3$(H$_2$O)$_2$ chelators, and the Ln(β-diketonate)$_3$dmphen chelators using Eu^{3+} as the central lanthanide.
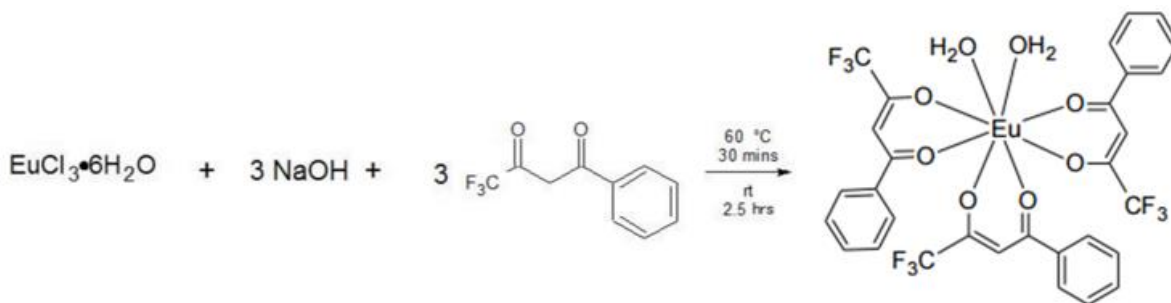
Scheme 3. General Reaction Scheme for the Synthesis of Ln(β-diketonate)$_3$(H$_2$O)$_2$
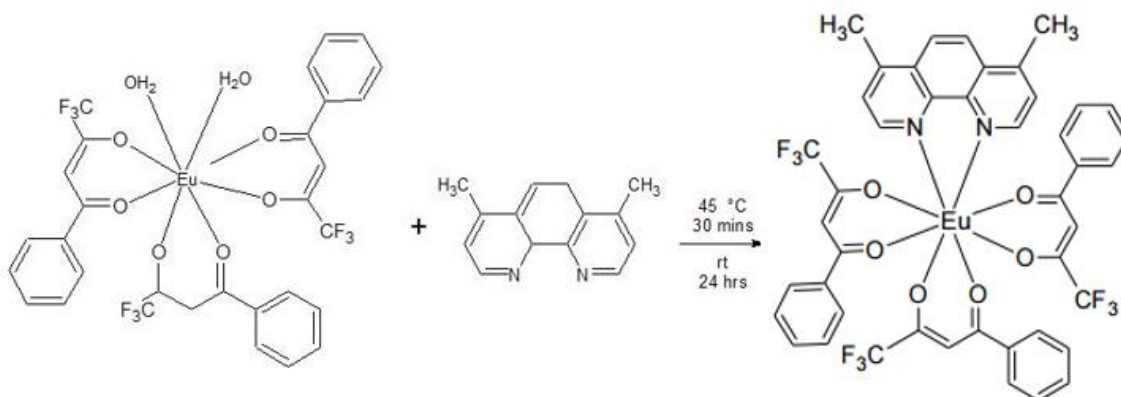
Scheme 4. General reaction scheme for the synthesis of Ln(β-diketonate)$_3$(N-donor Ligand) complex

20

2.2.1.2 Synthesis of Precursor Ln(β-diketonate)$_3$(H$_2$O)$_2$ Chelators

Hbtfa (648 mg,3 mmol) and NaOH (120 mg ,3 mmol) were added to Ar purged water (15 mL) and stirred until clear. This solution was added dropwise to a second solution of EuCl$_3$.6H$_2$O (366 mg,1 mmol) in Ar purged water (15mL). The reaction mixture was stirred at 60° C for 30 mins and then stirred at room temperature for an additional 2.5 hours. The precipitate was collected by vacuum filtration, washed with water (500 mL) and dried on the filter paper. An identical preparative and purification procedure was used for the synthesis of Er^{3+}, Gd^{3+}, Ho^{3+}, Tb^{3+}, Tm^{3+}, and Yb^{3+} complexes and is summarized in Table 4.

Table 4. Summary of the Synthesis of Ln(btfa)$_3$(H$_2$O)$_2$ Complexes

	Er	Ho	Gd	Tb	Tm	Yb
Ln (mg)	274	264	351	373	401	387
	(ErCl$_3$.H$_2$O)	(GdCl$_3$·H$_2$O)	(HoNO$_3$·H$_2$O)	(TbCl$_3$·6H$_2$O)	(TmCl$_3$·H$_2$O)	(YbCl$_3$·6H$_2$O)
Hbtfa (mg)	648	648	648	648	648	648
NaHO (mg)	120	120	120	120	120	120

2.2.1.3 Synthesis of Ln(β-diketonate)$_3$dmphen Chelators

Eu(btfa)$_3$(H$_2$O)$_2$ ((83.3 mg, 0.1 mmol) was dissolved in acetone (15 mL). To this solution, dmphen dissolved ((22.6 mg,0.1 mmol) in acetone (15 mL) was added. The reaction mixture was heated with stirring at 45° C for 30 mins and stirred at room temperature for 24 hrs. The reaction mixture was then recrystallized to obtain the product, Eu(btfa)$_3$dmphen. This procedure was repeated for the synthesis of Er^{3+}, Gd^{3+}, Ho^{3+}, Tb^{3+}, Tm^{3+}, and Yb^{3+} complexes and is summarized in Table 5.

Table 5. Summary of Ln(btfa)$_3$(H$_2$O)$_2$ to Ln(btfa)$_3$dmphen Synthesis

	Er	Ho	Gd	Tb	Tm	Yb
Ln (mg)	84.8	84.6	83.9	84	85	85.4
dmphen (mg)	22.6	22.6	22.6	22.6	22.6	22.6

2.2.1.4 Synthesis of Eu(btfa)$_3$dmphen Solgel Materials

After making the Ln(β-diketonate)$_3$dmphen chelators, the synthesis of silica based sol gel materials was attempted using four different processes. Solgel materials were made using acid catalysis, microemulsion, Stöber process, and the synthesis of a mixed lanthanide material sol gel.

2.2.1.4.1 Synthesis of Eu(btfa)$_3$(H$_2$O)$_2$ and Eu(btfa)$_3$dmphen Silica Sol Gels by Acid Catalysis

Eu(btfa)$_3$(H$_2$O)$_2$ or Eu(btfa)$_3$dmphen (100 mg) was added to a solution of nanopure H$_2$O (1.6 mL) and TEOS (4.5 mL) with stirring. Glacial acetic acid (9 mL) was added to the reaction mixture and shaken for 30s. The reaction mixture was reacted at room temperature for 30 mins with stirring. The sol gel material was centrifuged and washed with EtOH three times. The particles were air dried and dispersed in nanopure H$_2$O with sonication for 10 mins.

2.2.1.4.2 Synthesis of Eu(btfa)$_3$(H$_2$O)$_2$ and Eu(btfa)$_3$dmphen Sol Gels by Microemulsion

Eu(btfa)$_3$(H$_2$O)$_2$ or Eu(btfa)$_3$dmphen (30 mg) were dissolved in hexanol (2.30 mL). To this mixture, nanopure H$_2$O (1.10 mL), cyclohexane (9.31 mL), TEOS (200 μL), and triton x-100 (2.25 mL) were added and stirred until clear. To this mixture, a second solution of cyclohexane (9.31 mL), 30% NH$_4$OH (200 μL), and triton x-100 (2.25 mL) were added and the reaction mixture was stirred at room temperature for 24 hrs. The reaction mixture was stirred at room temperature for 24 hours. The silica

particles were precipitated using acetone (70 mL). The particles were centrifuged at 4750 g for 10 mins and then washed with EtOH three times. The particles were air dried and dispersed in nanopure H_2O with sonication for 10 mins. Two other versions followed the same procedure with the Eu chelator being first dissolved in MeOH or EtOH (1.5 mL).

2.2.1.4.3 Synthesis of Eu(btfa)$_3$(H_2O)$_2$ and Eu(btfa)$_3$dmphen Silica Sol Gels by Stöber Process[40-42]

Sol gel materials were synthesized using a modified Stöber process. Eu(btfa)$_3$(H_2O)$_2$ or Eu(btfa)$_3$dmphen (30 mg) was added to a solution of TEOS (2 mL) in EtOH (5 mL). To this solution, EtOH (25 mL) was added. 30% NH_4OH (1.5 mL) was added with stirring. The reaction mixture was stirred at room temperature for 24hr, and then sonicated for 10mins. The nanoparticles were centrifuged at 4750 g for 10 mins and then washed with EtOH with the procedure being repeated three times. The particles were air dried and dispersed in nanopure water with sonication.

Using procedures similar to the above synthesis, an in-situ reaction to make Eu(btfa)$_3$(H_2O)$_2$ or Eu(btfa)$_3$dmphen chelator complexes that would then be incorporated into a silica nanomaterial were performed. In place of the Eu(btfa)$_3$(H_2O)$_2$ (30 mg), btfa(23.2 mg) and EuCl$_3$.6H_2O (13.2 mg) were added to the TEOS (2 mL) in EtOH (5 mL). In place of Eu(btfa)$_3$dmphen (30 mg), btfa (19 mg), EuCl$_3$.6H_2O (10.7 mg), and dmphen (6.6 mg) were added to the TEOS (2 mL) in EtOH (5 mL).

2.2.2 Instrument Methods and Procedures

Methods used to characterize both chelators and sol gel materials include ICP-OES, UV-vis spectroscopy, Fluorescence spectroscopy, and carbon analysis. Sol gels were also characterized using STEM microscopy. Other characterization methods such as single crystal X-ray diffraction and lifetime studies were performed using other collaborators.

2.2.2.1 Varian VistaPro ICP-OES

2.2.2.1.1 Preparation of Lanthanide Standards and QC

A 100 mL stock of 100 ppm Eu^{3+}, Er^{3+}, Gd^{3+}, Ho^{3+}, Tb^{3+}, Tm^{3+}, and Yb^{3+} was prepared by weighing each lanthanide chloride or nitrate (Table 6) and diluting to volume with 10% aqua regia.

Table 6. Preparation Table for Mixed Lanthanide 100 ppm Stock Solutions

Element	FW (nitrate or chloride) (g)	Element Weight (g)	Amount added to Flask (g)
Eu	258.94	151.964	0.01700 g
Er	273.64	167.259	0.01636 g
Gd	263.61	157.25	0.016764 g
Ho	350.95	164.93033	0.0212787
Tb	344.94	158.92535	0.021705
Tm	354.95	168.93422	0.021011
Yb	387.48	173.045	0.022392

From the 100 ppm stock solution, standards of 2 ppm, 4 ppm, 6 ppm, 8 ppm, and 10 ppm were prepared according to Table 6 and diluted to volume with 10% aqua regia. In addition, a 10% aqua regia blank and 5 ppm QC were prepared according to Table 7 and diluted to volume with 10% aqua regia.

Table 7. Preparation Table for Mixed Lanthanide Standards and QC

Solution Type Prepared	ppm solution prepared	mL of 100 ppm Stock	mL 10% aqua regia
Blank	0.0	0	100
Standard 1	2.0	2	98
Standard 2	4.0	4	96
Standard 3	6.0	6	94
Standard 4	8.0	8	92
Standard 5	10.0	10	90
QC	5.0	5	95

2.2.3 Carbon Analysis

Carbon analysis of the lanthanide samples was performed using the LECO SC632 carbon/sulfur analyzer. 30 mg +/- 5 mg of sample was burned for analysis and compared to the calculated values.

2.2.4. Fluorescence spectroscopy

Fluorescence Spectroscopy of the Eu(btfa)$_3$dmphen chelator and chelator doped solgel material were performed using a Perkin Elmer LS-55 fluorescence spectrometer with a 5 nm slit width using quartz cuvettes and a scan speed of 200 nm/min. The excitation wavelength was 350 nm unless otherwise noted in data and results. Eu(btfa)$_3$dmphen chelator samples were prepared by making a 1×10^{-6} M concentration of sample in methylene chloride. Solgel material samples were prepared by dispersing 2 mg of solgel in 2 mL water. The solgels were sonicated at room temperature for 10 minutes prior to the spectra being collected.

2.2.5. UV-Vis Spectroscopy

UV-vis Spectroscopy of the Ln(btfa)$_3$dmphen chelators and chelator doped solgel materials were performed using Agilent 8453 UV-visible spectrometer. All samples were read from 200 nm to 700 nm using quartz cuvettes. Ln(btfa)$_3$dmphen chelator samples were prepared by making a 1×10^{-6} M concentration of sample in methylene chloride. Solgel material samples were prepared by dispersing 2 mg of solgel in 2 mL water. The solgels were sonicated at room temperature for 10 minutes prior to the spectra being collected. UV-visible spectra were recorded on an Agilent 8453 UV-visible spectrometer. Samples were prepared by dispersing 2 mg of the nanoparticle samples in 2 mL of solvent (water or dichloromethane). Nanoparticle samples were sonicated for 10 minutes at room temperature before collecting the spectra. The absorption spectra were collected from 200 nm to 700 nm using quartz cuvettes. Photoluminescence spectra were collected using a Perkin Elmer LS-55 fluorescence spectrometer with a 5 nm slit width using quartz cuvettes. The excitation wavelength was 350 nm. The emission spectra were collected from 200 nm to 700 nm using a scan speed of 200 nm/minute.

2.3. CALCULATIONS

2.3.1 Luminescent Quantum Yield Measurements

Luminescent quantum yield is the number of photons emitted vs the photons that are absorbed by a fluorescing material and in this case is a representation of efficiency. Luminescent quantum yield measurements were performed using a standard dye.

$$\varphi_S = \varphi_R (Abs_R/Abs_S)(A_S/A_R)(n_S^2/n_R^2)$$

where Abs, A and n are the absorbance at λ max, integrated area of the emission band of interest, and the refractive index of the solvent, respectively. Subscripts R and S refer to the reference and the sample, respectively

3.1. SYNTHESIS

All of the Ln(btfa)$_3$dmphen synthesized are in powder form with color that is darker than the corresponding Ln(btfa)$_3$(H$_2$O)$_2$ ranging from the off-yellow Eu(btfa)$_3$dmphen, Gd(btfa)$_3$dmphen, Tb(btfa)$_3$dmphen, Tm(btfa)$_3$dmphen, and Yb(btfa)$_3$dmphen, to the pink color of Er(btfa)$_3$dmphen and Ho(btfa)$_3$dmphen. All Ln(btfa)$_3$dmphen chelators are soluble in methylene chloride and chloroform and produce an amber solution when dissolved. When exposed to UV light, Eu(btfa)$_3$dmphen emits vivid red light characteristic of Eu^{3+} (Figure 8). Ho(btfa)$_3$dmphen produces a slight red emission and Tb(btfa)$_3$dmphen dimly glows the characteristic green light of Tb^{3+}.
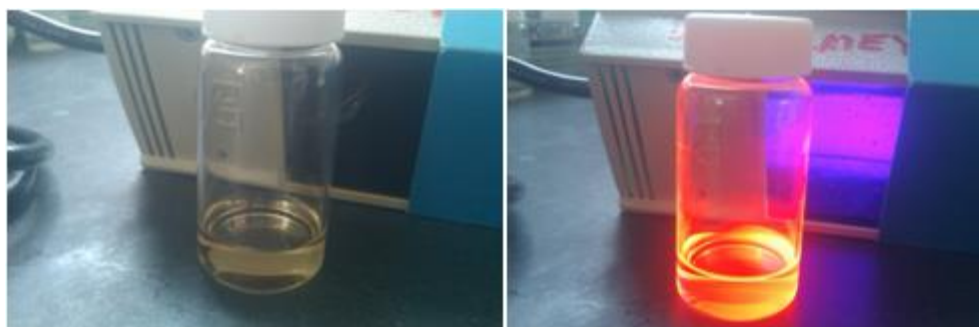
Figure 8. Eu(btfa)$_3$dmphen under visible and UV light conditions

3.2 X-RAY CRYSTAL STRUCTURES

3.2.1 General

Ln(btfa)$_3$dmphen chelators were slowly crystallized from a saturated acetone solution at room temperature for two to three weeks to produce pale yellow crystals. Crystals suitable for single crystal X-ray diffraction were collected and analyzed. The resolved crystal properties and parameters are summarized in Table 8-11.

Table 8. Resolved Ln(btfa)$_3$dmphen crystal characteristics

Ln	Eu	Er	Gd
Empirical formula	C44H30F9N2O6Eu	C44H30F9N2O6Er	C44 H30 F9 N2 O6 Gd
F.W	1005.66	1011.96	1001.95
Temp (K)	100(2)	293(2)	293(2)
Wavelength (A)	1.54178	0.71073	0.71073
Crystal system, space group	Monoclinic, C2/c	Monoclinic, C2/c	Monoclinic,C2/c
Unit cell dimensions	a=36.6051(10)A, alpha 90° b=10.8940(3)A,beta 111.9080(10)° c=22.261(6)A,gamma 90°	a=36.422(7)A alpha 90° b=11.045(2)A,beta 112.61(3)° c=22.290(5)Agamma a 90°	a=36.950(7)Aalpha 90° b=10.975(2)A,beta 112.51(3)° c=22.469(5)Agamma 90°
Volume (A^3)	8236.2(4)	8278(3)	8417(3)
Z	8	8	8
Calculated density (Mg/m^3)	1.622	1.624	1.581
Absorption coefficient (mm^-1)	11.717	2.113	1.660

F(000)	4000	4016	3984
Crystal size (mm)	0.45 x 0.29 x 0.20	0.24 x 0.12 x 0.12	0.23 x 0.08 x 0.08
Theta range for data collection°	2.60 to 66.97	2.69 to 25.05	2.92 to 25.05
Limiting indices	-43<=h<=43,-10<=k<=12,-26<=l<=26	-43<=h<=43, -12<=k<=13, -26<=l<=26	-44<=h<=40,-12<=k<=13,-26<=l<=26
Reflections collected / unique	44146/ 7190 [R(int)=0.0590]	34703 / 7331 [R(int)=0.0351]	24023 /7413 [R(int)=0.0571]
Completeness to theta =25.05	98.1 %	99.8 %	99.5 %
Absorption correction	Numerical	None	None
Max. and min. transmission	0.1985 and 0.0770	0.7856 and 0.6310	0.8787 and0.7014
Refinement method	Full-matrix least-squares on F^2	Full-matrix least-squares on F^2	Full-matrix least-squares on F^2
Data / restraints / parameters	7190 / 0 / 561	7331 / 0 / 559	7413 / 0 / 559
Goodness-of-fit on F^2	1.031	1.109	1.096
Final R indices [I>2sigma(I)]	R1 = 0.0401, wR2 = 0.1015	R1 = 0.0474, wR2 =0.1212	R1 =0.0598, wR2=0.1652

R indices (all data)	R1 = 0.0432, wR2 = 0.1039	R1 = 0.0545, wR2 = 0.1278	R1 = 0.0709, wR2=0.1804
Largest diff. peak and hole	1.255 and -0.802 e.A^-3	2.183 and -1.001 e.A^-3	2.045 and -1.157 e.A^-3

Table 9. Resolved Ln(btfa)$_3$dmphen crystal characteristics

Ln	Ho	Tb	Tm	Yb
Empirical formula	C44H30 F9 N2 O6Ho	C44H30F9N2O6Tb	C44H30F9N2O6Tm	C44H30F9N2O6Yb
F.W	1018.63	1003.62	1013.63	1026.74
Temp (K)	293(2)	293(2)	293(2)	293(2)
Wavelength (A)	0.71073	0.71073	0.71073	0.71073
Crystal system, space group	Monoclinic, C2/c	Monoclinic, C2/c	Monoclinic, C2/c	Monoclinic,C2/c
Unit cell dimensions	a=36.473(7)A,alpha 90° b=11.029(2)A,beta 112.55(3)° c=22.303(5)A,gamma 90°	a =36.814(7)A,alpha 90° b=10.992(2)A,beta 112.58(3)° c=22.438(5)A,gamma 90°	a=36.377(7)A, alpha 90° b=11.077(2)A, beta, 112.81(3)° c=22.309(5)A,gamma 90 °	a=36.245(7)A,alpha 90° b=11.091(2)A,beta 112.86(3)° c=22.239(4)A,gamma 90 °
Volume (A^3)	8286(3)	8384(3)	8286(3)	8238(3)
Z	8	8	8	8
Calculated	1.633	1.590	1.625	1.656

density (Mg/m^3)				
Absorption coefficient (mm^-1)	2.001	1.772	2.227	2.362
F(000)	4032	3992	4024	4056
Crystal size (mm)	0.22 x 0.12 x 0.09	0.33 x 0.08 x 0.05	0.31 x 0.07 x 0.05	0.26 x 0.11 x 0.10
Theta range for data collection°	2.93 to 25.05	3.33 to 25.05	2.70 to 25.05	2.60 to25.05
Limiting indices	-43<=h<=40,-13<=k<=11,-26<=l<=26	-43<=h<=43,-11<=k<=13, -26<=l<=26	-43<=h<=43, -13<=k<=13, -26<=l<=26	-41<=h<=43, -13<=k<=13, -26<=l<=24
Reflections collected/unique	31508 / 7328 [R(int)=0.0347]	34616 / 7387 [R(int)=0.0529]	34657 / 7344 [R(int)=0.0599]	31690 / 7294 [R(int)=0.0499]
Completeness to theta=25.05	99.7 %	99.6 %	99.9 %	99.7 %
Absorption correction	None	None	None	None
Max. and min. transmission	0.8405 and 0.6673	0.9166 and 0.5925	0.8968 and 0.5452	0.7981 and 0.5787
Refinement method	Full-matrix least-squares on F^2	Full-matrix least-squares on F^2	Full-matrix least-squares on F^2	Full-matrix least-squares on F^2
Data / restraints /parameters	7328 / 0 /559	7387 / 0 /560	7344 / 0 / 559	7294 / 0 /559
Goodness-of-fit	1.144	1.014	1.127	1.111

on F^2

Final R indices [I>2sigma(I)]	R1 = 0.0396, wR2 = 0.0975	R1 = 0.0536, wR2 = 0.1408	R1 = 0.0576, wR2 =0.1476	R1 =0.0423, wR2=0.0977
R indices (all data)	R1 = 0.0493, wR2 = 0.1072	R1 = 0.0637, wR2 = 0.1508	R1 = 0.0713, wR2 =0.1594	R1 = 0.0555, wR2=0.1090
Largest diff. peak and hole	2.106 and -0.950 e.A^-3	1.704 and -1.145 e.A^-3	2.255 and -1.286 e.A^-3	2.361 and -0.968 e.A^-3

Table 10. Bond Lengths for Ln(btfa)₃dmphen chelators

Ln	Eu	Er	Gd	Ho	Tb	Tm	Yb
Bond Length (A)	Eu-O(1) 2.384(2)	Er-O(1) 2.335(3)	Gd-O(1) 2.371(4)	Ho-O(1) 2.340(3)	Tb-O(1) 2.363(4)	Tm-O(1) 2.320(5)	Yb-O(1) 2.310(3)
	Eu-O(2) 2.365(3)	Er-O(2) 2.297(4)	Gd-O(2) 2.356(5)	Ho-O(2) 2.300(3)	Tb-O(2) 2.335(4)	Tm-O(2) 2.275(5)	Yb-O(2) 2.261(4)
	Eu-O(3) 2.344(3)	Er-O(3) 2.300(4)	Gd-O(3) 2.337(5)	Ho-O(3) 2.306(3)	Tb-O(3) 2.322(4)	Tm-O(3) 2.293(5)	Yb-O(3) 2.277(4)
	Eu-O(4) 2.388(3)	Er-O(4) 2.325(4)	Gd-O(4) 2.373(5)	Ho-O(4) 2.333(3)	Tb-O(4) 2.352(4)	Tm-O(4) 2.312(5)	Yb-O(4) 2.295(4)
	Eu-O(5) 2.348(3)	Er-O(5) 2.281(4)	Gd-O(5) 2.326(5)	Ho-O(5) 2.294(3)	Tb-O(5) 2.312(4)	Tm-O(5) 2.265(5)	Yb-O(5) 2.255(4)
	Eu-O(6) 2.344(3)	Er-O(6) 2.300(4)	Gd-O(6) 2.347(5)	Ho-O(6) 2.307(4)	Tb-O(6) 2.329(5)	Tm-O(6) 2.290(6)	Yb-O(6) 2.286(4)
	Eu-N(1) 2.560(4)	Er-N(1) 2.531(4)	Gd-N(1) 2.578(5)	Ho-N(1) 2.544(4)	Tb-N(1) 2.574(5)	Tm-N(1) 2.517(6)	Yb-N(1) 2.510(4)
	Eu-N(2) 2.607(3)	Er-N(2) 2.483(5)	Gd-N(2) 2.538(6)	Ho-N(2) 2.501(4)	Tb-N(2) 2.519(5)	Tm-N(2) 2.475(6)	Yb-N(2) 2.474(5)

Table 11. Bond Angles for the Ln(btfa)$_3$dmphen chelators

Eu	Er	Gd	Ho	Tb	Tm	Yb
O(3)-Eu-O(6) 80.64(10)	O(3)-Er-O(6) 78.91(15)	O(3)-Gd-O(6) 80.14(18)	O(3)-Ho-O(6) 79.17(13)	O(3)-Tb-O(6) 79.88(16)	O(6)-Tm-O(3) 78.35(19)	O(3)-Yb-O(6) 78.49(14)
O(3)-Eu-O(5) 140.75(10)	O(5)-Er-O(3) 142.01(14)	O(5)-Gd-O(3) 140.81(18)	O(5)-Ho-O(3) 141.89(12)	O(5)-Tb-O(3) 140.97(15)	O(5)-Tm-O(3) 142.3(2)	O(5)-Yb-O(3) 143.03(13)
O(6)-Eu-O(5) 73.40(12)	O(5)-Er-O(6) 74.59(17)	O(5)-Gd-O(6) 73.53(19)	O(5)-Ho-O(6) 74.45(14)	O(5)-Tb-O(6) 73.84(17)	O(5)-Tm-O(6) 75.2(2)	O(5)-Yb-O(6) 75.23(15)
O(3)-Eu-O(2) 78.28(9)	O(2)-Er-O(3) 77.84(14)	O(3)-Gd-O(2) 77.47(18)	O(2)-Ho-O(3) 77.82(12)	O(3)-Tb-O(2) 77.39(15)	O(2)-Tm-O(3) 77.80(19)	O(2)-Yb-O(3) 77.81(14)
O(6)-Eu-O(2) 75.55(10)	O(2)-Er-O(6) 74.23(15)	O(6)-Gd-O(2) 75.03(19)	O(2)-Ho-O(6) 74.51(13)	O(6)-Tb-O(2) 75.25(16)	O(6)-Tm-O(2) 73.8(2)	O(2)-Yb-O(6) 73.63(14)
O(5)-Eu-O(2) 121.31(11)	O(5)-Er-O(2) 119.20(16)	O(5)-Gd-O(2) 121.31(19)	O(5)-Ho-O(2) 119.64(14)	O(5)-Tb-O(2) 121.46(16)	O(5)-Tm-O(2) 118.9(2)	O(5)-Yb-O(2) 118.03(15)
O(3)-Eu-O(1) 141.38(9)	O(3)-Er-O(1) 140.98(13)	O(3)-Gd-O(1) 140.85(16)	O(3)-Ho-O(1) 140.98(11)	O(3)-Tb-O(1) 140.74(14)	O(3)-Tm-O(1) 140.84(17)	O(3)-Yb-O(1) 140.62(12)
O(6)-Eu-O(1) 112.89(10)	O(6)-Er-O(1) 115.46(14)	O(6)-Gd-O(1) 113.34(17)	O(6)-Ho-O(1) 115.03(12)	O(6)-Tb-O(1) 113.98(15)	O(6)-Tm-O(1) 116.13(19)	O(6)-Yb-O(1) 116.30(14)
O(5)-Eu-O(1) 76.97(10)	O(5)-Er-O(1) 76.04(14)	O(5)-Gd-O(1) 77.33(17)	O(5)-Ho-O(1) 76.17(12)	O(5)-Tb-O(1) 77.36(15)	O(5)-Tm-O(1) 75.97(19)	O(5)-Yb-O(1) 75.36(13)
O(2)-Eu-O(1) 71.20(9)	O(2)-Er-O(1) 72.47(13)	O(2)-Gd-O(1) 71.63(16)	O(3)-Ho-O(4) 72.70(12)	O(2)-Tb-O(1) 71.77(14)	O(2)-Tm-O(1) 72.69(17)	O(2)-Yb-O(1) 72.77(13)
O(3)-Eu-O(4) 71.62(9)	O(3)-Er-O(4) 73.05(13)	O(3)-Gd-O(4) 72.12(17)	O(6)-Ho-O(4) 79.60(13)	O(3)-Tb-O(4) 72.08(15)	O(3)-Tm-O(4) 73.29(18)	O(3)-Yb-O(4) 73.63(13)

O(6)-Eu-O(4) 79.25(10)	O(6)-Er-O(4) 79.71(15)	O(6)-Gd-O(4) 80.25(19)	O(5)-Ho-O(4) 75.83(12)	O(6)-Tb-O(4) 79.63(16)	O(6)-Tm-O(4) 79.7(2)	O(6)-Yb-O(4) 79.92(15)
O(5)-Eu-O(4) 74.95(10)	O(5)-Er-O(4) 75.81(14)	O(5)-Gd-O(4) 75.18(18)	O(2)-Ho-O(4) 143.76(12)	O(5)-Tb-O(4) 75.16(15)	O(5)-Tm-O(4) 75.82(19)	O(5)-Yb-O(4) 76.52(14)
O(2)-Eu-O(4) 143.32(10)	O(2)-Er-O(4) 143.99(14)	O(2)-Gd-O(4) 143.50(17)	O(4)-Ho-O(1) 143.07(12)	O(2)-Tb-O(4) 143.25(15)	O(2)-Tm-O(4) 144.02(18)	O(2)-Yb-O(4) 144.24(13)
O(1)-Eu-O(4) 144.41(9)	O(4)-Er-O(1) 142.58(14)	O(1)-Gd-O(4) 144.09(17)	O(3)-Ho-N(1) 76.76(12)	O(4)-Tb-O(1) 144.19(16)	O(4)-Tm-O(1) 142.31(18)	O(4)-Yb-O(1) 142.02(13)
O(3)-Eu-N(1) 109.49(10)	O(3)-Er-N(1) 76.70(14)	O(3)-Gd-N(1) 77.68(17)	O(6)-Ho-N(1) 147.57(13)	O(3)-Tb-N(1) 77.32(15)	O(3)-Tm-N(1) 76.07(18)	O(3)-Yb-N(1) 75.63(13)
O(6)-Eu-N(1) 145.82(11)	O(6)-Er-N(1) 147.25(14)	O(6)-Gd-N(1) 149.04(18)	O(2)-Ho-O(1) 72.23(11)	O(6)-Tb-N(1) 148.52(16)	O(6)-Tm-N(1) 146.19(18)	O(6)-Yb-N(1) 146.06(14)
O(5)-Eu-N(1) 79.58(12)	O(5)-Er-N(1) 136.67(16)	O(5)-Gd-N(1) 135.95(18)	O(5)-Ho-N(1) 136.52(13)	O(5)-Tb-N(1) 136.22(16)	O(5)-Tm-N(1) 137.2(2)	O(5)-Yb-N(1) 137.21(15)
O(2)-Eu-N(1) 137.73(10)	O(2)-Er-N(1) 79.51(14)	O(2)-Gd-N(1) 79.26(17)	O(2)-Ho-N(1) 79.40(12)	O(2)-Tb-N(1) 78.79(15)	O(2)-Tm-N(1) 79.45(19)	O(2)-Yb-N(1) 79.70(14)
O(1)-Eu-N(1) 80.08(9)	O(1)-Er-N(1) 73.51(13)	O(1)-Gd-N(1) 73.49(16)	O(1)-Ho-N(1) 73.67(12)	O(1)-Tb-N(1) 73.39(15)	O(1)-Tm-N(1) 73.73(18)	O(1)-Yb-N(1) 73.86(13)
O(4)-Eu-N(1) 73.75(10)	O(4)-Er-N(1) 113.06(14)	O(4)-Gd-N(1) 112.57(17)	O(4)-Ho-N(1) 112.96(12)	O(4)-Tb-N(1) 113.01(15)	O(4)-Tm-N(1) 113.02(19)	O(4)-Yb-N(1) 112.75(14)
O(3)-Eu-N(2) 78.48(9)	O(3)-Er-N(2) 110.97(15)	O(3)-Gd-N(2) 110.43(18)	O(3)-Ho-N(2) 110.70(12)	O(3)-Tb-N(2) 110.46(16)	O(3)-Tm-N(2) 111.15(19)	O(3)-Yb-N(2) 111.17(15)
O(6)-Eu-N(2) 150.03(10)	O(6)-Er-N(2) 146.55(15)	O(6)-Gd-N(2) 146.28(19)	O(6)-Ho-N(2) 146.50(13)	O(6)-Tb-N(2) 146.45(16)	O(6)-Tm-N(2) 147.0(2)	O(6)-Yb-N(2) 146.91(14)
O(5)-Eu-N(2) 134.94(11)	O(5)-Er-N(2) 79.71(17)	O(5)-Gd-N(2) 79.57(19)	O(5)-Ho-N(2) 79.73(14)	O(5)-Tb-N(2) 79.57(17)	O(5)-Tm-N(2) 79.7(2)	O(5)-Yb-N(2) 79.88(16)

O(2)-Eu-N(2)	O(2)-Er-N(2)	O(2)-Gd-N(2)	O(2)-Ho-N(2)	O(2)-Tb-N(2)	O(2)-Tm-N(2)	O(2)-Yb-N(2)
79.32(9)	138.26(14)	137.73(17)	138.06(12)	137.40(15)	138.25(19)	138.50(13)
O(1)-Eu-N(2)	O(1)-Er-N(2)	O(1)-Gd-N(2)	O(1)-Ho-N(2)	O(1)-Tb-N(2)	O(1)-Tm-N(2)	O(1)-Yb-N(2)
73.15(9)	77.70(14)	79.27(17)	78.13(12)	78.83(15)	77.20(18)	77.07(14)
O(4)-Eu-N(2)	O(4)-Er-N(2)	O(4)-Gd-N(2)	O(4)-Ho-N(2)	O(4)-Tb-N(2)	O(4)-Tm-N(2)	O(4)-Yb-N(2)
113.64(9)	73.44(15)	73.43(17)	73.60(13)	74.01(16)	73.6(2)	73.28(14)
N(2)-Eu-N(1)	N(2)-Er-N(1)	N(2)-Gd-N(1)	N(2)-Ho-N(1)	N(2)-Tb-N(1)	N(2)-Tm-N(1)	N(2)-Yb-N(1)
62.76(10)	64.28(14)	63.22(17)	64.02(12)	63.44(15)	64.63(19)	64.82(14)

All resolved Ln(btfa)₃dmphen crystals have a general empirical formula of $C_{44}\,H_{30}\,F_9\,N_2\,O_6$ Ln and belong to the centrosymetric monoclinc space group, C2/c. The molecular structures reveal an octa-coordinated central Ln atom with six coordinating oxygens and two nitrogens from the btfa and dmphen ligands, respectively. The coordination polyhedrons can all be described as distorted square anti-prisms (Figures 9 &10).
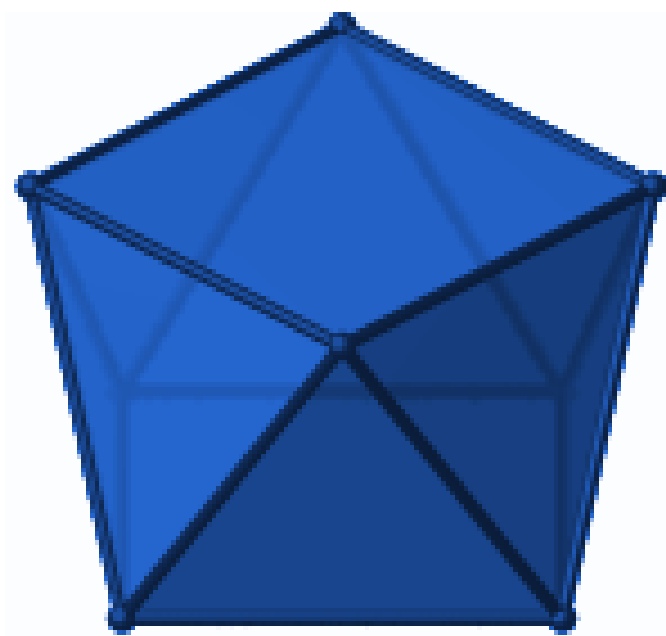
Figure 9. Square antiprisim polyhedron
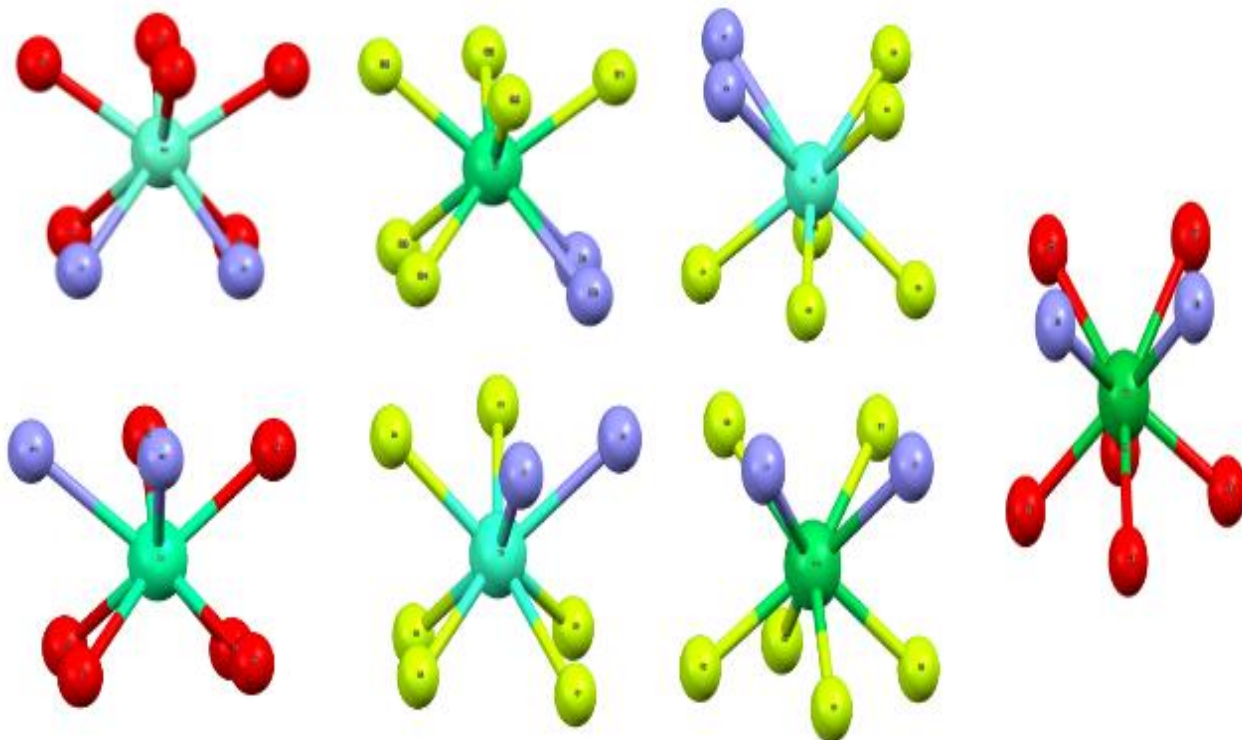
Figure 10. Coordination spheres of Ln(btfa)₃dmphen complexes

Calculations show that the atoms of the dmphen ligand are nearly coplanar for each resolved crystal. Ln-N bond distances (2.474-2.607 A, average 2.529 A) Ln-O bond distances (2.255-2.388 A, average 2.320 A) are within the average bond distances observed for similar lanthanide complexes (Table 9 and 10).

Volumes of the crystals ranged from 8236.2 to 8417 A³ with an average volume of 8303.6 A³. The calculated density of the crystals ranges from 1.581 to 1.656 mg/m³ with an average density of 1.618 mg/m³. The crystal sizes range from 0.22 x 0.12 x 0.09 to 0.45 x 0.29 x 0.20 nm with an average size of 0.29 x 0.12 x 0.099 nm. Unit cell dimensions ranged from a= 36.245-36.950 A (average 36.555) alpha = 90 deg, b = 10.8940- 11.091 (average 11.015) A beta=111.9080-112.86 (average 112.55) deg. , and c = 22.239- 22.469 (average 22.330) A gamma = 90 deg. All crystal sizes show a length that is roughly twice the amount of the width or depth. The width and depth tend to be equal, though there is a trend of the width being bigger than the depth if there is a distortion.

The calculated unit cells (Figure 11) have eight Ln(btfa)$_3$ dmphen molecules arranged in a pattern of 2-4-2. π-π stacking of the molecules occurs at the dmphen ligand with the 4,7 methyl groups being reflected and overlaid from the connecting dmphen while being offset stacked. The unit cell is also held by the hydrogen bonding between from the fluorinated methyl group of one btfa to the benzene ring of another btfa ligand.
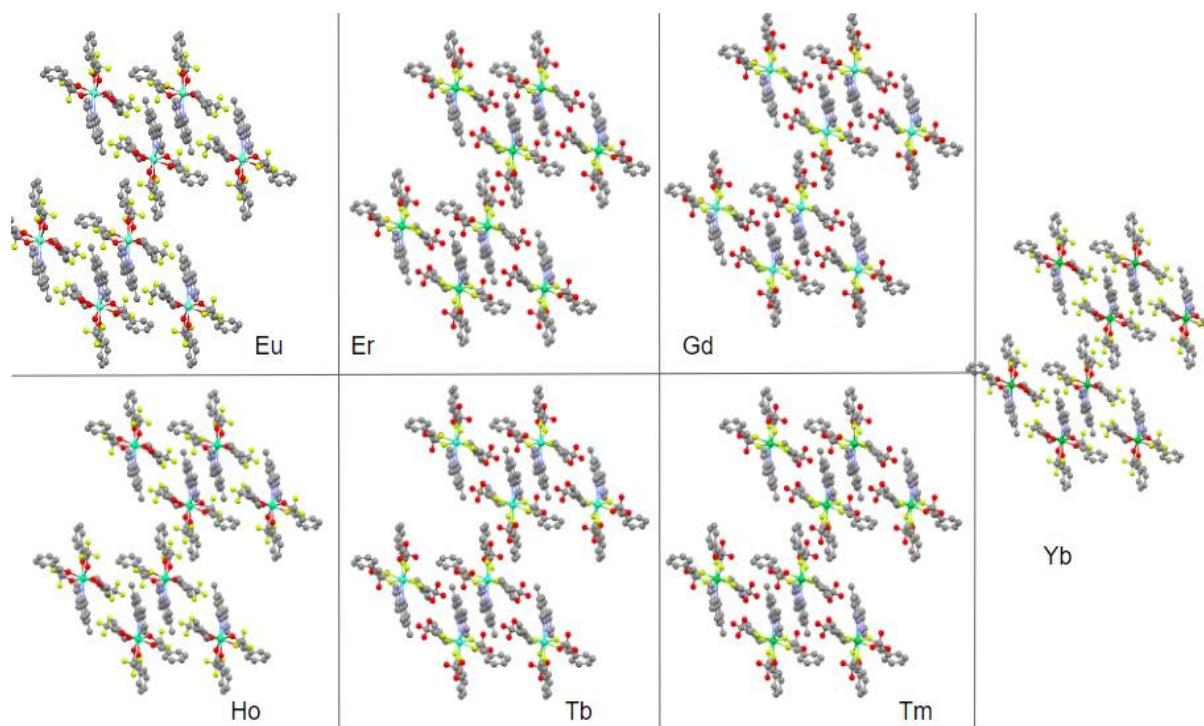
Figure 11. Calculated Unit Cells for the Ln(btfa)$_3$dmphen complexes

3.2.2 Eu(btfa)$_3$ dmphen

Eu(btfa)$_3$ dmphen crystalizes in the centrosymetric monoclinc space group C2/c. The molecular structure reveals a central europium atom situated with six coordinating oxygens and two nitrogens from the btfa and dmphen ligands, respectively. The coordination polyhedron (Figure 12) can be best described by a distorted square antiprism.
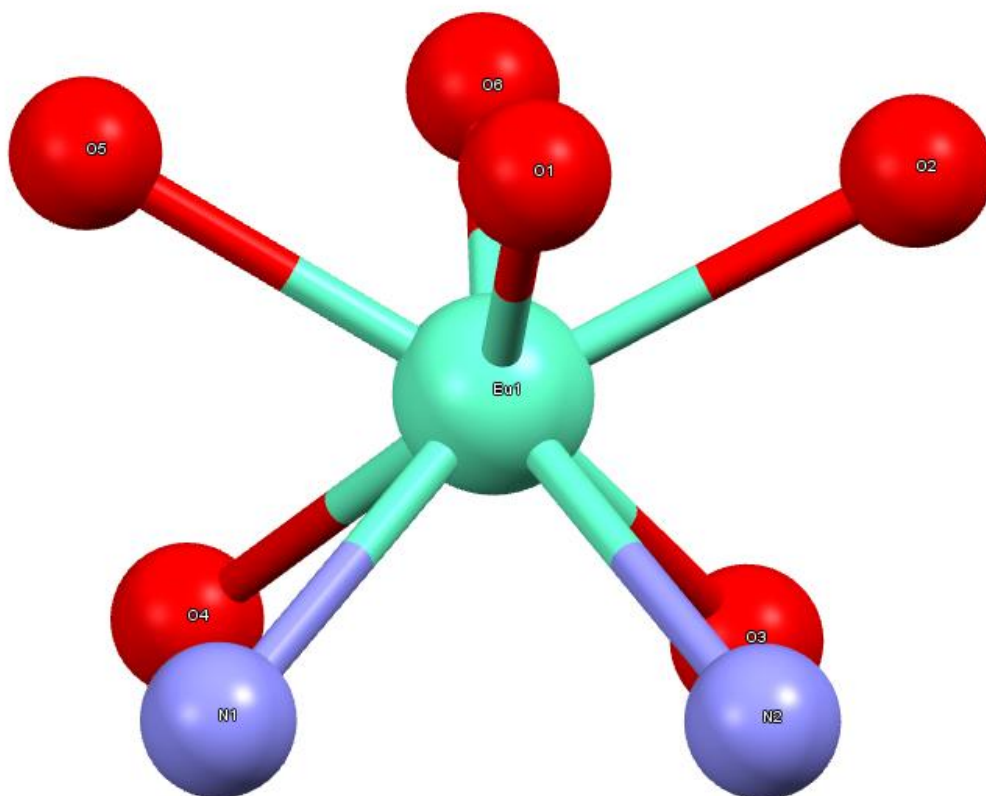
Figure 12. Coordination polyhedron of Eu(btfa)₃dmphen complex

The Eu-N bond distances (2.560-2.607, average 2.584) and Eu-O bond distances (2.344(3)-2.388, average 2.362) are in agreement with previously reported europium b-diketonate complexes. N atoms of dmphen ligand is nearly co-planar.

The crystal was 0.45 x 0.29 x 0.20 mm in size with a volume of 8236.2 A^3, and density of 1.622 mg/m^3 making it the largest crystal resolved while being the 4th densest with a least volume. Unit cell dimensions are a = 36.6051(10) A   alpha = 90 deg, b = 10.8940(3) A   beta = 111.9080(10) deg., and c = 22.2613(6) A   gamma = 90 deg. The crystal had an absorption coefficient of 11.717 which is 5 times larger than any of the other resolved crystals suggesting that there is a great amount of absorption from the crystal which is then transferred to the central Eu atoms for luminescence. The crystal exhibits the characteristic red luminescence of Eu^{3+} luminescence when exposed to UV light. The calculated unit cell

(Figure 13) has eight Eu(btfa)$_3$dmphen molecules. The molecules are arranged in a pattern of 2-4-2. π-π stacking of the molecules occurs at the dmphen ligand with the 4,7 methyl groups being reflected and overlaid from the connecting dmphen while being offset stacked. The unit cell is also held by F-H type hydrogen bonding from the fluorinated methyl group of one btfa to the benzene ring of another btfa ligand.

Figure 13. Calculated Unit Cell of Eu(btfa)$_3$dmphen complex

3.2.3 Er(btfa)₃ dmphen

Er(btfa)₃ dmphen crystalizes in the centroscymetric monoclinc space group C2/c. The molecular structure (Figure 14) reveals a central erbium atom situated with six coordinating oxygens and two nitrogens from the btfa and dmphen ligands respectively. The coordination polyhedron (Figure 15) can be described as a distorted square antiprism.

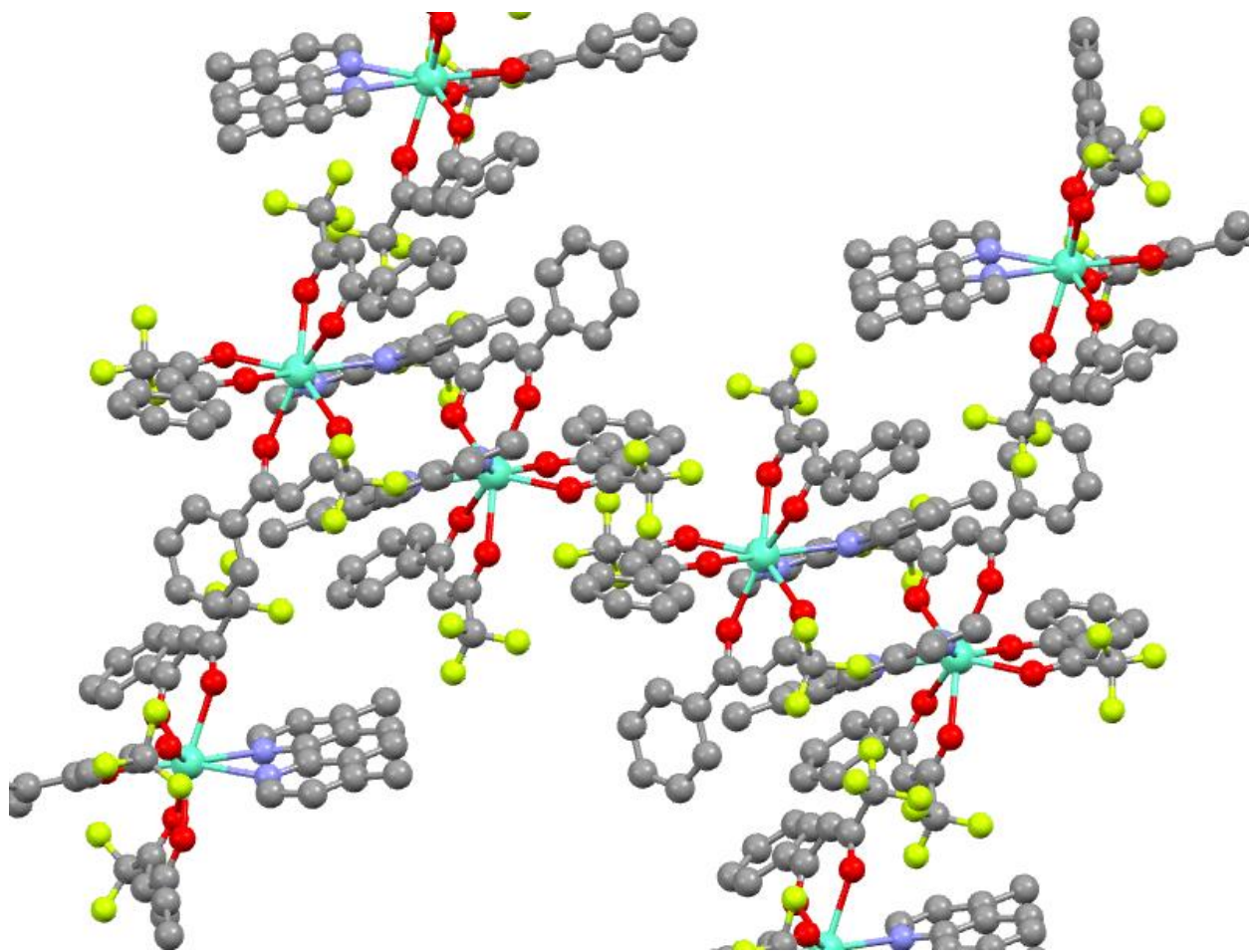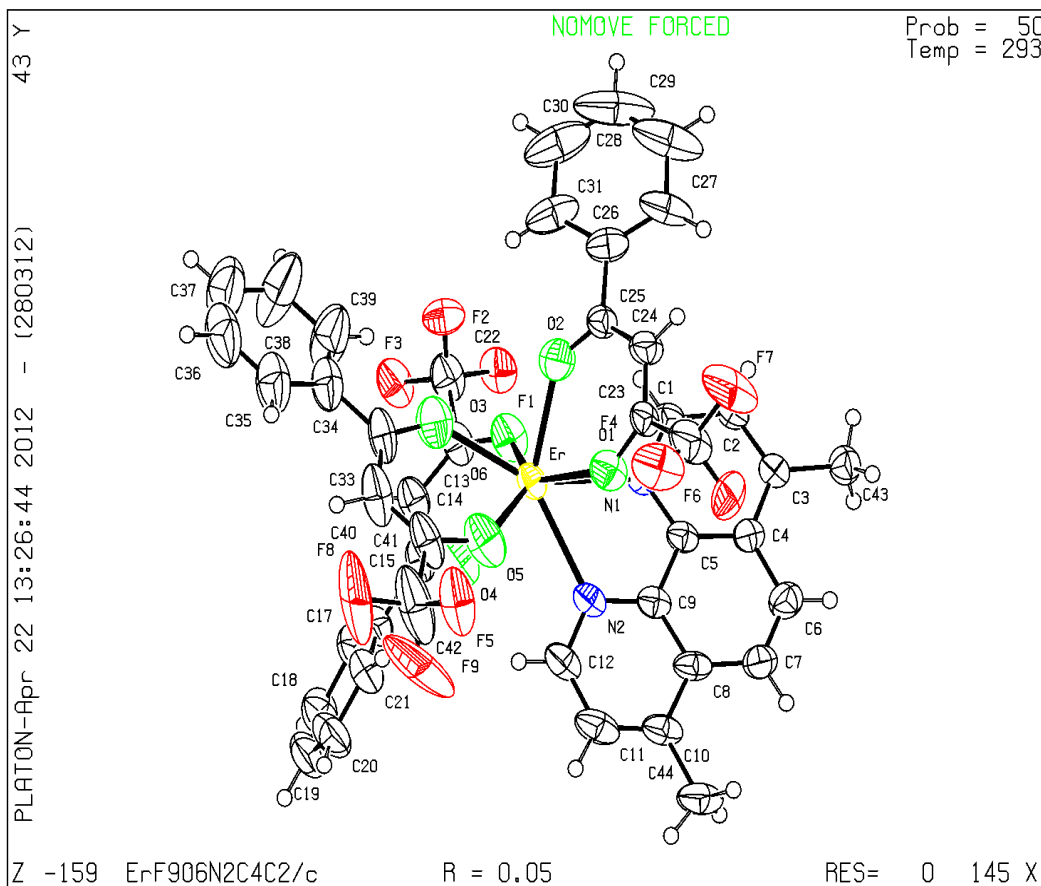**Figure 14.** Structure of Er(btfa)₃dmphen.
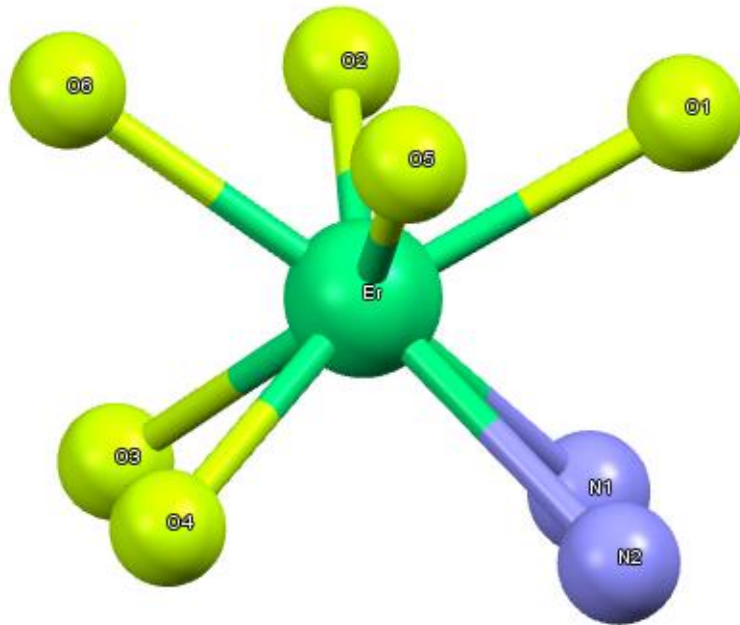
Figure 15. Coordination polyhedron of Er(btfa)₃dmphen complex

Calculations show that the atoms of the dmphen ligand are nearly coplanar.

The Er-N bond distances (2.483-2.531(average 2.507) and Er-O bond distances (2.281-2.355, average 2.306). The crystal was   0.24 x 0.12 x 0.12 mm in size with a volume of 8278, and density of 1.624 mg/m^3 making it the third smallest crystal resolved while having the third least volume and fourth densest. Unit cell dimensions were a = 36.422(10) A   alpha = 90 deg, b = 11.045(3) A   beta = 112.61 deg., and c = 22.290 A   gamma = 90 deg. The crystal had an absorption coefficient of 2.113 which is the fourth largest. The crystal shows no visible luminescence under UV light. The calculated unit cell (Figure 16) has eight Er(btfa)₃dmphen molecules. The molecules are arranged in a pattern of 2-4-2. π-π stacking of the molecules occurs at the dmphen ligand with the 4,7 methyl groups being reflected and overlaid from the connecting dmphen while being offset stacked. The unit cell is also held by F-H hydrogen bonding from the fluorinated methyl group of one btfa to the benzene ring of another btfa ligand.

Figure 16. Calculated Unit Cell of Er(btfa)$_3$dmphen

3.2.4 Gd(btfa)$_3$ dmphen

Gd(btfa)$_3$ dmphen crystalizes in the centroscymetric monoclinc space group C2/c. The molecular structure (Figure 17) reveals a central gadolinium atom situated with six coordinating oxygens and two nitrogens from the btfa and dmphen ligands respectively. The coordination polyhedron (Figure 18) can be described as a distorted square antiprism.

Figure 17. Structure of Gd(btfa)₃dmphen.
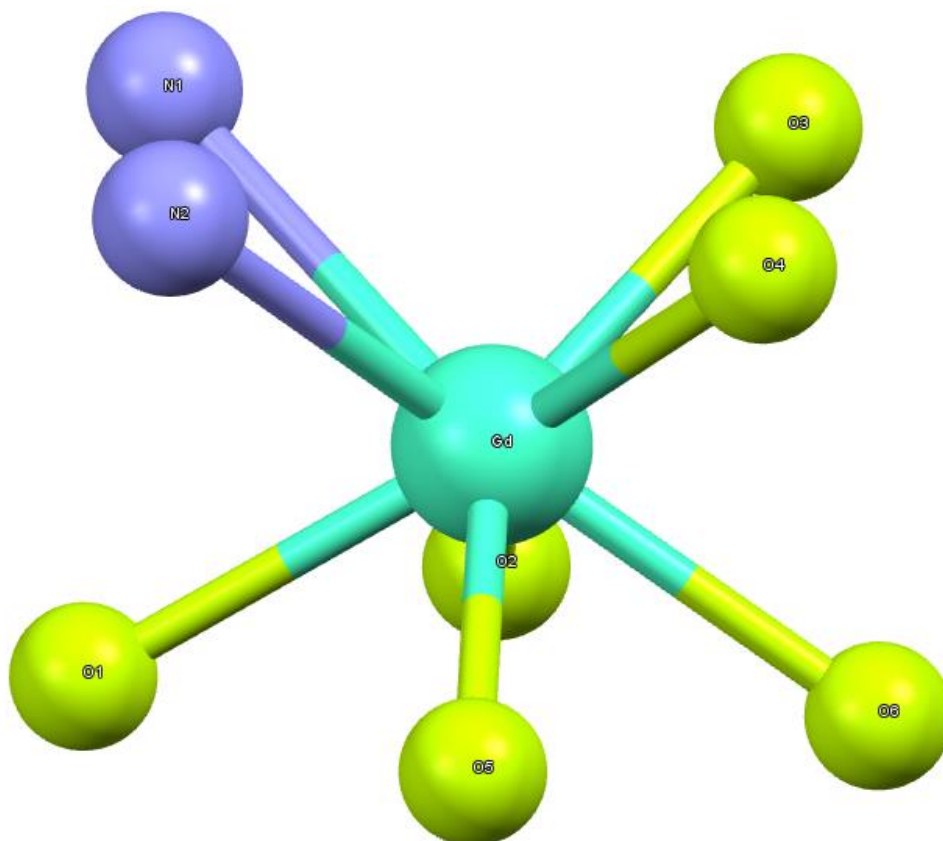
Figure 18. Coordination polyhedron of Gd(btfa)₃dmphen complex

Calculations show that the atoms of the dmphen ligand are nearly coplanar. The Gd-N bond distances (2.538-2.578, average 2.558) and Gd-O bond distances (2.326-2.373, average 2.351) The crystal was 0.23 x 0.08 x 0.08 mm in size with a volume of 8417 A^3, and density of 1.581 mg/m^3 making it the third smallest crystal resolved while having the smallest density and largest volume. Unit cell dimensions were a = 36.950 A   alpha = 90 deg,b = 10.975(3) A   beta = 112.5 deg. , and c = 22.469(6) A   gamma = 90 deg. The crystal has the smallest absorption coefficient at 1.660 and displays no visible luminescence under UV light. The calculated unit cell (Figure 19) has eight Gd(btfa)₃ dmphen molecules. The molecules arranged in a pattern of 2-4-2. π-π stacking of the molecules occurs at the dmphen ligand with the 4,7 methyl groups being reflected and overlaid from the connecting dmphen while being offset

stacked. The unit cell is also held by F-H bonding from the fluorinated methyl group of one btfa to the benzene ring of another btfa ligand.


Figure 19. Calculated Unit Cell of Gd(btfa)$_3$dmphen

3.2.5 Ho(btfa)$_3$ dmphen

Ho(btfa)$_3$ dmphen crystallizes in the centroscymetric monoclinc space group C2/c. The molecular structure (Figure 20) reveals a central holmium atom situated with six coordinating oxygens and two nitrogens from the btfa and dmphen ligands respectively. The coordination polyhedron (Figure 21) can be described as a distorted square antiprism.
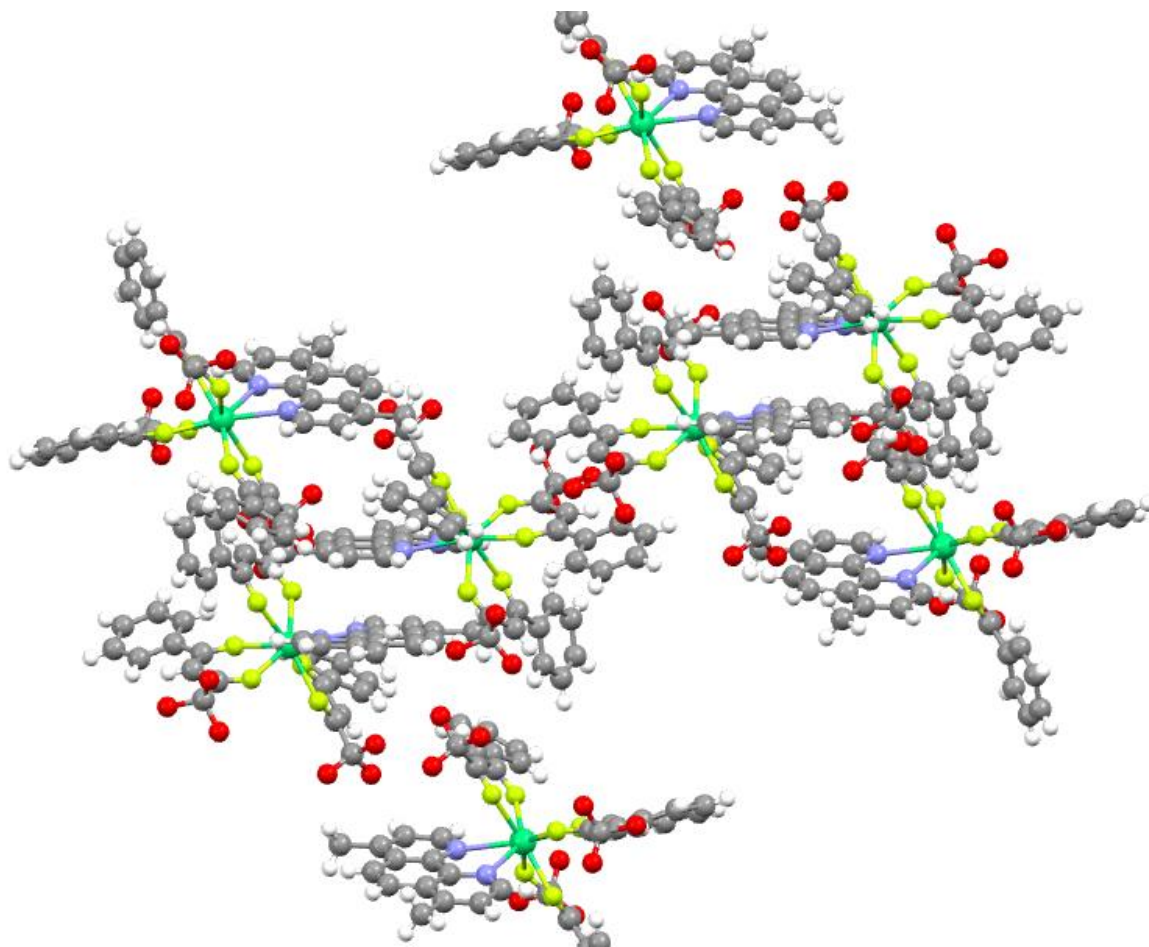
47
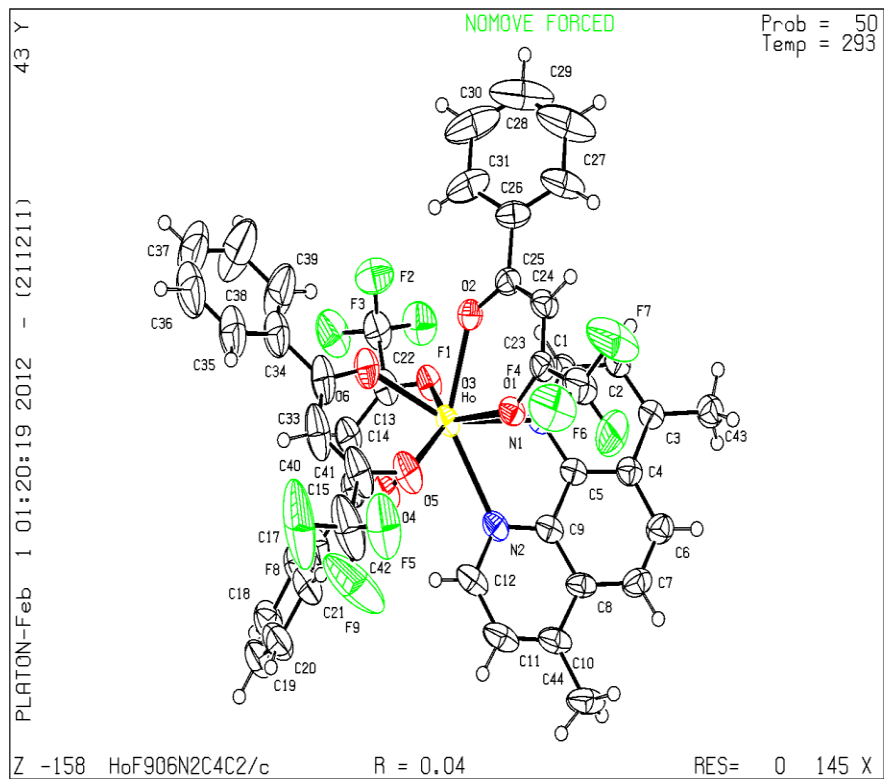
Figure 20. Structure of Ho(btfa)₃dmphen.
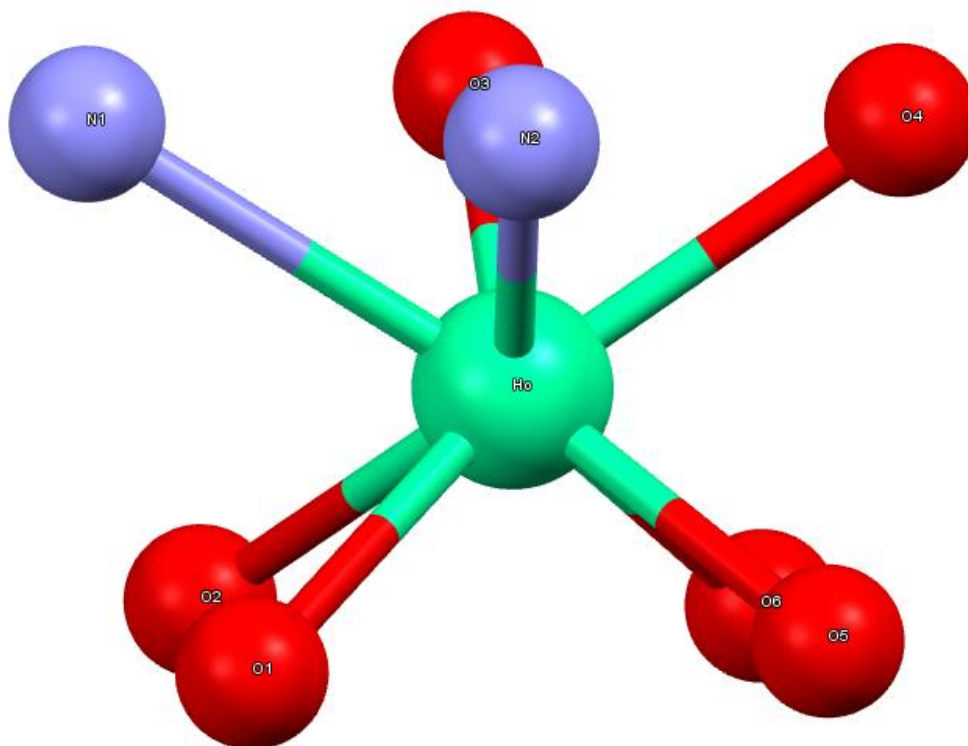
Figure 21. Coordination polyhedron of Ho(btfa)3dmphen complexes

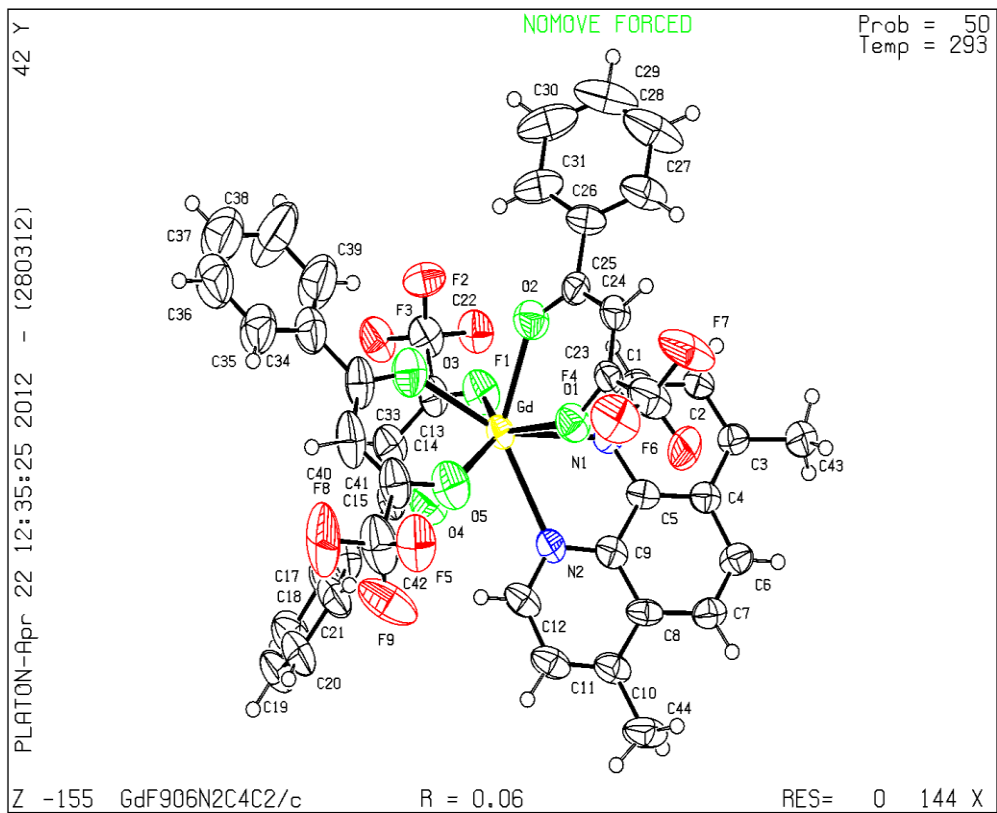Calculations show that the atoms of the dmphen ligand are nearly coplanar.

The Ho-N bond distances (2.501(4)-2.544(3), average 2.523) and Eu-O bond distances (2.294(3)-2.340, average 2.313) are within the average bond distances observed for similar complexes. The crystal was 0.22 x 0.12 x 0.09 mm in size with a volume of 8286 A^3, and density of 1.633 mg/m^3 making it the smallest crystal resolved while having the second largest density and tied with Tm(btfa)$_3$dmphen for the fourth smallest volume. Unit cell dimensions were a = 36.473(10) A   alpha = 90 deg, b = 11.029 A beta = 112.55 deg., and c = 22.303(6) A   gamma = 90 deg. The crystal has the fourth largest absorption coefficient at 2.001 and displays a faint red luminescence under UV light. The calculated unit cell (Figure 22) has eight Ho(btfa)$_3$ dmphen molecules. The molecules arranged in a pattern of 2-4-2. π-π stacking of the molecules occurs at the dmphen ligand with the 4,7 methyl groups

being reflected and overlaid from the connecting dmphen while being offset stacked. The unit cell is also held by F-H bonding from the fluorinated methyl group of one btfa to the benzene ring of another btfa ligand.

Figure 22. Calculated Unit Cell of Ho(btfa)₃dmphen

3.2.6 Tb(btfa)₃ dmphen

Tb(btfa)₃ dmphen crystalizes in the centroscymetric monoclinc space group C2/c. The molecular structure (Figure 23) reveals a central terbium atom situated with six coordinating oxygens and two nitrogens from the btfa and dmphen ligands respectively. The coordination polyhedron (Figure 24) can be described as a distorted square antiprism.
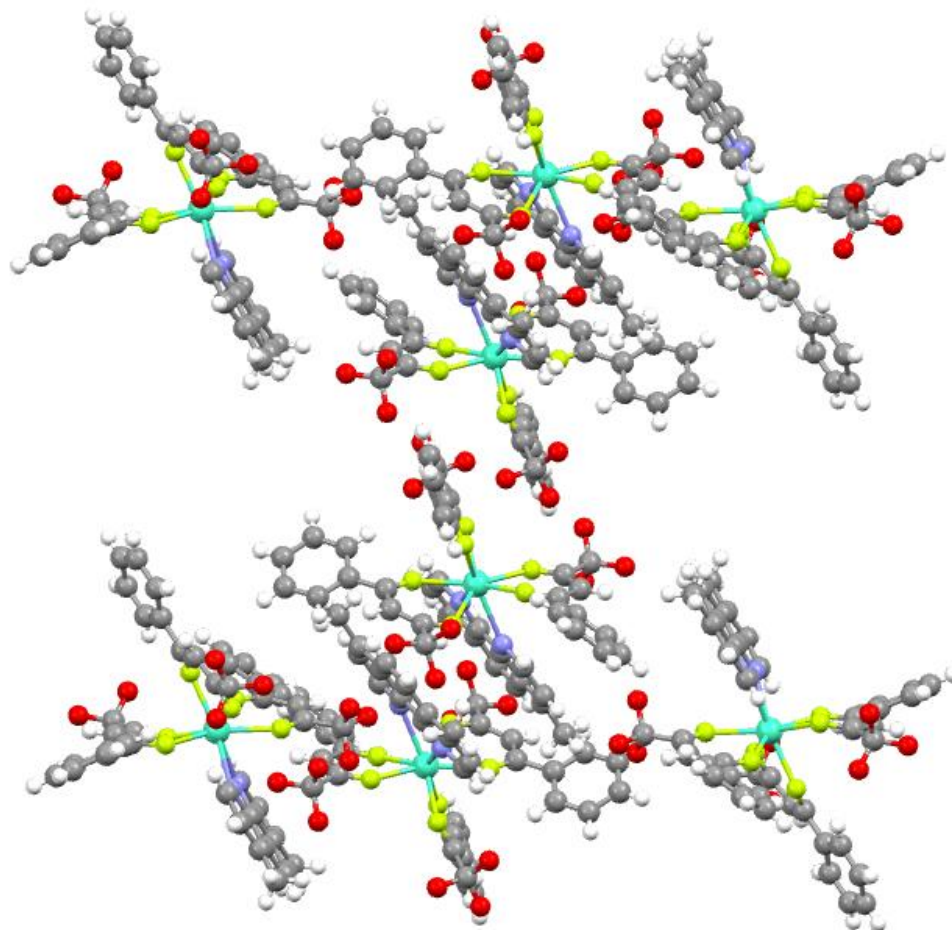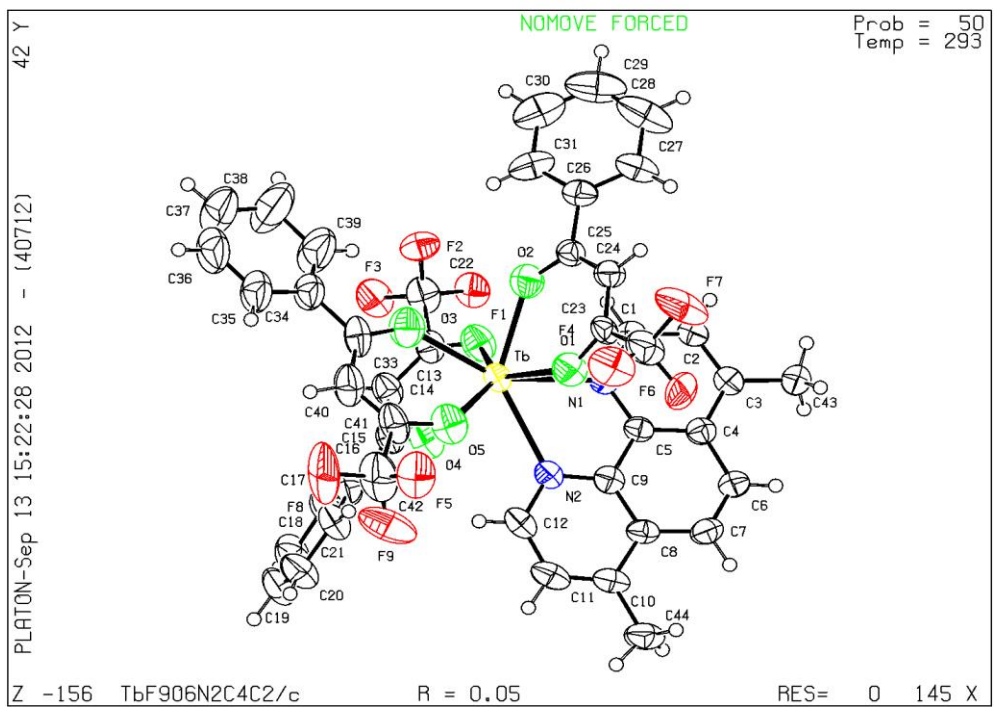
Figure 23. Structure of Tb(btfa)$_3$dmphen.
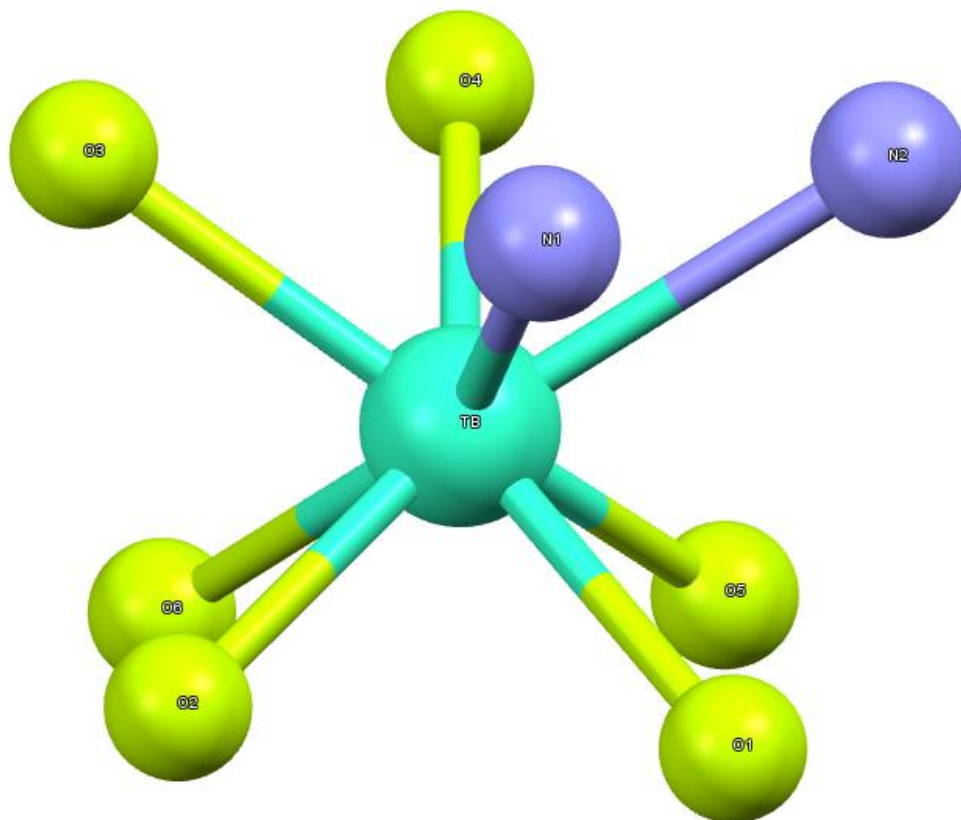
Figure 24. Coordination polyhedron of Tb(btfa)₃dmphen complex

Calculations show that the atoms of the dmphen ligand are nearly coplanar.

The Tb-N bond distances (2.519(4)-2.574(3), average 2.547) and Tb-O bond distances (2.312(3)-2.363, average 2.336) are within the values observed for similar complexes. The crystal was   0.33 x 0.08 x 0.05 mm in size with a volume of 8384 A^3, and density of 1.590 mg/m³ making it the second largest crystal resolved while being the second least dense and second highest volume. Unit cell dimensions were a = 36.814(10) A   alpha = 90 deg, b = 10.992(3) A   beta = 112.58 deg., and c = 22.438 A   gamma = 90 deg.   The crystal has the second smallest absorption coefficient at 1.772 and just barely glows the characteristic green luminescence of Tb³⁺. The calculated unit cell (Figure 25) has eight Tb(btfa)₃dmphen molecules. The molecules are arranged in a pattern of 2-4-2. π-π stacking of the molecules occurs at the dmphen ligand with the 4,7 methyl groups being reflected and overlaid from the connecting dmphen

while being offset stacked. The unit cell is also held by F-H bonding from the fluorinated methyl group of one btfa to the benzene ring of another btfa ligand.


Figure 25. Calculated Unit Cell of Tb(btfa)$_3$dmphen

3.2.7 Tm(btfa)$_3$ dmphen

Tm(btfa)$_3$ dmphen crystalizes in the centroscymetric monoclinc space group C2/c. The molecular structure (Figure 26) reveals a central thulim atom situated with six coordinating oxygens and two nitrogens from the btfa and dmphen ligands, respectively. The coordination polyhedron (Figure 27) can be described as a distorted square antiprism.
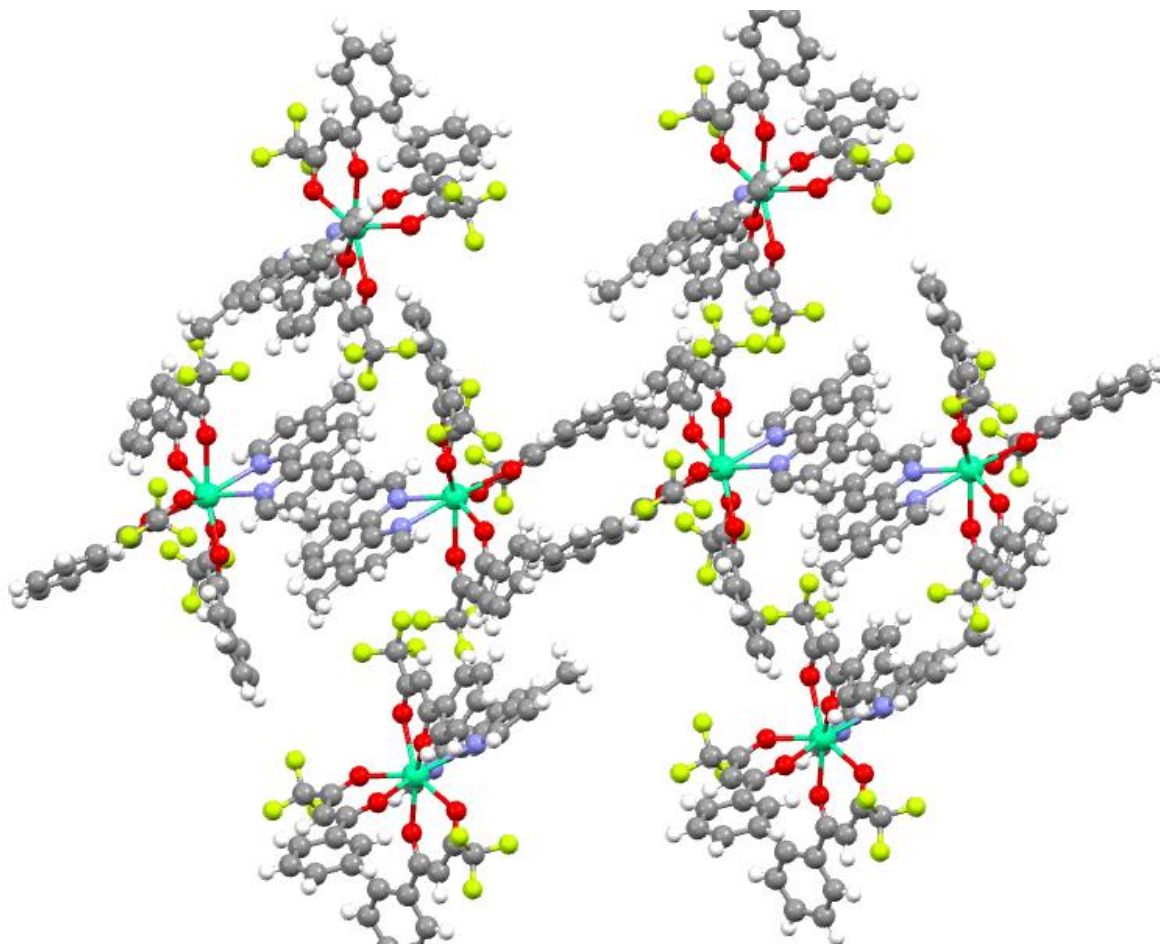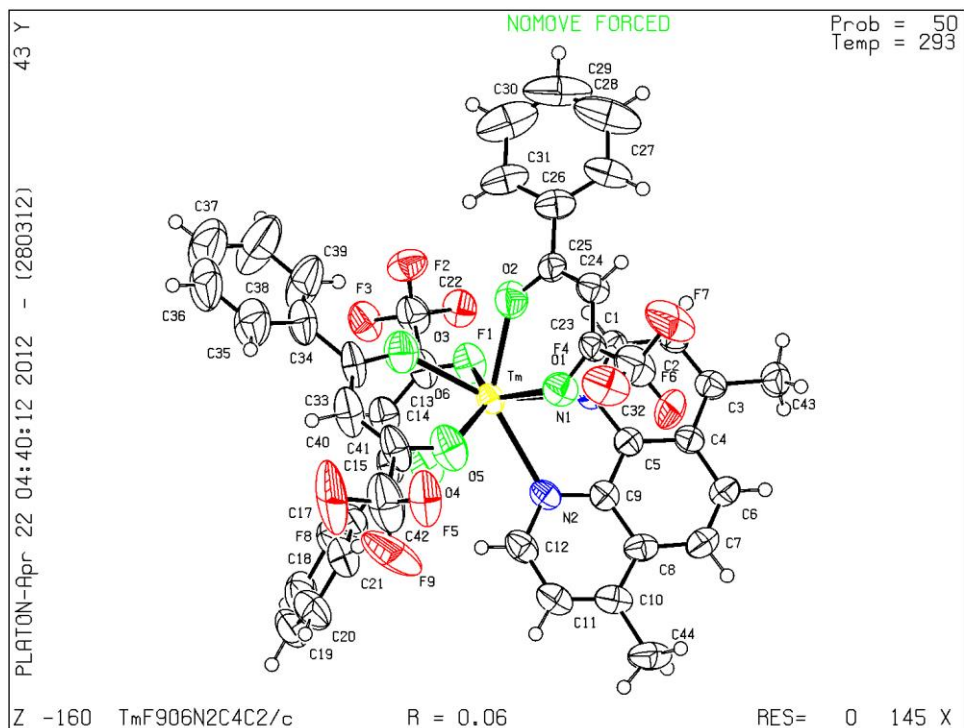
Figure 26. Structure of Tm(btfa)₃dmphen.
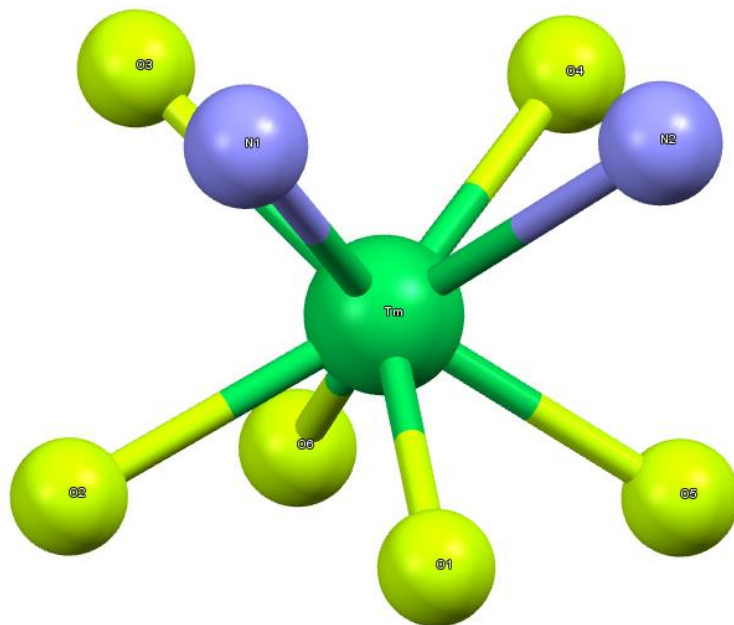
Figure 27. Coordination polyhedron of Tm(btfa)₃dmphen complex

Calculations show that the atoms of the dmphen ligand are nearly coplanar.

The Tm-N bond distances (2.475(4)-2.517(3), average 2.496) and Tm-O bond distances (2.275(3)-2.320, average 2.293) are within the average bond distances observed for similar complexes. The crystal was 0.31 x 0.07 x 0.05 mm in size with a volume of 8286 A^3, and density of 1.625 mg/m^3 making it the third largest crystal resolved while being the third densest and tied with Ho(btfa)$_3$dmphen for fourth most voluminous. Unit cell dimensions were a = 36.377 A alpha = 90 deg, b = 11.077 A   beta = 112.81deg., and c = 22.309 A   gamma = 90 deg. Crystal has the third largest absorption coefficient at 2.227 and displays no visible luminescence when exposed to UV light. The calculated unit cell (Figure 28) has eight Tm(btfa)$_3$dmphen molecules.   The molecules arranged in a pattern of 2-4-2. π-π stacking of the molecules occurs at the dmphen ligand with the 4,7 methyl groups being reflected and overlaid from the connecting dmphen while being offset stacked.   The unit cell is also held by F-H bonding from the fluorinated methyl group of one btfa to the benzene ring of another btfa ligand.
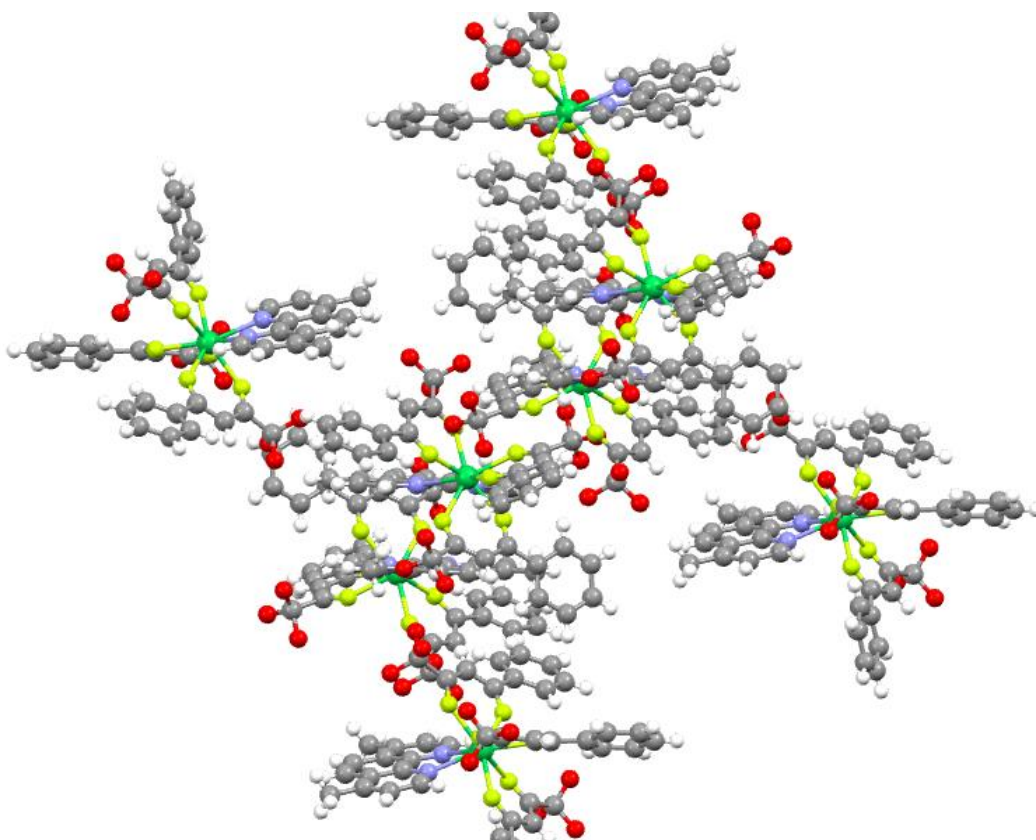

Figure 28. Calculated Unit Cell of Tm(btfa)$_3$dmphen

55

3.2.8 Yb(btfa)₃ dmphen

Yb(btfa)₃ dmphen crystalizes in the centroscymetric monoclinc space group C2/c. The molecular structure (Figure 29) reveals a central ytterbium atom situated with six coordinating oxygens and two nitrogens from the btfa and dmphen ligands, respectively. The coordination polyhedron (Figure 30) can be described as a distorted square antiprism.
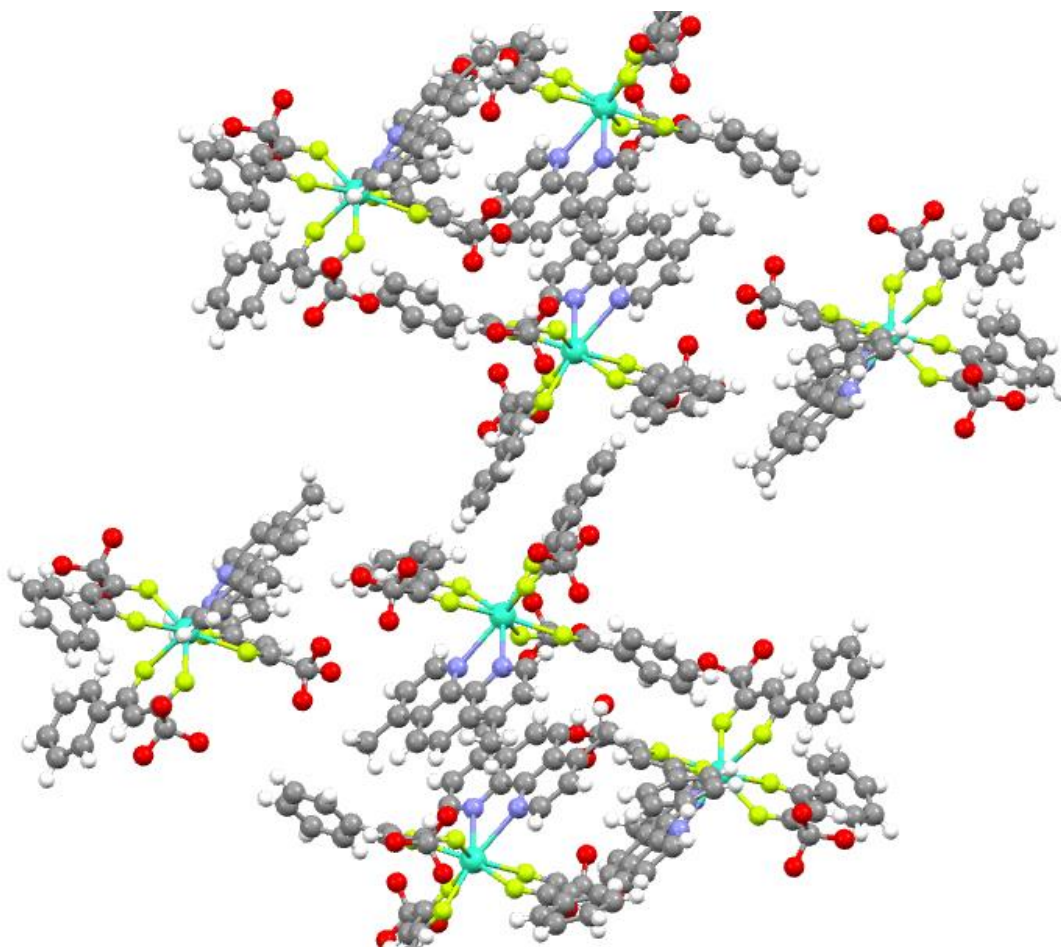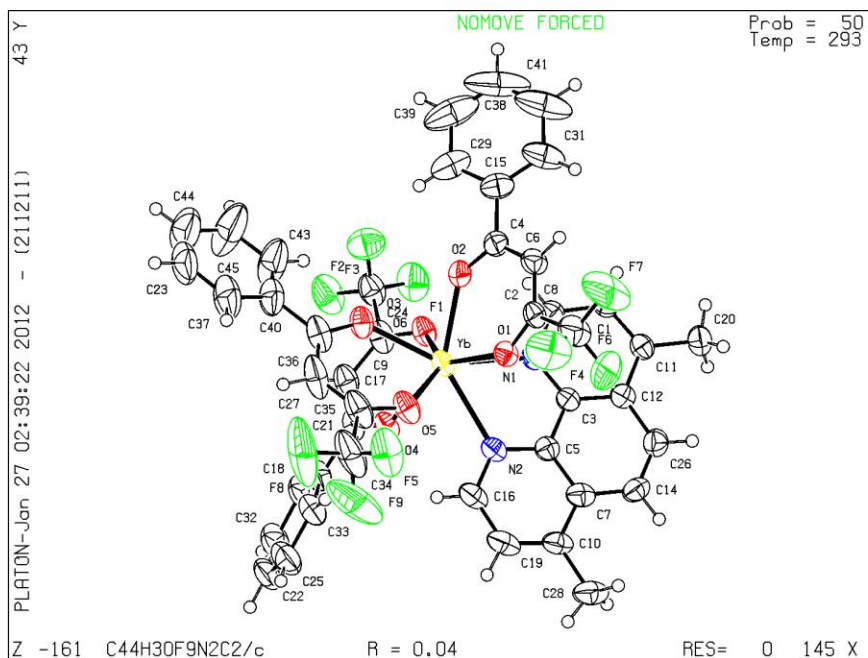

Figure 29. Structure of Yb(btfa)₃dmphen.
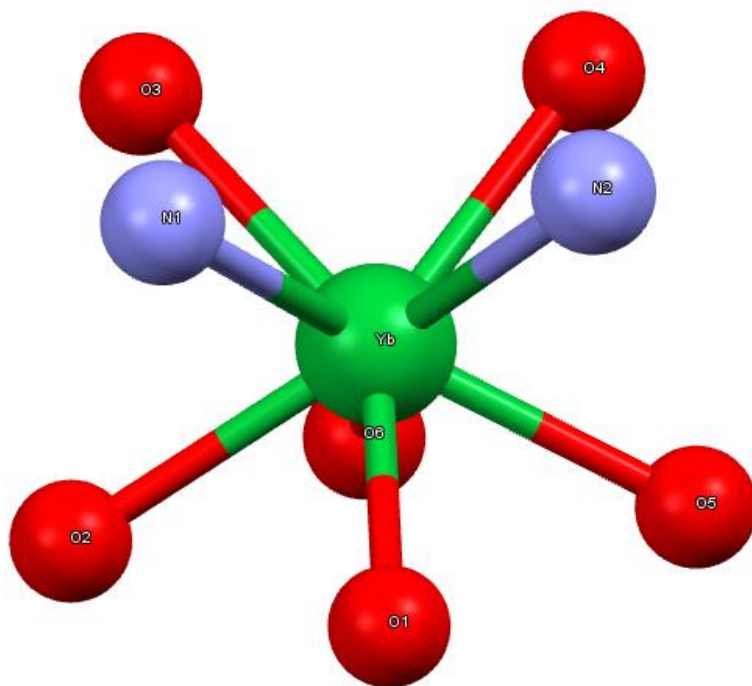
Figure 30. Coordination polyhedron of Yb(btfa)₃dmphen complex

Calculations show that the atoms of the dmphen ligand are nearly coplanar.

The Yb-N bond distances (2.474(4)-2.510(3), average 2.492) and Yb-O bond distances (2.55(3)-2.510, average 2.281) are within the average bond distances observed for similar complexes. The crystal was 0.26 x 0.09 x 0.10 mm in size with a volume of 8238 A^3, and density of 1.656 mg/m³ making it the fourth largest crystal resolved while having the greatest density and second smallest volume. Unit cell dimensions were a = 36.6051(10) A   alpha = 90 deg, b = 10.8940(3) A   beta = 111.9080(10) deg. , and c=22.2613(6)A gamma=90deg. The calculated unit cell (Figure 31) has eight Yb(btfa)₃ dmphen molecules. The molecules are arranged in a pattern of 2-4-2. π-π stacking of the molecules occurs at the dmphen ligand with the 4,7 methyl groups being reflected and overlaid from the connecting dmphen

while being offset stacked. The unit cell is also held by F-H bonding from the fluorinated methyl group of one btfa to the benzene ring of another btfa ligand.
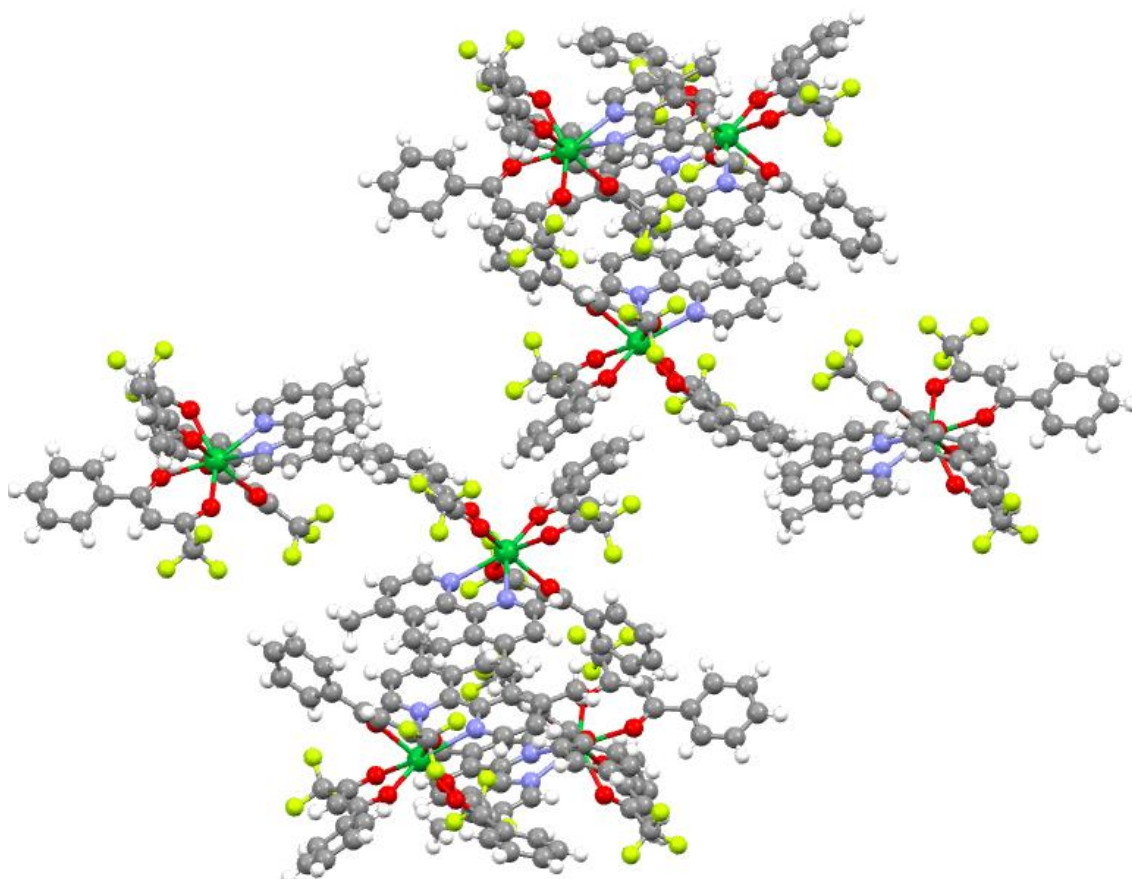

**Figure 31.** Calculated Unit Cell of Yb(btfa)$_3$dmphen

3.3 ABSORPTION STUDIES

UV-vis absorbance of the Ln(btfa)$_3$ dmphen complexes (Figure 32) was measured in methylene chloride solution for the λmax values (Table 12) and plotted with a representative water complex, Eu(btfa)$_3$(H$_2$O)$_2$ for comparison.
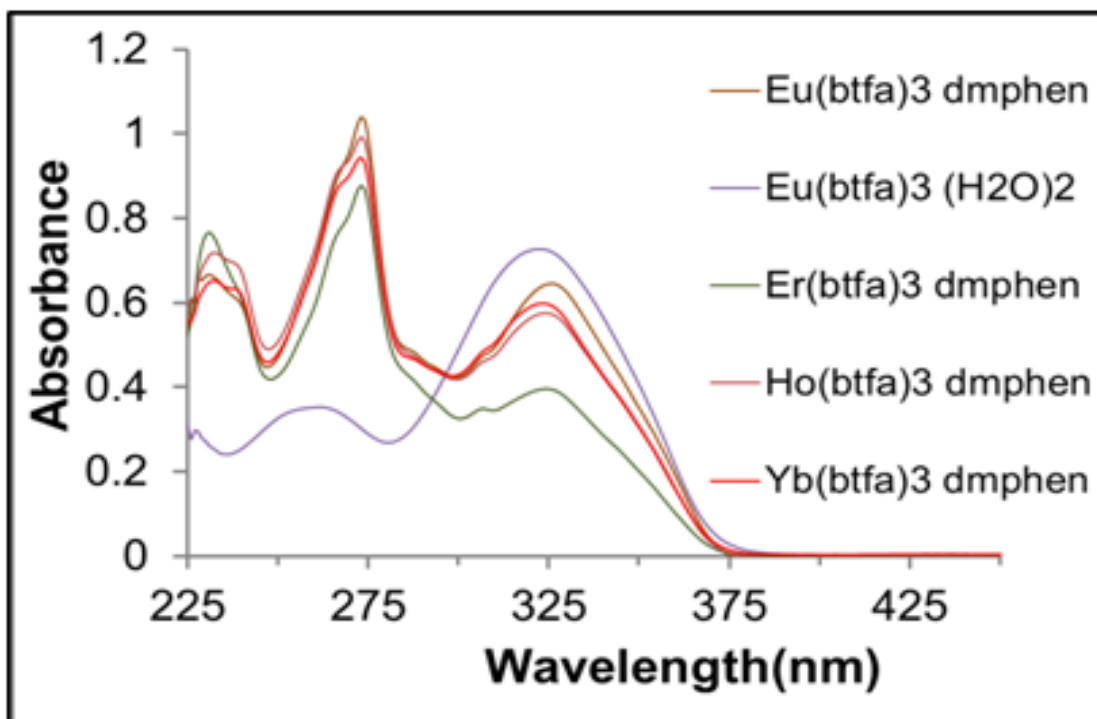
Figure 32. UV-vis absorption studies of Ln(btfa)$_3$ dmphen complexes

Table 12. λmax values for Ln(btfa)$_3$dmphen complexes

Chelator	Wavelength (nm)	Abs
Eu(btfa)3 dmphen	231	0.6666
	273	1.0389
	326	0.6459
Er(btfa)3 dmphen	231	0.7667
	273	0.8768
	324	0.3961
Gd(btfa)3 dmphen	232	0.6529
	273	0.9437
	325	0.5965
Ho(btfa)3 dmphen	232	0.7181
	273	0.9919
	325	0.5750
Tb(btfa)3 dmphen	233	0.5510
	265	0.8269
	328	0.3825
Tm(btfa)3 dmphen	233	0.3494
	273	0.6289
	327	0.3115

Yb(btfa)3 dmphen	232	0.6529
	273	0.9437
	323	0.5984

The btfa and dmphen ligand combination in the Ln(btfa)$_3$dmphen complex has three absorption peaks with wavelengths ranging from 231-233 nm , 265-273 nm, and 323-326 nm. All of the Ln(btfa)$_3$dmphen chelators have the characteristic pattern of three peaks with the middle peak being the largest peak.

3.4. LUMINESCENT STUDIES

The Excitation data was taken for the Eu(btfa)$_3$dmphen at 1×10^{-6} M concentration in methylene chloride solution (Figure 33) and the highest intensities are listed in Table 13.
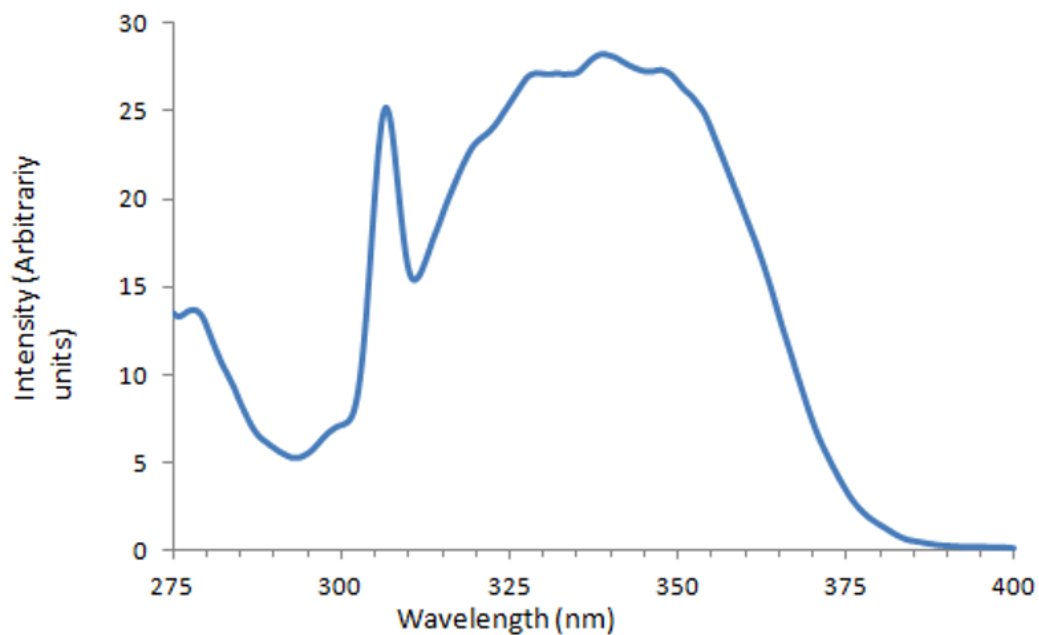
Figure 33. Excitation spectrum for Eu(btfa)$_3$dmphen

Table 13. Excitation Wavelengths with highest intensity for Eu(btfa)$_3$dmphen

Wavelength (nm)	Intensity (a.u)
272	15.013048
332	27.194924
339	28.282965

The Eu(btfa)$_3$ dmphen chelator has a broad peak of excitation with higher peak intensities at 272 nm, 332 nm, and 339 nm and values of 15.01 a.u, 27.19 a.u, and 28.28 a.u. The best excitation values for the btfa/dmphen ligand combination is between 340 nm and 350 nm though values as low as 325 nm can be used to excite the ligand system. This broad range of excitation may contribute to the tunability of the Eu(btfa)$_3$ dmphen complex.

Luminescent data from 500 nm to 680 nm for the Eu(btfa)$_3$ dmphen chelator was taken at 350 nm excitation and 1×10^{-6} M concentration (Figure 34) and 325 excitation nm and 1×10^{-6} M concentration (Figure 35) in methylene chloride with the highest peak intensities shown in Table 14.
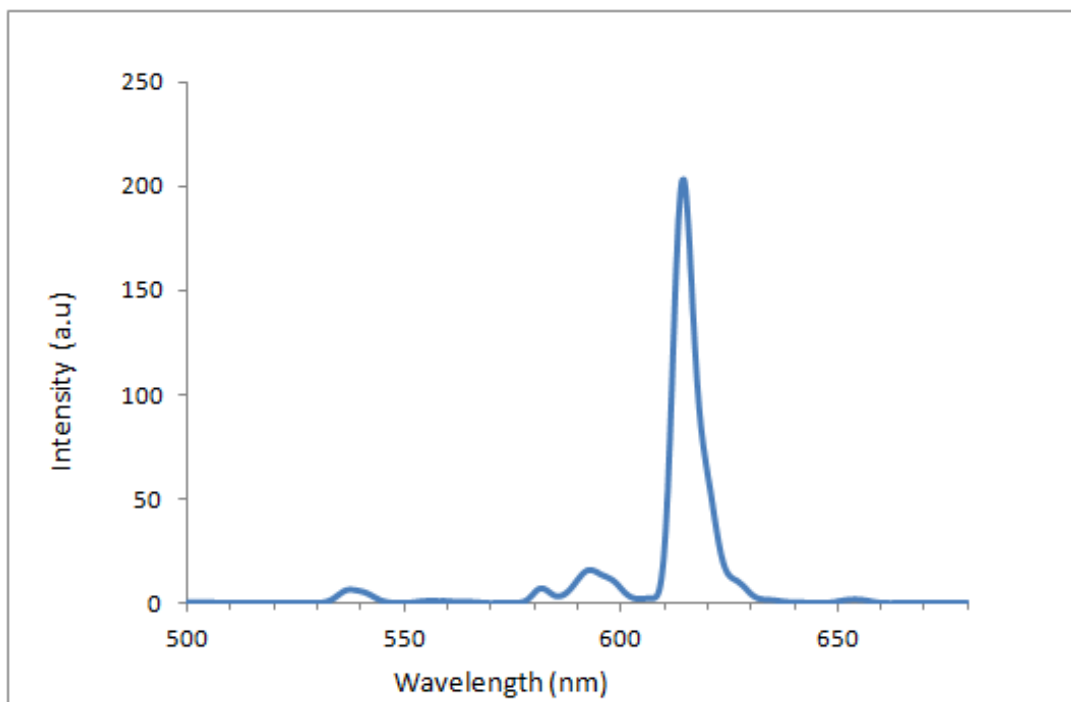
Figure 34. Eu(btfa)$_3$ dmphen emission from 500 nm to 680 nm at 325 nm excitation
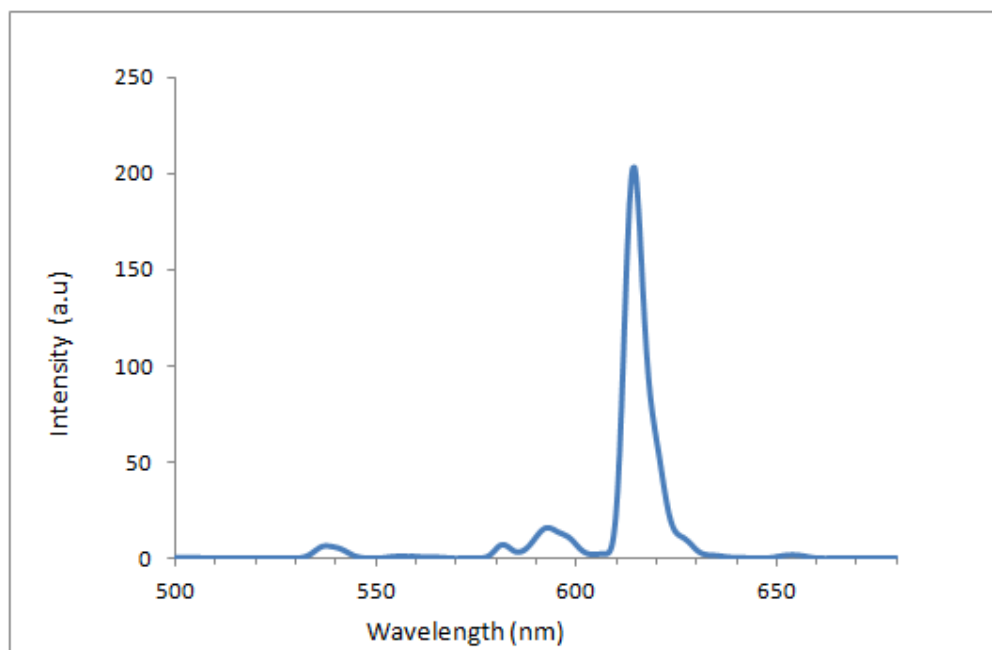
Figure 35. Eu(btfa)$_3$ dmphen emission from 500 nm to 680 nm at 350 nm excitation

Table 14. Highest peak intensities for Eu(btfa)$_3$dmphen emission from 500 nm to 680 nm at 325 nm and 350 nm excitation

Wavelength (nm)	325 nm Excitation (a.u)	350 nm Excitation (a.u)
538	8.026436	6.48705
582	8.444747	7.110492
594	19.00239	15.338398
614	256.5862	202.766896
651	38.0157	1.252737

The results were compared to the emission spectra of the Eu(btfa)$_3$(H$_2$O)$_2$ complex (Figure 36) .
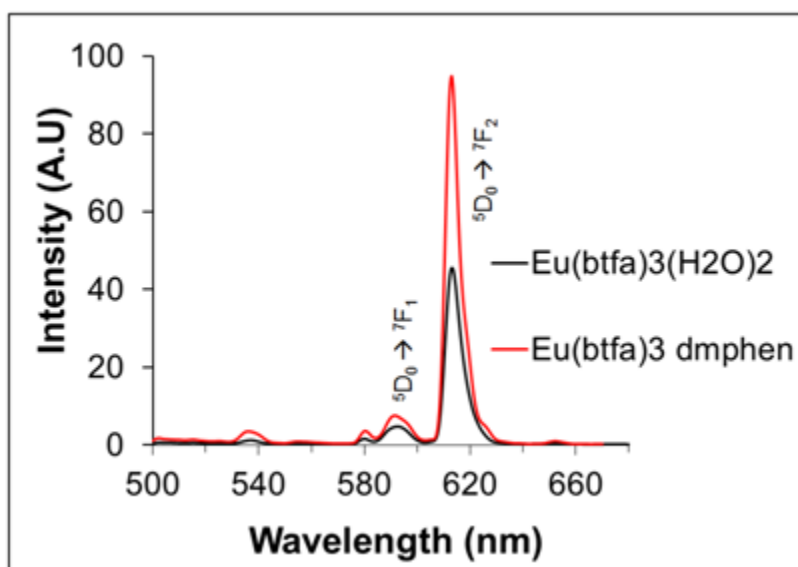
Figure 36. Comparison of Eu(btfa)$_3$ dmphen and Eu(btfa)$_3$(H$_2$O)$_2$ emission

Both complexes have the emission characteristics of $^5D_0$ to $^7F_1$ transition and $^5D_0$ to $^7F_2$ transition of Eu^{3+}. The Eu(btfa)$_3$(H$_2$O)$_2$ complex has a relative intensity of 45 A.U at its most intense peak at 614 nm compared to the 95 A.U of the Eu(btfa)$_3$dmphen at its most intense peak at 614 nm. The relationship for the peaks at 540 nm, 595 nm, and 614 nm all follow a trend of the Eu(btfa)$_3$(H$_2$O)$_2$ intensities being roughly half the value of the Eu(btfa)$_3$dmphen intensities.   This is due to vibrational quenching effects of

the H_2O ligands of the $Eu(btfa)_3(H_2O)_2$ complex. The intense peak of both the $Eu(btfa)_3(H_2O)_2$ and $Eu(btfa)_3$dmphen complexes means that energy is absorbed through the ligand system, with the energy transfer going from the excited singlet state of the ligands to the triplet state of the antenna ligands, then a transfer from the triplet state of the ligands to the triplet state of the Eu, and finally a transfer to the singlet state of the Eu and a relaxation down producing Eu-centered luminescence. The dmphen contribution is more than the water ligands, leading to the higher luminescence intensity.

Luminescent lifetime decay data for the $Eu(btfa)_3$dmphen complex was taken for dry chelator and dissolved in methylene chloride and compared to the water complex under the same conditions. Lifetimes were measured at 355 nm excitation (Figure 37) and 465 nm excitation (Figure 38). 355 mm can be used to excite the ligand, while 465 nm is good for direct excitation of the Eu^{3+}. The results of the lifetime decays for the $Eu(btfa)_3$dmphen and $Eu(btfa)_3(H_2O)_2$ are summarized in Table 15.
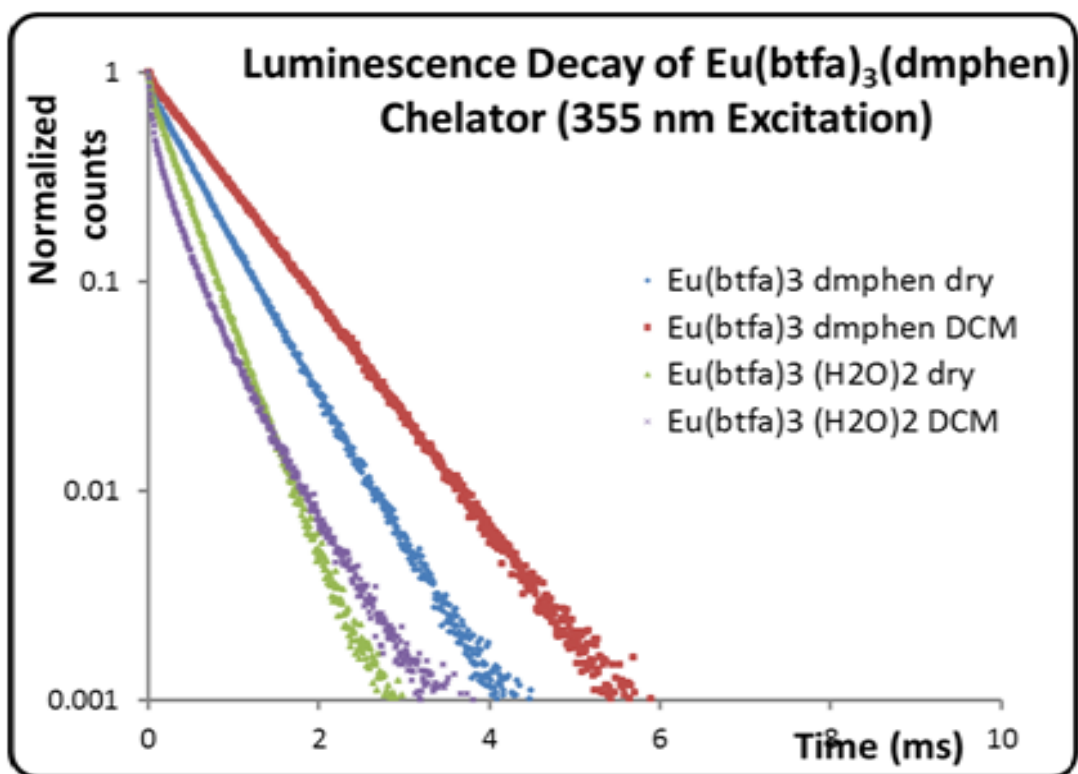
Figure 37. Luminescent decay curves of $Eu(btfa)_3$dmphen and $Eu(btfa)_3(H_2O)_2$ at 355 nm excitation
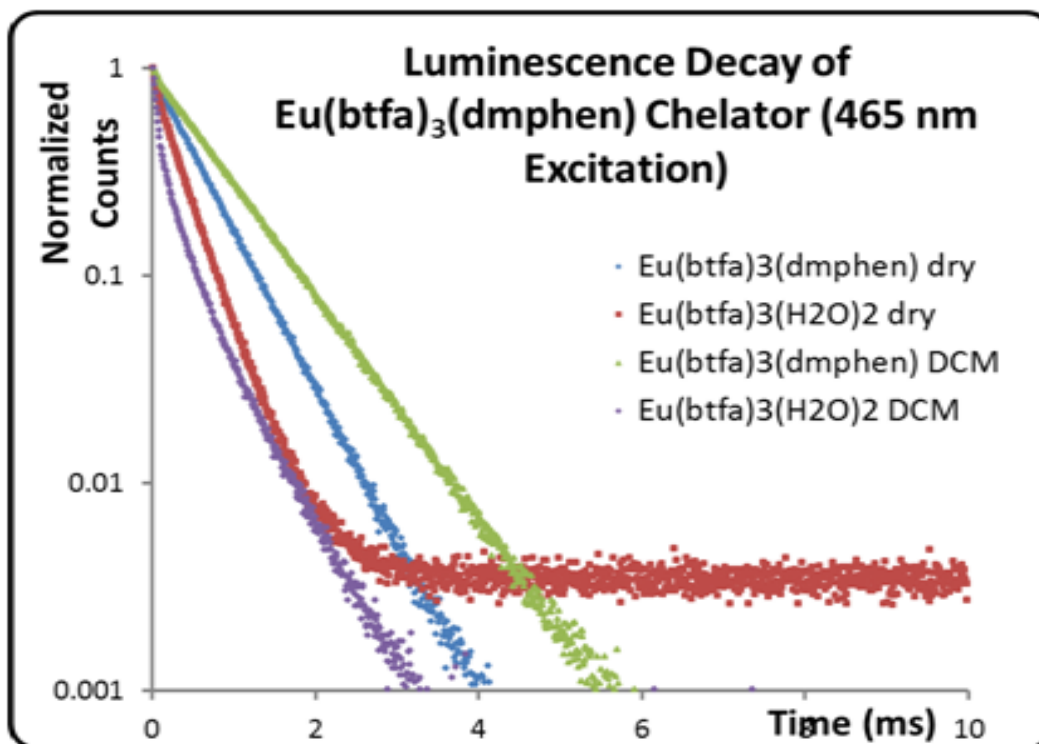
Figure 38. Luminescent decay curves of Eu(btfa)$_3$dmphen and Eu(btfa)$_3$(H$_2$O)$_2$ at 465 nm excitation

Table 15. Comparison of luminescent lifetimes for Eu(btfa)$_3$dmphen and Eu(btfa)$_3$(H$_2$O)$_2$ at 355 nm and 465 nm excitation

Material	Lifetime at 355 nm Excitation (ms)	Lifetime at 465 nm Excitation (ms)
Eu(btfa)$_3$dmphen (dry)	0.593	0.572
Eu(btfa)$_3$dmphen (in CH$_2$Cl$_2$)	0.813	0.811
Eu(btfa)$_3$(H$_2$O)$_2$ (dry)	0.384	0.371
Eu(btfa)$_3$(H$_2$O)$_2$ (CH$_2$Cl$_2$)	0.470	0.474

The dry Eu(btfa)$_3$dmphen had lifetimes of 0.593 ms at 355 nm excitation and 0.572 ms at 465 nm excitation, while the methylene chloride dissolved chelator had a lifetime 0.813 ms at 355 nm excitation and 0.811 ms at 465 nm excitation. This is a 0.22 ms shorter lifetime at 355 nm and 0.239 ms shorter lifetime at 465 nm for the dry material compared to the chelator dissolved in methylene chloride. This

65

equates to a 27.06% shorter lifetime at 355 nm and 29.47% shorter lifetime at 465 nm for the dry Eu(btfa)$_3$dmphen compared to the Eu(btfa)$_3$dmphen dissolved in methylene chloride.

The dry Eu(btfa)$_3$(H$_2$O)$_2$ had lifetimes of 0.384 ms at 355 nm excitation and 0.371 ms at 465 nm excitation, while the methylene chloride dissolved version had lifetimes of 0.470 ms at 355 nm and 0.474 nm at 465 nm. This is a 0.086 ms shorter lifetime at 355 nm and 0.103 ms shorter lifetime at 465 nm for the dry material compared to the methylene chloride dissolved chelator. This equates to a 18.30% shorter lifetime at 355 nm and 21.73% shorter lifetime at 465 nm than the Eu(btfa)$_3$(H$_2$O)$_2$ dissolved in methylene chloride

The dry Eu(btfa)$_3$(H$_2$O)$_2$ also had lifetimes that were 0.209 ms shorter at 355 nm and 0.201 ms shorter at 465 nm compared to the dry Eu(btfa)$_3$dmphen chelator and 0.429 ms shorter lifetime at 355 nm and 0.440 ms shorter lifetime at 465 nm compared to the Eu(btfa)$_3$dmphen chelator dissolved in methylene chloride. This equates to a 35.52% shorter lifetime at 355 nm and 35.14% shorter lifetime at 465 nm compared to the dry Eu(btfa)$_3$dmphen chelator and a 52.77% shorter lifetime at 355 nm and 54.25% shorter lifetime at 465 nm compared to the Eu(btfa)$_3$dmphen chelator dissolved in methylene chloride.

The methylene chloride dissolved in Eu(btfa)$_3$(H$_2$O)$_2$ had lifetimes that were 0.123 ms shorter at 355 nm and 0.098 ms shorter at 465 nm compared to the dry Eu(btfa)$_3$dmphen chelator and 0.343 ms shorter at 355 nm and 0.337 ms shorter at 465 nm compared to the Eu(btfa)$_3$dmphen chelator dissolved in methylene chloride. This equates to a 20.74% shorter lifetime at 355 nm and 17.13% shorter lifetime compared to the dry Eu(btfa)$_3$dmphen and 42.22% shorter lifetime at 355 nm and 41.55% shorter lifetime at 465 nm compared to the Eu(btfa)$_3$dmphen dissolved in methylene chloride. The Eu(btfa)$_3$dmphen complex has limited solubility in water and so suffers from the quenching effects of water instead of the longer lifetime in methylene chloride, but still has a significantly longer luminescence lifetime than the Eu(btfa)$_3$(H$_2$O)$_2$ complex that could allow for longer relaxation time of background fluorescence before taking measurements and is a promising candidate to be incorporated into silica solgel materials. Substitution of H$_2$O ligands by dmphen ligand greatly enhances the luminescence intensity of the

complex. This may be attributed to two reasons. (i) H_2O ligands may be responsible for vibrational quenching of the Eu(III)-centered luminescence; (ii) The dmphen ligand may adjust the triplet level of the ligand system to make it more suitable for an efficient ligand-to-metal energy transfer process resulting in improved luminescence intensity. The luminescent lifetime of the dmphen complex is significantly higher than the lifetime of the H_2O complex. The measured luminescent lifetimes of 0.59 to 0.61 ms are sufficient for the suppression of cell background fluorescence and are useful for imaging applications after silica encapsulation.

Luminescent quantum yield was measured for the Eu(btfa)₃dmphen and compared to Rhodamine 6G in methylene chloride (0.88) as a standard (Table 16).

Table 16. Luminescent quantum yield of Eu(btfa)₃dmphen and Rhodamine 6G[43-50] in methylene chloride

Compound	Quantum Yield
Eu(btfa)₃dmphen	0.539
Rhodamine 6G	0.88

The Eu(btfa)₃dmphen complex has a quantum yield of 0.593 in methylene chloride. That is 0.341 less than the Rhodamine 6G standard for a difference in efficiency of 38.97% in methylene chloride. While not as high yield as the standard, the relative cost of Eu(btfa)₃dmphen complex is more than sufficient for imaging applications due to the high intensity of the emission and long luminescence lifetime. Er(btfa)₃ dmphen was measured from 350 nm to 1150 nm with a 60 s integration (Figure 39). The highest peak intensity is listed in Table 17.
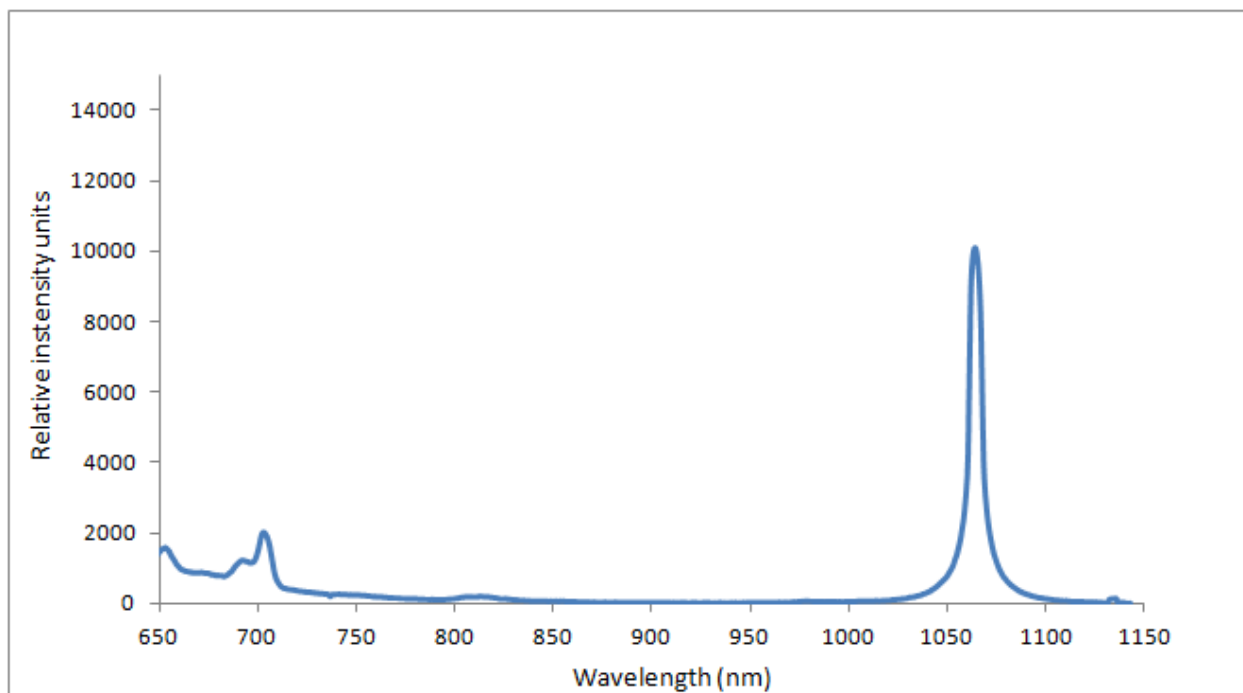
Figure 39. Luminescent studies of Er(btfa)$_3$dmphen using 350 nm excitation

Table 17. Peak Intensity values for Er(btfa)$_3$ dmphen

Wavelength (nm)	Intensity (a.u)
1063	10114

The Er(btfa)$_3$dmphen complex has one strong emission peak at 1063 nm in the infrared region with a peak intensity of 10114 a.u. The Er(btfa)$_3$dmphen complex has a strong emission in the infrared portion of the electromagnetic spectrum.   The complex absorbs energy through the ligand system similar to Eu(btfa)$_3$dmphen complex.   This emission is shifted significantly down from cell background fluorescence that it could be measured directly with minimal background fluorescence. A strong intensity also provides potential applications that would use only a small amount of material as a tracer.

Luminescence of Ho(btfa)$_3$dmphen was measured from 350 nm to 1150 nm with a 40 s integration (Figure 40). The highest peak intensity is listed in Table 18.

68
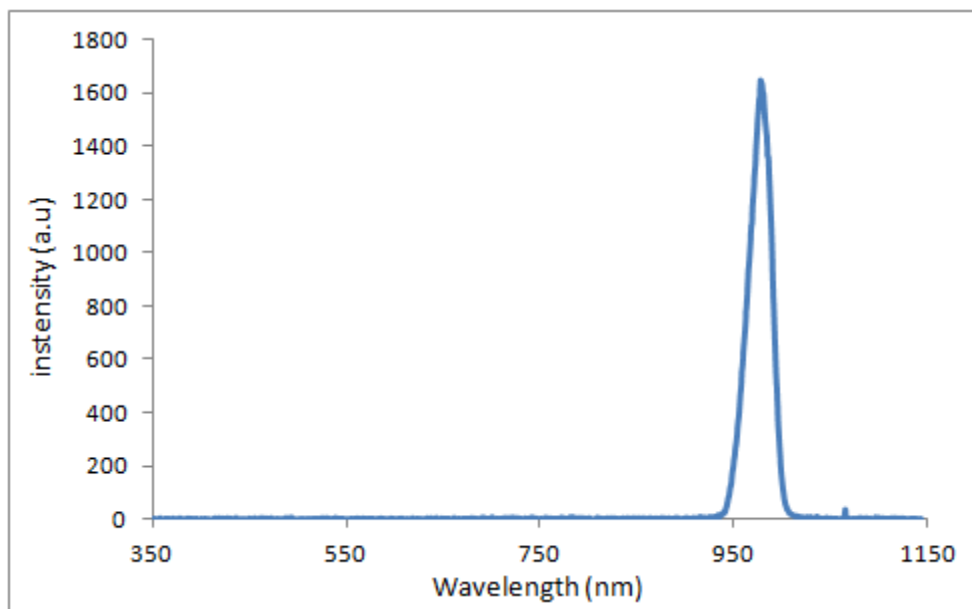
Figure 40. Luminescent studies of Ho(btfa)₃dmphen upon 350 nm excitation

Table 18. Peak Intensity values for Ho(btfa)$_3$ dmphen

Wavelength (nm)	Intensity (a.u)
977	1647

The Ho(btfa)₃dmphen complex has one strong emission peak in the near infrared region at 977 nm with a peak intensity of 1647 a.u.   This emission in the near infrared is sufficient to provide the Ho(btfa)₃dmphen complex a slight red glow under UU-light.   The intensity is high enough to be potentially useful in a luminescent solgel material, and is far enough from cell background fluorescence to be measured without any interferences.   Like Eu(btfa)₃dmphen and Er(btfa)₃dmphen complexes, energy is absorbed through the ligand system in the Ho(btfa)₃dmphen complex.

The lifetime decay for Ho(btfa)₃dmphen was measured (Figure 41) with the summary of results in Table 19.
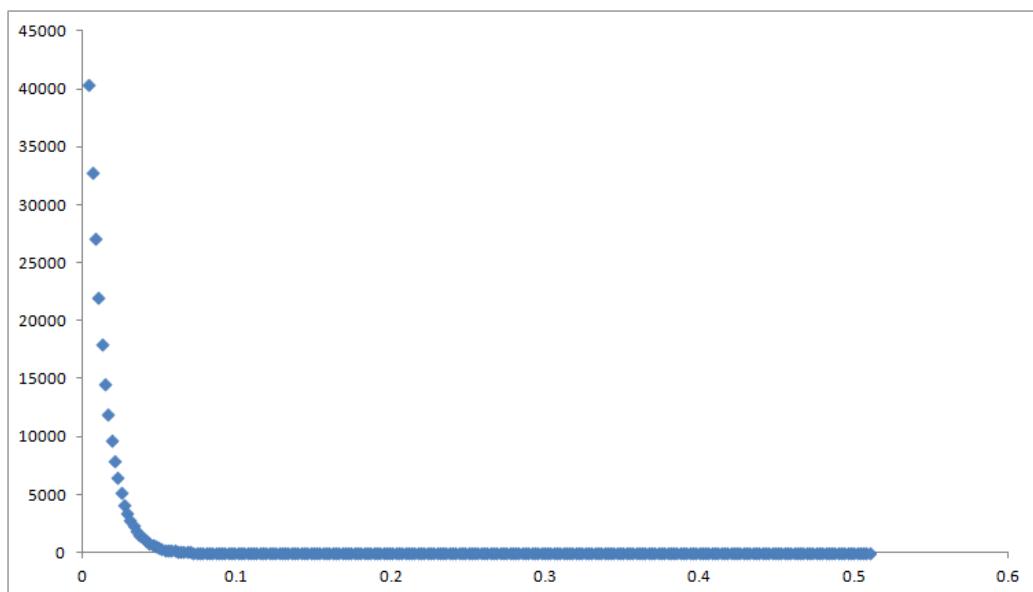
Figure 41. Lifetime Decay of Ho(btfa)$_3$dmphen

Table 19. Lifetime Decay of Ho(btfa)$_3$dmphen

Time (ms)	Intensity (A.U)
0.0492	475

The Ho(btfa)$_3$dmphen chelator complex had a lifetime of 0.0492 ms with complete decay by 0.05 ms. This is a significantly weaker lifetime luminescence than the < 0.5 ms lifetime of the Eu(btfa)$_3$dmphen complex. This order of magnitude difference does not make the Ho(btfa)$_3$dmphen as good a choice for imaging applications as the Eu(btfa)$_3$dmphen, but it could have some use due to be even further removed from background fluorescence, and the observed longer luminescent lifetime which is higher than those values observed for traditional organic dyes.

3.5 ICP-OES AND OTHER CHARACTERIZATION.

By percentage, the Ln amount in the chelator complex should be within 1% of the 92 atom components of the complex. The Ln(btfa)$_3$dmphen chelator complexes were evaluated for Ln percentages using ICP-OES (Table 20).

Table 20. Ln percentages (Ln %) for the Ln(btfa)$_3$dmphen chelators

Sample	Theoretical Ln%	Actual Ln%
Eu(btfa)$_3$ dmphen	1.51%	1.050
Er(btfa)$_3$ dmphen	1.64%	0.988
Gd(btfa)$_3$ dmphen	1.56%	1.004
Ho(btfa)$_3$ dmphen	1.62%	1.020
Tb(btfa)$_3$ dmphen	1.57%	0.995
Tm(btfa)$_3$ dmphen	1.65%	1.060
Yb(btfa)$_3$ dmphen	1.69%	1.038

The lanthanide percentages are 1.050% (Eu), 0.988% (Er), 1.004% (Gd), 1.020% (Ho), 0.995% (Tb), 1.060% (Tm), and 1.038% (Yb). The seven lanthanide targets ranged in percentage of total complex from 0.995% to 1.06% and are within instrumental errors suggesting the successful synthesis of each of the target Ln(btfa)$_3$dmphen complexes.

The Ln(btfa)$_3$dmphen chelator complex has a chemical formula of $C_{44}H_{30}F_9N_2O_6Ln$. It has 92 atom components with 44 of them being carbon for approximately 48 percent of the total compound mass. The Ln(btfa)$_3$dmphen chelator complexes were analyzed for carbon percentages (Table 21).

Table 21. Carbon Percentages for Ln(btfa)$_3$ dmphen complexes

Sample	Theoretical C%	Actual C%
Eu(btfa)$_3$ dmphen	52.55	48.2
Er(btfa)$_3$ dmphen	51.76	48.3
Gd(btfa)$_3$ dmphen	52.28	47.8
Ho(btfa)$_3$ dmphen	51.88	48.1
Tb(btfa)$_3$ dmphen	52.12	48.1
Tm(btfa)$_3$ dmphen	51.68	47.9
Yb(btfa)$_3$ dmphen	51.47	47.9

The range of the actual C% ranged from 47.9 to 48.3%. This range falls within the expected value and confirms that the Ln(btfa)$_3$(H$_2$O)$_2$ chelators were reacted successfully to form the Ln(btfa)$_3$dmphen chelators. The 0.1% to 0.3% difference from the expected value for each chelator can be attributed to minor impurities and trace amounts of the original materials.

CHAPTER 4: SILICA SOLGEL MATERIAL RESULTS

4.1 PHOTOPHYSICAL CHARACTERISTICS AND STEM IMAGING

Eu(btfa)$_3$(H$_2$O)$_2$ and Eu(btfa)$_3$dmphen chelators were doped into a silica solgel matrix and the materials were examined under UV light excitation. The chelator-doped sol gel materials produced vivid red luminescence which is characteristic of the Eu^{3+} ions. The bulk silica solgel materials when dried had no other distinguishing visible characteristics and were all white powders. The bulk materials were examined by STEM imaging (Figure 42.)
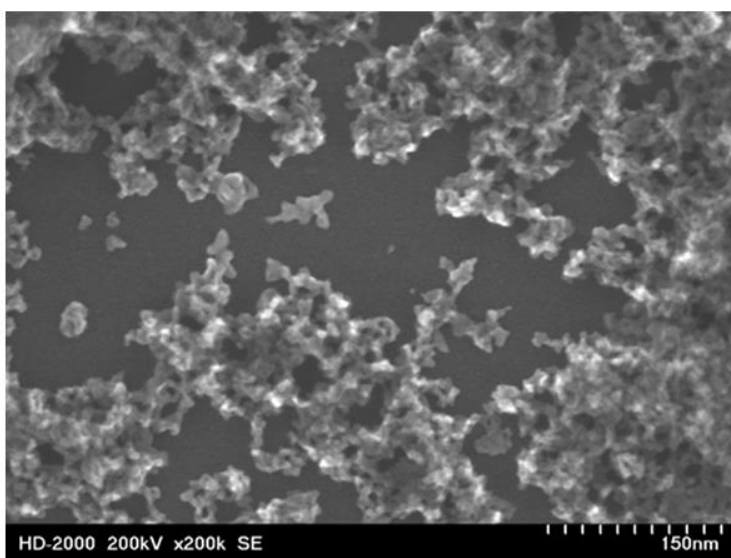
Figure 42. STEM Image of Eu(btfa)$_3$dmphen chelator-doped silica matrix

The Eu(btfa)$_3$dmphen solgel has components of varying shapes and sizes ranging from ~20 nm across to portions bigger than 150 nm and confirming the formation of a bulk solgel material. The presence of successful chelator doping can be seen in the white regions (Figure 41). Chelator doping ranges in distribution from spread to clustered.

4.2 ABSORPTION STUDIES

Eu(btfa)$_3$dmphen solgel absorption in water was measured using UV-vis spectroscopy (Figure 42).
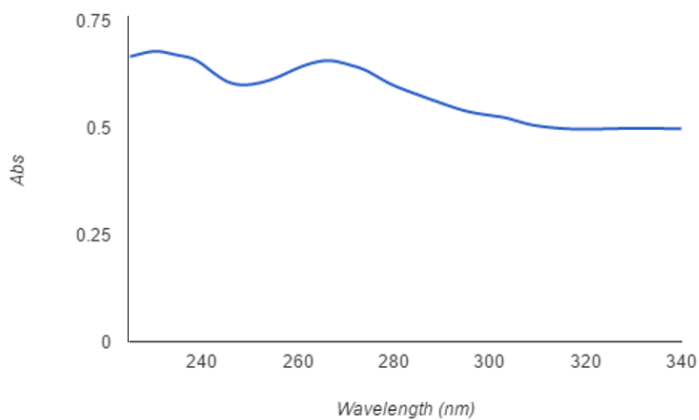
Figure 43. Absorption studies of Eu(btfa)₃dmphen solgel in water

The Eu(btfa)₃dmphen has absorption peaks at 231 nm, 273 nm, and 326 nm. The solgel material has absorption peaks at 231 nm, 273 nm, and 328 nm with λmax values of 0.6792, 0.6402, and 0.4989, respectively. The three peaks confirm the doping of the Eu(btfa)₃dmphen chelator into the silica based material.

4.3 LUMINESCENT STUDIES

Excitation data was taken for the solgel material at 1×10^{-6} M concentration in water from 275 nm to 400 nm (Figure 44) and the highest intensities are listed in Table 22.
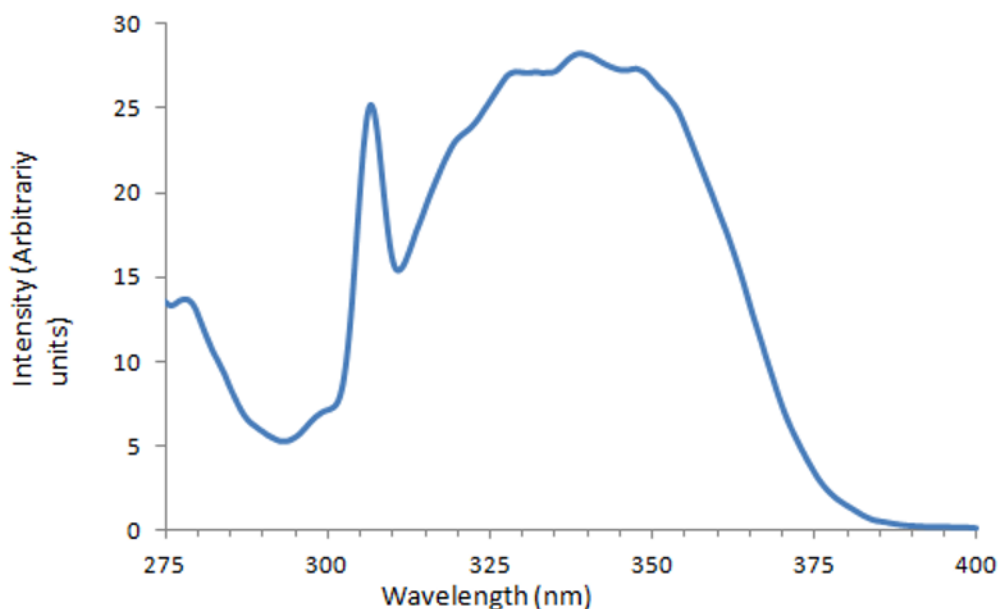
Figure 44. Excitation spectrum of Eu(btfa)$_3$dmphen solgel material

Table 22. Excitation Wavelengths with highest intensity for Eu(btfa)$_3$dmphen solgel material

Wavelength (nm)	Intensity (a.u)
272	15.013048
332	27.194924
339	28.282965

The solgel material has a broad peak of excitation with the highest peak intensities at 272 nm, 332 nm, and 339 nm and values of 15.01 a.u, 27.19 a.u, and 28.28 a.u.   This matches the curve of the Eu(btfa)$_3$dmphen chelator and confirms doping of Eu(btfa)$_3$dmphen into the silica matrix. The silica of the solgel material does not appear to change the excitation curve in any way. Like the pure chelator, the Eu(btfa)$_3$dmphen solgel material can utilize the broad excitation of the ligand system to channel energy to the Eu^{3+} ion. Luminescent data from 500 nm to 680 nm for the solgel material was taken at 280 nm, 330 nm, 340 nm, and 350 nm excitation at 1×10^{-6} M concentration in water (Figure 45) with the highest peak intensities listed Table 23.
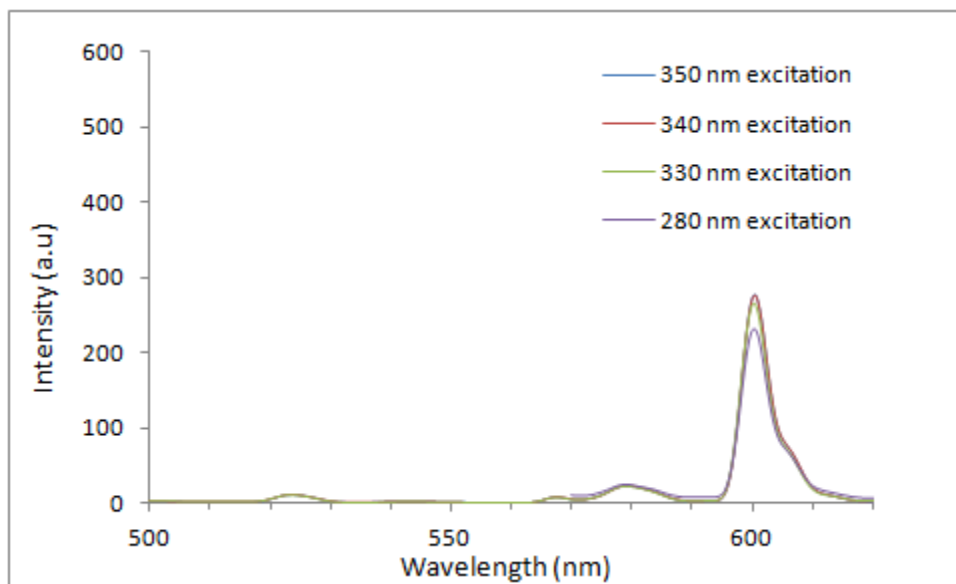
Figure 45. Luminescent studies of the Eu(btfa)₃dmphen chelator-doped solgel material

Table 23. Excitation Wavelengths with highest intensity for Eu(btfa)₃dmphen chelator-doped solgel material

Wavelength (nm)	Intensity (a.u)
280	227.78828
330	263.747254
340	274.490383
350	275.008992

The solgel material has a sharp intensity peak at 600 nm and intensities of 227.79 a.u at 280 nm excitation, 263.74 a.u at 330 nm, 274.49 a.u at 340 nm, and 275.01 a.u at 350 nm. The intensity of emission is strongest at 350 nm, but is less than 5% more intense than the 20 nm range between 330 nm and 350 nm excitation, but 18.78% more intense than the 280 nm excitation. The best luminescence for this system was observed at excitation wavelengths around 350 nm. The chelator-doped solgel matrix luminescence lifetime was measured at 355 nm (Figure 45) and 465 nm (Figure 46) excitation wavelengths. The dry form of the Eu(btfa)₃dmphen solgel was measured and compared to the water dispersed forms of the Eu(btfa)₃dmphen and Eu(btfa)₃ (H₂O)₂ solgels.
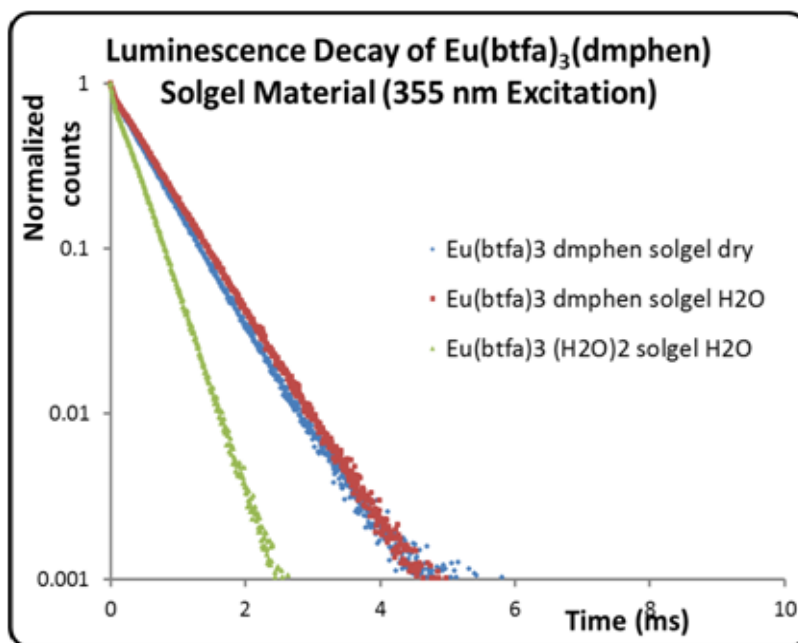
Figure 46. Luminescent decay curves of Eu(btfa)₃dmphen solgel at 355 nm excitation
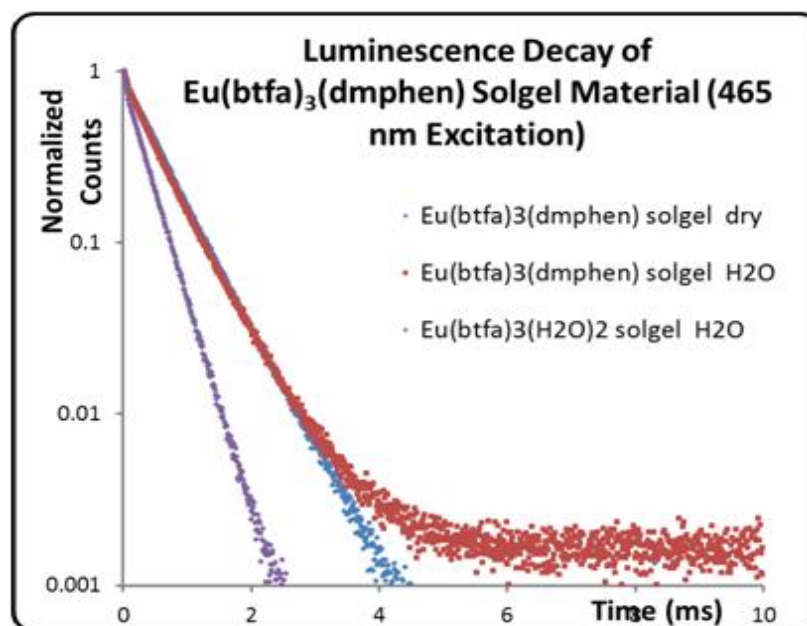
Figure 47. Luminescent decay curves of Eu(btfa)₃dmphen solgel at 465 nm excitation

Both Figures 46 and 47 show a steep lifetime decay curve for the Eu(btfa)$_3$(H$_2$O)$_2$ solgels with full decay

at just under 3 ms. The lifetime decay curve for the Eu(btfa)$_3$dmphen solgels is not as steep, and exhibits

a lifetime decay of nearly two times higher than that of the Eu(btfa)$_3$(H$_2$O)$_2$ solgels at approximately 6-7

with full decay for the dry Eu(btfa)$_3$dmphen solgel not reaching complete decay after even 10 ms. The lifetime decay time of the solgels are listed in Table 24.

Table 24. Summary of Eu(btfa)$_3$dmphen and The Eu(btfa)$_3$(H$_2$O)$_2$ solgel lifetime analysis

Material	Lifetime at 355 nm Excitation (ms)	Lifetime at 465 nm Excitation (ms)	% difference in lifetime length from dry chelator	%difference in lifetime length dissolved chelator water
Eu(btfa)$_3$dmphen (sol- gel, dry)	0.616	0.595	+3.734 (355 nm)	-31.98 (355 nm)
			+3.866 (465 nm)	-36.30 (465 nm)
Eu(btfa)$_3$dmphen (sol- gel in H$_2$O)	0.655	0.588	+9.463 (355 nm)	-24.12 (355 nm)
			+2.721 (465 nm)	-37.93 (465 nm)
Eu(btfa)$_3$ (H$_2$O)$_2$ (sol- gel, H$_2$O)	0.360	0.345	-64.72 (355 nm)	-125.8 (355 nm)
			-39.69 (465 nm)	-135.1 (465 nm)

The Eu(btfa)$_3$dmphen solgel had a lifetime of 0.616 ms at 355 nm and 0.595 ms at 465 nm while dry, and a lifetime.of 0.655 ms at 355 nm and 0.588 ms at 465 nm excitation when dispersed. This is a 0.023 ms longer lifetime at 355 nm and 465 nm excitation than the dry Eu(btfa)$_3$dmphen chelator, but 0.197 ms shorter lifetime at 355 nm and 0.216 ms shorter lifetime at 465 nm excitation than the Eu(btfa)$_3$dmphen dissolved in methylene chloride for the dry Eu(btfa)$_3$dmphen solgel. This is 3.734% longer lifetime at 355nm and 3.866% at 465nm excitation for the dry material and 31.98.43% at 355 nm and 36.30% at 465 nm excitation shorter lifetime compared to the Eu(btfa)$_3$dmphen chelator dissolved in methylene chloride. The Eu(btfa)$_3$dmphen water dispersed solgel material had a lifetime 0.062 ms longer lifetime at 355 nm and 0.016 ms longer lifetime at 465 nm excitation than the dry Eu(btfa)$_3$dmphen chelator, and 0.158 ms shorter lifetime at 355 nm and 0.223 ms shorter lifetime at 465 nm excitation than the Eu(btfa)$_3$dmphen chelator dissolved in methylene chloride. This is 9.463% longer lifetime at 355 nm and 2.721% longer

lifetime at 465 nm excitation for the water dispersed material and 24.12% shorter lifetime at 355 nm and 37.93% at shorter lifetime at 465 nm excitation compared to the Eu(btfa)$_3$dmphen chelator dissolved in methylene chloride. The Eu(btfa)$_3$(H$_2$O)$_2$ water dispersed solgel material had a lifetime 0.233 ms shorter lifetime at 355 nm and 0.227 ms shorter lifetime at 465 nm excitation than the dry Eu(btfa)$_3$dmphen chelator, and 0.453 ms shorter lifetime at 355 nm and 0.466 ms shorter lifetime at 465 nm excitation than the Eu(btfa)$_3$dmphen chelator dissolved in methylene chloride. This is 64..72.% shorter lifetime at 355 nm and 39.69% shorter lifetime at 465 nm excitation compared to the Eu(btfa)$_3$dmphen water dispersed solgel material and 125.8% shorter lifetime at 355 nm and 135.1% shorter lifetime at 465 nm excitation compared to the Eu(btfa)$_3$dmphen chelator dissolved in methylene chloride.

4.4 ICP-OES ANALYSIS OF THE SOLGEL MATERIALS

ICP-OES data was taken for the solgel material to determine doping percentage (Table 25).

Table 25. Eu doping percentage of Eu(btfa)$_3$dmphen doped solgel

Compound	Eu%
Eu(btfa)$_3$dmphen doped solgel	3.02

The amount of europium metal ions in the solgel material was 3.02%.

CHAPTER 5: CONCLUSIONS

5.1 LANTHANIDE β-DIKETONATE CHELATOR COMPLEXES

A series of seven octaccoordinated lanthanide β-diketonate chelator complexes based on the btfa/dmphen ligand system were synthesized and characterized. The complexes were characterizedusing single crystal X-ray diffraction studies. Seven chelators of the form Ln(btfa)$_3$dmphen (where Ln= Eu^{3+}, Er^{3+}, Gd^{3+}, Ho^{3+}, Tb^{3+}, Tm^{3+}, and Yb$^{3+)}$ produced crystal structures with a square antprism coordination sphere. The complexes have maximum absorption peaks at 270 nm and 325 nm. Eu complexes exhibit vivid red luminescence at 615 nm while Er, Yb, and Ho complexes show infra-red luminescence upon UV excitation. The complexes exhibit ligand-to-metal energy transfer processes. The best excitation values for the btfa/dmphen ligand combination is between 340 nm and 350 nm though values as low as 325 nm can be used to excite the ligand system. This broad range of excitation may contribute to the tunability of the complex pending on the Ln^{3+} chosen.

The luminescent lifetimes of the Eu(btfa)$_3$dmphen complex were 0.593 ms at 355 nm excitation and 0.572 ms at 465 nm excitation for the dry chelator and 0.813 ms and 0.811 ms in methylene chloride solution. This demonstrates that the luminescent lanthanide complexes have much longer lifetimes outside of a water environment. This appears to be related to vibrational quenching effects on the lanthanide centered luminescence. The Eu(btfa)$_3$dmphen chelator complex was doped into a solgel matrix. The lifetimes of the solgel materials were 0.616 ms at 355 nm excitation and 0.595 ms at 465 nm excitation for the dry solgel, and 0.655 ms and 0.588 ms in a water dispersion. The Eu(btfa)$_3$dmphen complex has a luminescent lifetime that is nearly twice as the value observed for the Eu(btfa)$_3$(H$_2$O)$_2$ chelator.

The Eu(btfa)$_3$dmphen complex has limited solubility in water and so suffers from the quenching effects of water instead of the longer lifetime in methylene chloride, but still has a significantly longer luminescence lifetime than the Eu(btfa)$_3$(H$_2$O)$_2$ complex that could allow for longer relaxation time of background fluorescence before taking measurements and is a promising candidate to be incorporated into silica

solgel materials. The luminescence lifetime of the dmphen complex is significantly higher than the lifetime of the H_2O complex. The measured luminescence lifetimes of 0.59 to 0.61 ms are sufficient for the suppression of cell background fluorescence and are useful for imaging applications after silica encapsulation.

Quantum Yield was measured for the Eu(btfa)$_3$dmphen and compared to Rhodamine 6G in methylene chloride (0.88). The Eu(btfa)$_3$dmphen complex has a quantum yield of 0.593. That is 0.341 less than the Rhodamine 6G standard for a difference in efficiency of 38.97% in methylene chloride. While not as high yield as the standard, the relative cost of Eu(btfa)$_3$dmphen complex is more than sufficient for imaging applications due to the high intensity of the emission and long luminescent lifetimes.

5.2 Eu(BTFA)$_3$DMPHEN SOLGEL MATERIALS.

The second part of this work attempted to encapsulate the Eu(btfa)$_3$dmphen complex into a silica solgel material. Eu(btfa)$_3$dmphen was chosen for this part due to its high luminescence and quantum yield. The Eu(btfa)$_3$(H$_2$O)$_2$ and Eu(btfa)$_3$dmphen chelators were doped into a silica solgel matrix via methods of microemulsion, acid catalysis, and Stöber process. The methods of Stöber process, microemulsion, and acid catalysis produced solgel materials that had no visible defining characteristics among them and their ability to disperse into a water environment. All three methods take the relative same amount of time and produce quantities of material that are similar to each other. This suggests that there may not be a preferred method for generating the studied materials. The STEM image of the sol gel material shows a doped bulk material of varying size, shape, and chelator distribution. This indicates that the materials are not uniform. The other indication is that all three methods tried did not produce a well encapsulated material matrix, diminishing use in a biological system due to being able to leak or being exposed on the surface rather than encapsulated. This also suggests possible luminescent interference and inefficiencies due to the range of shapes, sizes, and distribution of doped material. The produced silica solgel materials were a white powdery substance. Upon excitation by the UV light, all dry materials with either Eu(btfa)$_3$(H$_2$O)$_2$ or Eu(btfa)$_3$dmphen exhibited vivid red luminescence characteristic of Eu^{3+} and

81

confirmed the doping of chelators into the silica matrix. Luminescence of the dry chelator doped material was less intense for $Eu(btfa)_3(H_2O)_2$, while the $Eu(btfa)_3dmphen$ material was visibly more intense. Once dispersed into water, both wet materials appeared more intense, suggesting effective dispersion of the solgel material. Dry and water dispersed solgels were measured for lifetime decay at 355 nm and 465 nm. All life times were higher at 355 nm and water dispersed solgel material suggesting that 355 nm is the optimal excitation value, with the 465 nm excitation being comparable to the 355 nm excitation with a lifetime reading difference of 0.067 ms or 10.23% faster decay time for $Eu(btfa)_3dmphen$ that is not a characteristic of the chelator dissolved in methylene chloride.

REFERENCES

1. Aspinall H.C. *Chemistry of the f-block elements*. CRC Press. 2001.8.

2. Hammond C.R. "Section 4; The Elements." *CRC Handbook of Chemistry and Physics.* 89ed.

3. Binnemans, K.; et al. *Hand Book on the Physics & Chemistry of Rare Earths. 2005, 35, 107*

4. Eliseevaa S. V. , Bünzli J.C G.. Lanthanide luminescence for functional materials and bio-sciences. *Chem. Soc. Rev.*, 2010,39, 189-227

5. Hemmilä, I. Laitala. Progress in Lanthanides as Luminescent Probes
V. *J Fluoresc* 2005. 15,4 529-542.

6. Yuan, J. ,Wang G.Lanthanide Complex-Based Fluorescence Label for Time-Resolved Fluorescence Bioassay. *J Fluoresc* 2005. 15: 559-568.

7. Hagan A.K; T. Zuchner. Lanthanide-based time-resolved luminescence immunoassays

Anal Bioanalytical Chemistry 2011, 400,2847–2864.

8. Leonard, J.P,   Cidalia M.G.dos Santos, Plush. S.E, McCabea,T Sally E. Plush and Thorfinnur G.

pH driven self-assembly of a ternary lanthanide luminescence complex: the sensing of anions using a β-

diketonate-Eu(III) displacement assay.*Chem. Commun.*, 2007, 129-131

9.Hebbink, G. A., Stouwdam, J.W., Reinhoudt, D.N. and van Veggel, F.C.J.M. Lanthanide(III)-Doped

Nanoparticles That Emit in the Near-Infrared. *Adv. Mater*. 2002, 14: 1147–1150.

10. Nyk M., R. Kumar, T.Y. Ohulchanskyy, E.J. Bergey, P.N. Prasad. *Nano Lett. 2008.* 8,11, 3832-3838

11.Yang C., Yume C., Hongmei W., Zuhong L. *Anal. Chem.* 2007, 79,3, 960-965

12.Faulkner S.; J.A Simon J.A.P., B.P B-P. *Appl Spectrosc Rev.*2005, 40, 1-31

13.Carter A. *Optical fibers for high-power eye-safe lasing applications.* 28 October 2007, SPIE

Newsroom.

14.Svelto, O. *Principles of Lasers 5ᵗʰ ed*. 2010, Springer

15. De Silva, C. R.; Vagner, J.; Lynch, R.; Gillies, R. J.; Hruby, V. J. "Optimization of Time-Resolved Fluorescence Assay for Detection of Eu-DOTA-labeled Ligand-Receptor Interactions" *Analytical Biochemistry* 2010, 398, 15.

16.Soukka, Tero, et al. "Supersensitive time-resolved immunofluorometric assay of free prostate-specific antigen with nanoparticle label technology."*Clinical chemistry* 47.7 (2001): 1269-1278.

17. Handl, L.H.; Robert, J.; Gillies, R. J. Lanthanide-based luminescent assays for ligand-receptor interactions. *Life Sciences,* 2005, 77 361 − 371. 10.

18. Josan, J. S.; De Silva, C. R.; Vagner, J.; Yoo, B.; Lynch, R.; Pagel, M. D.; Hruby, V.J. "Fluorescent and Lanthanide Labeling for Ligand Screens, Assays, and Imaging " invited chapter (in press) **2010**, *Methods in Molecular Biology-Protocols* - Special Issue on Drug Design and Discovery.

19.Fagge, Tim, et al. "Variation in concentration of prion protein in the peripheral blood of patients with variant and sporadic Creutzfeldt-Jakob disease detected by dissociation enhanced lanthanide fluoroimmunoassay and flow cytometry." *Transfusion* 45.4 (2005): 504-513.

20.Elliott, C T., K. S. Francis,W. J. McCaughey. "Investigation of dissociation enhanced lanthanide fluoroimmunoassay as an alternative screening test for veterinary drug residues." *Analyst* 119.12 (1994): 2565-2569.

21. Tan, M.; Wang G.; Hai, X.; Ye, Z.; Yuan, J. Development of functionalized fluorescent europium nanoparticles for biolabeling and time-resolved fluorometric applications. *J. Mater Chem* , 2004, 14: 2896-2901. 9.

22.Philippot, C.; Bourdolle, A.; Maury, O.; Dubois, F.; Boury, B.; Brustlein, S.; Brasselet, S.; Andraud, C.; Ibanez, A. Doped silica nanoparticles containing two photon luminescent Eu(III)complexes for the development of water stable biolabels. J. Mater. Chem., 2011, 21, 18613-18622. 14.

23.Escribano, P.; López, B. J.; Aragó, J. P.; Cordoncillo, E.; Viana, B.; Sanchez, C. Photonic and nanobiophotonic properties of luminescent lanthanide-doped hybrid organic–inorganic materials. *J. Mater. Chem.*, 2008, 18, 23-40. 13.

24.Page, A. B.; Page, A. M.; Noel, C. A new fluorimetric assay for cytotoxicity measurements in vitro. Int. J. Oncol. 1993, 3, 473–476.

25.Diamente, P. R.; Veggel, F.C.J.M.V. Water-Soluble Ln3+ Doped LaF3 Nanoparticles: Retention of Strong Luminescence and Potentials as Biolabels. *J. Fluor.* 2005, 15, 350. 4.

26.Coll, J. L. Cancer optical imaging using fluorescent nanoparticles. J. Nanomedicine 2012, 6, 7

27.Liu, Q.; Sun, Y.; Yang, T.; Feng, W.; Li, C.; Fuyou Li, F. Sub-10 nm Hexagonal 80 Lanthanide-Doped NaLuF4 Upconversion Nanocrystals for Sensitive Bioimaging in Vivo. J. Am. Chem. Soc, 2011, 133 (43), 17122–17125. 12.

28. Sigel, A.; Sigel, H. Metal ions in biological system, the lanthanides and their interaction with biosystem. 2003, Volume 40. 32.

29.Weissman, S. I. Intramolecular Energy Transfer The Fluorescence of Complexes of Europium .*J. Chem. Phys*. 1942, 10, 214.

30 Chen Y.T. R Aggeler, J. Bradford, Y.Wu, M.Rhodes, M. Janes, H.C. Kang, I.Johnson. *Molecular MM Probes^{TM} Labeling and Detection Technologies*, Invitrogen Corporation.

31.De Silva, C. R.; Maeyer, J.R.; Wang, R.; Nichol, G.S.; Zheng, Z. "Adducts of Europium ß-diketonates with Nitrogen *p,p'*-disubstituted Bipyridine and Phenanthroline Ligands: Synthesis, Structural Characterization, and Luminescence Studies" *Inorganica Chimica Acta* **2007**, 360, 3543.

32.De Silva, C. R**.**; Li, J.; Zheng, Z.; Corrales, L. R. "Correlation of Calculated Excited-state Energies and Experimental Quantum Yields of Luminescent Tb(III) ß-diketonates" *Journal of Physical Chemistry A* 2008, 112, 4527.

33. Lal, M.; Levy, L.; Kim, K. S.; He, G. S.; Wang, X.; Min, Y. H.; Pakatchi, S.; Prasad, P. N. Silica nanobubbles containing an organic dye in a multilayered organic/inorganic heterostructure with enhance luminescence. Chem. Mater. 2000, 12, 2632-2639. 3.

34. Wang, H.; Wang, L. Synthesis and sensing application of highly luminescent and water stable polyaspartate functionalized LaF3 nanocrystals J. Mater. Chem. C, 2013, 1, 1105-1110.

35.Galaup, C.; Azéma, J.; Tisnès, P.; Picard, C.; Ramos, P.; Juanes, O.; Brunet, E.; Rodríguez-Ubis, J. C. Luminescence of Eu+3 and Tb+3 Complexes of Two Macrobicyclic Ligands Derived from a Tetralactam Ring and a Chromophoric Antenna. Helvetica chemical acta, 2002, 85, 1613-1625. 8.

36. Nihonyanagi, S.; Kanemitsu, Y. Enhanced luminescence from electron–hole droplets in silicon nanolayers. Appl Phys. Lett. 2004, 85, 5721. 26.

37.Zhang H, Xu Y, Yang W ,and Li Q.Dual-Lanthanide-Chelated Silica Nanoparticles as Labels for Highly Sensitive Time-Resolved Fluorometry.*Chem. Mater.*, 2007, 19 (24), pp 5875–5881

38. Daojun Zhang D, Xuemin Wang X, Qiao Z, Tang D, Liu Y ,Huo Q.Synthesis and Characterization of Novel Lanthanide(III) Complexes-Functionalized Mesoporous Silica Nanoparticles as Fluorescent Nanomaterials *J. Phys. Chem.* C, 2010, 114 (29), 12505–12510

39. De Silva C, Vagner J, Lynch R, Gillies R, Hruby V.Optimization of time-resolved fluorescence assay for detection of europium-tetraazacyclododecyltetraacetic acid–labeled ligand–receptor interactions. *Anal Biochem. 2010* 398:15–23

40. Stöber W; A. Fink, E.J. Bohn. *J. Colloid. Interf. Sci. 1968, 26, 62.*

41.SS Rossi L.M.; L. Shi, F. Quina, Z. Rosenzweig. *Langmuir. 2005, 21, 4277-4280.*

42.Ibrahim, I. A. M.; Zikry, A. A. F.; Sharaf, M. A. Preparation of spherical silica nanoparticles: Stober silica. J. Amer Sci, 2010, 6(11), 985-989

43. Kubin, R. F. and A. N. Fletcher (1982) Fluorescence quantum yields of some rhodamine dyes. J. Luminescence 27, 455-462.

44. L U Y., Penzkofe A . R..“Absorption Behaviour of Methanolic Rhodamine 6G solutions at High Concentration.” *Chemical Physics 1986.* 107 175-184

45.Bindhu C V, Harilal S S, Nampoor VPN,CPG Vallabhan I. Studies of nonlinear absorption and aggregation in aqueous solutions of rhodamine 6G using a transient thermal lens technique J. Phys. D: *Appl. Phys.* 1999.32. 407–411

46.Genger U.R, Rurack K. Determination of the photoluminescence quantum yield of dilute dye

solutions (IUPAC Technical Report). Pure and Applied Chemistry 2013, 85:10.

47. Würth C, González M. G, Niessner R, Panne U, Haisch C, Genger U.R. Determination of the absolute fluorescence quantum yield of rhodamine 6G with optical and photoacoustic methods – Providing the basis for fluorescence quantum yield standards. *Talanta* 2012 90, 30-37.

48.González M. G.Determination of the photoluminescence quantum yield of diluted dye solutions in highly scattering media by pulsed photoacoustic spectroscopy. *Applied Optics* 2010 49:36, 6850.

49. Magde D, Wong R, Seybold P. G. Fluorescence Quantum Yields and Their Relation to Lifetimes of Rhodamine 6G and Fluorescein in Nine Solvents: Improved Absolute Standards for Quantum Yields. *Photochemistry and Photobiology* 2007 **75**:4, 327.

50. Zehentbauer F. M, Moretto C, Stephen R, Thevar T, Gilchrist J.R, Pokrajac D, Richard K. L, Kiefer J.Fluorescence spectroscopy of Rhodamine 6G: Concentration and solvent effects. Spectrochimica Acta Part A: *Molecular and Biomolecular Spectroscopy* 2014, 121, 147-151.